



THESIS APPROVAL
GRADUATE SCHOOL, KASETSART UNIVERSITY

Master of Science (Chemistry)

DEGREE

Chemistry

FIELD

Chemistry

DEPARTMENT

TITLE: Preparation of N-doped TiO₂ to Use as Catalysts in Photodegradation
 Reaction of PAHs and Phenol

NAME: Mr. Weekit Sirisaksoontorn

THIS THESIS HAS BEEN ACCEPTED BY

THESIS ADVISOR

(Associate Professor Apisit Songsasen, Ph.D.)

THESIS CO-ADVISOR

(Associate Professor Waraporn Parasuk, Dr.rer.nat.)

THESIS CO-ADVISOR

(Assistant Professor Surasak Chiangga, Dr.rer.nat.)

DEPARTMENT HEAD

(Assistant Professor Noojaree Prasitpan, Ph.D.)

APPROVED BY THE GRADUATE SCHOOL ON _____

DEAN

(Associate Professor Gunjana Theeragool, D.Agr.)

THESIS

PREPARATION OF N-DOPED TiO_2 TO USE AS CATALYSTS IN PHOTODEGRADATION REACTION OF PAHs AND PHENOL

WEEKIT SIRISAKSOONTORN

A Thesis Submitted in Partial Fulfillment of
the Requirements for the Degree of
Master of Science (Chemistry)
Graduate School, Kasetsart University
2009

Weekit Sirisaksoontorn 2009: Preparation of N-doped TiO₂ to Use as Catalysts in Photodegradation Reaction of PAHs and Phenol. Master of Science (Chemistry), Major Field: Chemistry, Department of Chemistry. Thesis Advisor: Associate Professor Apisit Songsasen, Ph.D. 165 pages.

N-doped TiO₂ was prepared via the sol-gel method, which varied titania precursors and nitrogen sources. From the characterization results, it was found that N-doped TiO₂ using titanium(IV) tetraisopropoxide with ammonia solution and calcined at 673 K provided the most appropriate properties for acting as the photocatalyst. TGA, Raman and XRD results indicated that this N-doped TiO₂ catalyst had high crystallinity because its titania precursor was simply hydrolyzed completely so no organic contents blocked initial phase construction. SEM and TEM results demonstrated that its surface morphology was spherical like fluffy powders. Moreover, with increasing calcination temperature, its anatase-to-rutile phase transformation was retarded by the incorporated nitrogen. Elemental Analysis and UV-Vis/DR results also suggested that nitrogen could be dormant in the TiO₂ lattice with strong bonds, causing the effect on the band gap structure by adding energy states nearly valence band of TiO₂. All of these properties enhanced the photocatalytic activity of N-doped TiO₂ under visible light.

Regarding the photocatalytic activity, N-doped TiO₂ using titanium(IV) tetraisopropoxide with ammonia solution and calcined at 673 K succeeded in degrading phenanthrene, benz[a]anthracene and phenol with the highest efficiency. However, its photocatalytic activity was drastically decreased when it was calcined at higher temperature. Additionally, the plausible mechanism was also proposed in case of photodegradation of phenanthrene based on two detected intermediates by GC/MS; bis(2-ethylhexyl)benzene-1,2-dicarboxylate and dimethyl-4-methyl-1,2-benzene dicarboxylate.

Student's signature

Thesis Advisor's signature

— / — / —

ACKNOWLEDGEMENTS

I would like to express my profound appreciation to my supervisor, Associate Professor Dr. Apisit Songsasen for his valuable guidance and encouragement throughout the span of my study and research. I also wish to express my sincere gratitude to Associate Professor Dr. Waraporn Parasuk, a member of committee, and Mr. Apipol Piriyaagagoon, a graduate student in physical chemistry field, for their advantageous suggestions on the quantum chemical calculation part. Additionally, I am so appreciative to Assistant Professor Dr. Surasak Chiangga, a member of committee, and his post-graduate student, Mr. Suchat Suwannatus, for their mutual collaboration and inventing the photoreactor used in my research.

I would also like to thank Faculty of Science, Kasetsart University for giving me the BRC (Bilateral Research Cooperation) grant. This grant provided me with the great opportunity to further do my research at the School of Chemistry, University of Bristol. Concomitantly, I gratefully thank Dr. Sean Davis, a senior lecturer at University of Bristol, Mr. Jonathan Jones and Mr. John Mitchels, both skillful technicians, for training me on the use of advanced SEM and TEM techniques.

In addition, I myself would like to thank the Development and Promotion of Science and Technology Talents Project (DPST) and Center of Excellent for Innovation in Chemistry: Postgraduate Education and Research Program in Chemistry (PERCH-CIC) for financial support and the Department of Chemistry, Faculty of Science, Kasetsart University for all research facilities.

I am specially appreciated my parents for continuously boosting my morale, encouraging me to overcome the obstacles and giving me financial assistance. Honestly speaking, I especially thank my colleagues and my friends for endorsing me and devoting their valuable time to helping me during my graduate study.

Weekit Sirisaksoontorn

April, 2009

TABLE OF CONTENTS

	Page
TABLE OF CONTENTS	i
LIST OF TABLES	ii
LIST OF FIGURES	v
LIST OF ABBREVIATIONS	xii
INTRODUCTION	1
OBJECTIVES	16
LITERATURE REVIEW	17
MATERIALS AND METHODS	29
Materials	29
Methods	30
RESULTS AND DISCUSSION	42
CONCLUSION AND RECOMMENDATIONS	115
Conclusion	115
Recommendations	116
LITERATURE CITED	117
APPENDICES	124
Appendix A	125
Calculation of crystallite sizes, phase composition and unit cell volume	
Appendix B	130
The procedure for the determination of the absorption edge of UV-Vis/DR results	
Appendix C	132
The supplementary data on the structural deter- mination by using quantum chemical calculation	
Appendix D	137
Raw data of all photodegradation reactions	
Appendix E	157
Calculation of rate constants of each photodegradation reactions	
Appendix F	163
The gas chromatogram of phenanthrene and intermediate products	
CURRICULUM VITAE	165

LIST OF TABLES

Table		Page
1	Some crystal properties of the three main polymorphs of TiO ₂	3
2	Structures and general properties of phenanthrene and benz[a]anthracene	14
3	The structure and general properties of phenol	15
4	Different nitrogen sources which were employed with their concentrations, volumes and the mole equality of nitrogen	31
5	Effect of titania precursors and calcination temperatures on the crystallite sizes and phase content of N-doped TiO ₂ and P25 TiO ₂	54
6	Effect of calcination temperatures on the unit cell volume of N-doped TiO ₂ and P25 TiO ₂	55
7	Energy gap (E _g) values of all N-doped TiO ₂ and P25 TiO ₂	76
8	The amount of nitrogen and carbon of N-doped TiO ₂ with various types of titania precursors	79
9	Effect of the nitrogen sources on the crystallite size and phase composition of N-doped TiO ₂	91
10	The amount of nitrogen and carbon of N-doped TiO ₂ with various types of nitrogen sources	99
11	%Conversion and rate constants of photodegradation reactions of phenanthrene by N-doped TiO ₂ using NH ₃ and various types of titania precursors at two different temperatures and by P25 TiO ₂	105
12	%Conversion and rate constants of photodegradation reactions of phenanthrene by N-doped TiO ₂ using titanium(IV) tetraisopropoxide and various types of nitrogen sources at 673 K	108
13	%Conversion and rate constants of photodegradation reactions of three substrates by N-doped TiO ₂ using titanium(IV) tetraisopropoxide mixed with NH ₃ and calcined at 673 K	114

LIST OF TABLES (Continued)

Appendix Table		Page
C1	The total energy, optimized bond lengths and bond angles of titanium(IV) bis(ethyl acetoacetato)diisopropoxide	134
C2	The total energy, optimized bond lengths and bond angles of titanium(IV) tetra-n-butoxide	135
C3	The total energy, optimized bond lengths and bond angles of titanium(IV) tetraisopropoxide	136
D1	Raw data of the photodegradation reaction of phenanthrene by N-doped TiO ₂ using titanium(IV) bis(ethyl acetoacetato) diisopropoxide mixed with NH ₃ and calcined at 673 K	140
D2	Raw data of the photodegradation reaction of phenanthrene by N-doped TiO ₂ using titanium(IV) bis(ethyl acetoacetato) diisopropoxide mixed with NH ₃ and calcined at 773 K	141
D3	Raw data of the photodegradation reaction of phenanthrene by N-doped TiO ₂ using titanium(IV) tetra-n-butoxide mixed with NH ₃ and calcined at 673 K	142
D4	Raw data of the photodegradation reaction of phenanthrene by N-doped TiO ₂ using titanium(IV) tetra-n-butoxide mixed with NH ₃ and calcined at 773 K	143
D5	Raw data of the photodegradation reaction of phenanthrene by N-doped TiO ₂ using titanium(IV) tetraisopropoxide mixed with NH ₃ and calcined at 673 K	144
D6	Raw data of the photodegradation reaction of phenanthrene by N-doped TiO ₂ using titanium(IV) tetraisopropoxide mixed with NH ₃ and calcined at 773 K	145

LIST OF TABLES (Continued)

Appendix Table	Page
D7 Raw data of the photodegradation reaction of phenanthrene by P25 TiO ₂	146
D8 Raw data of the photodegradation reaction of phenanthrene without catalysts	147
D9 Raw data of the photodegradation reaction of phenanthrene by N-doped TiO ₂ using titanium(IV) bis(ethyl acetoacetato) diisopropoxide mixed with (NH ₂) ₂ CO and calcined at 673 K	148
D10 Raw data of the photodegradation reaction of phenanthrene by N-doped TiO ₂ using titanium(IV) bis(ethyl acetoacetato) diisopropoxide mixed with NH ₄ Cl and calcined at 673 K	149
D11 Raw data of the photodegradation reaction of phenanthrene by N-doped TiO ₂ using titanium(IV) bis(ethyl acetoacetato) diisopropoxide mixed with N ₂ H ₄ ·H ₂ O and calcined at 673 K	150
D12 Raw data of the photodegradation reaction of benz[a]anthracene by N-doped TiO ₂ using titanium(IV) tetraisopropoxide mixed with NH ₃ and calcined at 673 K	151
D13 Raw data of the photodegradation reaction of benz[a]anthracene by P25 TiO ₂	152
D14 Raw data of the photodegradation reaction of benz[a]anthracene without catalysts	153
D15 Raw data of the photodegradation reaction of phenol by N-doped TiO ₂ using titanium(IV) tetraisopropoxide mixed with NH ₃ and calcined at 673 K	154
D16 Raw data of the photodegradation reaction of phenol by P25 TiO ₂	155
D17 Raw data of the photodegradation reaction of phenol without catalysts	156

LIST OF FIGURES

Figure		Page
1	Crystal structures of anatase, rutile and brookite	2
2	Principal processes on the TiO ₂ particles; e ⁻ + h ⁺ generation, oxidation of donors (D), reduction of acceptors (A), and e ⁻ - h ⁺ recombination at surface and in bulk	5
3	Secondary reactions with activated oxygen species in the photoelectronchemical mechanism	6
4	Schematic illustration of the expected energy bands for N-doped TiO ₂ (anatase) together with some photoinduced electronic process	8
5	Model structures for substitutional and interstitial N-dopants in anatase TiO ₂ phase	9
6	Electronic structures computed with PBE density function for substitutional and interstitial models	9
7	Priority listed PAHs by US EPA	12
8	The graphic picture of the inventive photoreactor; the photoreactor set, the stirrer set and the lamp set	36
9	The TG curve of as-prepared N-doped TiO ₂ using titanium(IV) bis(ethyl acetoacetato)diisopropoxide as a titania precursor	42
10	The TG curve of as-prepared N-doped TiO ₂ using titanium(IV) tetra-n-butoxide as a titania precursor	43
11	The TG curve of as-prepared N-doped TiO ₂ using titanium(IV) tetraisopropoxide as a titania precursor	44
12	Expected products from the hydrolysis reaction of titanium(IV) bis(ethyl acetoacetato)diisopropoxide; titanium(IV) tetra-n-butoxide and titanium(IV) tetraisopropoxide	45
13	Temperature-Programmed Oxidation (TPO) of as prepared N-doped TiO ₂	47

LIST OF FIGURES (Continued)

Figure		Page
14	The XRD patterns of N-doped TiO ₂ using titanium(IV) bis(ethyl acetoacetato)diisopropoxide as a titania precursor with different calcination temperatures and P25 TiO ₂	48
15	The XRD patterns of N-doped TiO ₂ using titanium(IV) tetra-n-butoxide as a titania precursor with different calcination temperatures	50
16	The XRD patterns of N-doped TiO ₂ using titanium(IV) tetraisopropoxide as a titania precursor with different calcination temperatures	51
17	Raman spectra of N-doped TiO ₂ using titanium(IV) bis(ethyl acetoacetato)diisopropoxide as a titania precursor with different calcination temperatures	56
18	Raman spectra of N-doped TiO ₂ using titanium(IV) tetra-n-butoxide as a titania precursor with different calcination temperatures	57
19	Raman spectra of N-doped TiO ₂ using titanium(IV) tetraisopropoxide as a titania precursor with different calcination temperatures	58
20	SEM and TEM images of N-doped TiO ₂ using titanium(IV) bis(ethyl acetoacetato)diisopropoxide as a titania precursor and calcined at 673 K	60
21	SEM and TEM images of N-doped TiO ₂ using titanium(IV) bis(ethyl acetoacetato)diisopropoxide as a titania precursor and calcined at 773 K	61
22	SEM and TEM images of N-doped TiO ₂ using titanium(IV) bis(ethyl acetoacetato)diisopropoxide as a titania precursor and calcined at 873 K	62

LIST OF FIGURES (Continued)

Figure		Page
23	SEM and TEM images of N-doped TiO ₂ using titanium(IV) tetra-n-butoxide as a titania precursor and calcined at 673 K	64
24	SEM and TEM images of N-doped TiO ₂ using titanium(IV) tetra-n-butoxide as a titania precursor and calcined at 773 K	65
25	SEM and TEM images of N-doped TiO ₂ using titanium(IV) tetra-n-butoxide as a titania precursor and calcined at 873 K	66
26	SEM and TEM images of N-doped TiO ₂ using titanium(IV) tetraisopropoxide as a titania precursor and calcined at 673 K	68
27	SEM and TEM images of N-doped TiO ₂ using titanium(IV) tetraisopropoxide as a titania precursor and calcined at 773 K	69
28	SEM and TEM images of N-doped TiO ₂ using titanium(IV) tetraisopropoxide as a titania precursor and calcined at 873 K	70
29	SEM and TEM images of P25 TiO ₂	72
30	UV-Vis/DR spectra of N-doped TiO ₂ using titanium(IV) bis(ethyl acetoacetato)diisopropoxide as a titania precursor and P25 TiO ₂	73
31	UV-Vis/DR spectra of N-doped TiO ₂ using titanium(IV) tetra-n-butoxide as a titania precursor	74
32	UV-Vis/DR spectra of N-doped TiO ₂ using titanium(IV) tetraisopropoxide as a titania precursor	75
33	XPS spectra of N-doped TiO ₂ using titanium(IV) bis(ethyl acetoacetato)diisopropoxide as a titania precursor with binding energy of Ti 2p, O 1s and N 1s	81
34	The optimized structure of titanium(IV) bis(ethyl acetoacetato)diisopropoxide	82
35	The optimized structure of titanium(IV) tetra-n-butoxide	83
36	The optimized structure of titanium(IV) tetraisopropoxide	83

LIST OF FIGURES (Continued)

Figure		Page
37	The TG curve of as-prepared N-doped TiO ₂ using (NH ₂) ₂ CO as a nitrogen source	85
38	The TG curve of as-prepared N-doped TiO ₂ using NH ₄ Cl as a nitrogen source	86
39	The TG curve of as-prepared N-doped TiO ₂ using NH ₃ as a nitrogen source	87
40	The TG curve of as-prepared N-doped TiO ₂ using N ₂ H ₄ .H ₂ O as a nitrogen source	88
41	The XRD patterns of N-doped TiO ₂ using various types of nitrogen sources; (NH ₂) ₂ CO, NH ₄ Cl, NH ₃ and N ₂ H ₄ .H ₂ O with fixed calcination temperature at 673 K	89
42	Raman spectra of N-doped TiO ₂ using various types of nitrogen sources; (NH ₂) ₂ CO, NH ₄ Cl, NH ₃ and N ₂ H ₄ .H ₂ O with fixed calcination temperature at 673 K	92
43	SEM and TEM images of N-doped TiO ₂ using (NH ₂) ₂ CO as a nitrogen source and calcined at 673 K	93
44	SEM and TEM images of N-doped TiO ₂ using NH ₄ Cl as a nitrogen source and calcined at 673 K	94
45	SEM and TEM images of N-doped TiO ₂ using NH ₃ as a nitrogen source and calcined at 673 K	95
46	SEM and TEM images of N-doped TiO ₂ using N ₂ H ₄ .H ₂ O as a nitrogen source and calcined at 673 K	96
47	Photodegradation of phenanthrene by N-doped TiO ₂ using NH ₃ and various types of titania precursors; titanium(IV) tetraisopropoxide, titanium(IV) tetra-n-butoxide, titanium(IV) bis(ethyl acetoacetato) diisopropoxide, and calcined at 673 K, compared to P25 TiO ₂ and without catalysts	100

LIST OF FIGURES (Continued)

Figure		Page
48	Photodegradation of phenanthrene by N-doped TiO ₂ using NH ₃ and various types of titania precursors; titanium(IV) tetraisopropoxide, titanium(IV) tetra-n-butoxide, titanium(IV) bis(ethyl acetoacetato) diisopropoxide, and calcined at 773 K, compared to P25 TiO ₂	103
49	Photodegradation of phenanthrene by N-doped TiO ₂ using titanium(IV) bis(ethyl acetoacetato)diisopropoxide and various types of nitrogen sources; NH ₃ , (NH ₂) ₂ CO, NH ₄ Cl and N ₂ H ₄ .H ₂ O, and calcined at 673 K	106
50	The chemical structures of two detected intermediate products; bis(2-ethylhexyl)benzene-1,2-dicarboxylate and dimethyl-4-methyl-1,2-benzene dicarboxylate	109
51	Possibly proposed mechanism of photodegradation of phenanthrene by using N-doped TiO ₂ calcined at 673 K	110
52	Photodegradation of benz[a]anthracene by using N-doped TiO ₂ calcined at 673 K, P25 TiO ₂ and without catalysts	111
53	Photodegradation of phenol by using N-doped TiO ₂ calcined at 673 K, P25 TiO ₂ and without catalysts	112
 Appendix Figure		
A1	The XRD pattern of N-doped TiO ₂ using titanium(IV) tetraisopropoxide mixed with NH ₃ and calcined at 673 K	126
A2	The XRD pattern of N-doped TiO ₂ using titanium(IV) tetra-n-butoxide mixed with NH ₃ and calcined at 873 K	127
A3	The XRD pattern of N-doped TiO ₂ using titanium(IV) tetraisopropoxide mixed with NH ₃ and calcined at 673 K	129

LIST OF FIGURES (Continued)

Appendix Figure	Page
A4 The XRD pattern of N-doped TiO ₂ using titanium(IV) tetra-n-butoxide mixed with NH ₃ and calcined at 873 K	129
B1 The UV-Vis/DR spectrum of N-doped TiO ₂ using titanium(IV) tetraisopropoxide mixed with NH ₃ and calcined at 773 K	131
C1 The optimized structure of titanium(IV) bis(ethyl acetoacetato) diisopropoxide	133
C2 The optimized structure of titanium(IV) tetra-n-butoxide	133
C3 The optimized structure of titanium(IV) tetraisopropoxide	135
D1 The linear calibration curve of phenanthrene	138
D2 The linear calibration curve of benz[a]anthracene	138
D3 The linear calibration curve of phenol	139
E1 The relation between $\ln C_0/C$ and time (h) of photodegradation reaction of phenanthrene by N-doped TiO ₂ using the variation of titania precursors; titanium(IV) bis(ethyl acetoacetato)diisopropoxide, titanium(IV) tetra-n-butoxide and titanium(IV) tetraisopropoxide, and calcined at 673 K	158
E2 The relation between $\ln C_0/C$ and time (h) of photodegradation reaction of phenanthrene by N-doped TiO ₂ using the variation of titania precursors; titanium(IV) bis(ethyl acetoacetato)diisopropoxide, titanium(IV) tetra-n-butoxide and titanium(IV) tetraisopropoxide, and calcined at 773 K	159
E3 The relation between $\ln C_0/C$ and time (h) of photodegradation reaction of phenanthrene by N-doped TiO ₂ using the variation of nitrogen sources; NH ₃ , (NH ₂) ₂ CO, NH ₄ Cl and N ₂ H ₄ .H ₂ O and calcined at 673 K	160
E4 The relation between $\ln C_0/C$ and time (h) of photodegradation reaction of phenanthrene by P25 TiO ₂	160

LIST OF FIGURES (Continued)

Appendix Figure		Page
E5	The relation between $\ln C_0/C$ and time (h) of photodegradation reaction of benz[a]anthracene by N-doped TiO_2 using titanium(IV) tetraisopropoxide mixed with NH_3 and calcined at 673 K and P25- TiO_2	161
E6	The relation between $\ln C_0/C$ and time (h) of photodegradation reaction of phenol by N-doped TiO_2 using titanium(IV) tetraisopropoxide mixed with NH_3 and calcined at 673 K and P25- TiO_2	162
F1	The gas chromatogram of phenanthrene and intermediate products	164

LIST OF ABBREVIATIONS

BET	=	Brunauer-Emmett- Teller
B3LYP	=	Becke-Lee, Yang and Parr correlation functional
DFT	=	Density Functional Theory
EA	=	Elemental Analysis
GC/MS	=	Gas Chromatography/Mass Spectrometry
JCPDS	=	Joint Committee on Powder Diffraction Standard
PBE	=	Population Balance Equation
PAHs	=	Polycyclic Aromatic Hydrocarbons
SEM	=	Scanning Electron Microscopy
TEM	=	Transmission Electron Microscopy
TGA	=	Thermal Gravimetric Analysis
TPO	=	Temperature-Programmed Oxidation
US EPA	=	US Environmental Protection Agency
UV-Vis/DR	=	UV-Vis Diffuse Reflectance Spectrophotometry
XPS	=	X-ray Photoelectron Spectroscopy
XRD	=	X-ray Diffraction

PREPARATION OF N-DOPED TiO_2 TO USE AS CATALYSTS IN PHOTODEGRADATION REACTION OF PAHs AND PHENOL

INTRODUCTION

Titanium dioxide (TiO_2)

Titanium dioxide (TiO_2) is naturally found in the mineral sources such as ilmenite, rutile, anatase and brookite. First, ilmenite (FeTiO_2) or titanite iron ore is a grey mineral containing magnetic black iron. It was firstly discovered at Ural Ilmen Mountain (Russia) in 1827 by Kupffer who named it. The majority of the ilmenite mined is used as a raw material for pigment production. The product is titanium dioxide, which is ground into a fine powder and is a highly white substance used as a base in high-quality paint, paper and plastics applications. Second, rutile is a mineral composed primarily of titanium dioxide, TiO_2 , and found in 1803 by Werner in Spain. It is commonly reddish brown but sometimes yellowish, bluish or violet and naturally contains up to 10% of iron and other impurities as well. The main uses for rutile are the manufacture of refractory ceramic, as a pigment, or for the production of titanium metal. Third, anatase, earlier called octahedrite, was named by Haüy in 1801. It is always found as small, isolated and sharply developed crystals and a more commonly occurring modification of titanium dioxide. Last, brookite is a dark brown to greenish black mineral mainly consisting of titanium oxide, TiO_2 . Brookite occurs rarely compared to the anatase and rutile forms of titanium dioxide. However, it was firstly found by A Levy in 1825 at Snowden (England).

1. Crystal structures and properties

There are three principal crystal structures, anatase (tetragonal), rutile (tetragonal) and brookite (orthorhombic) found in nature (Figure 1). Even though their structures are similarly based on octahedrals (TiO_6), they still differ from one another by the distortion of each octahedral and by the assembly patterns of the octahedral

chains. Anatase is built up from octahedra which are mainly connected by their vertices. Octahedral structures in rutile are mostly connected by the edges. Both vertical and edge connections are found in the octahedral structure of the brookite form. Although both anatase and rutile are the same tetragonal system, anatase has longer its vertical axis of the crystals than rutile. Meanwhile, brookite crystallizes in the orthorhombic system.

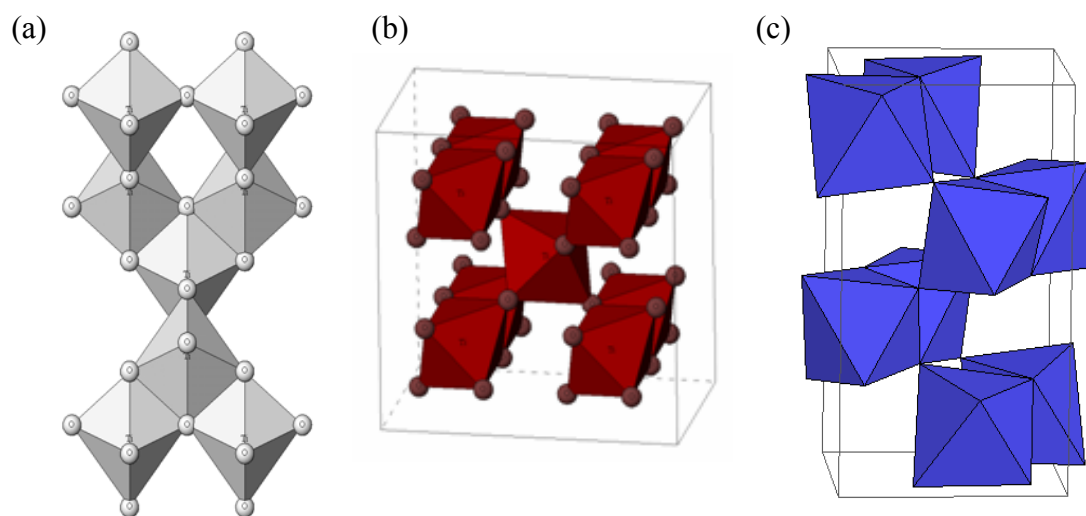


Figure 1 Crystal structures of (a) anatase, (b) rutile and (c) brookite.

Source: Namura (2002)

Moreover, rutile is the most stable phase of titanium dioxide while anatase and brookite are metastable phases. The metastable structures are almost as stable as rutile at normal pressure and temperature because of small difference in the Gibbs free energy (4-20 kJ/mol) between three phases (Carp *et al.*, 2004). Regarding the band gap energy, 3.26 eV (~380 nm) is the band gap energy of anatase and in rutile 3.05 eV (~406 nm) is its energy (Carp *et al.*, 2002). Other crystal properties of all three forms of TiO_2 are shown in Table 1.

Table 1 Some crystal properties of the three main polymorphs of TiO₂.

Crystal structure	System	Space group	Lattice constants (nm)			Density (kg/m ³)	Band gap (eV)
			a	b	c		
Anatase	Tetragonal	I4 ₁ /amd	0.3733	0.3733	0.937	3830	3.26
Rutile	Tetragonal	P4 ₂ /mmm	0.4584	0.4584	0.2953	4240	3.05
Brookite	Orthorhombic	Pbca	0.5436	0.9166	0.5134	4170	-

Source: Carp *et al.* (2004)

2. TiO₂ applications

Nowadays, titanium dioxide (TiO₂) has widely gained a great deal of attention because of its chemical stability, non toxicity, low cost and other advantageous properties. It, therefore, has been used in worldwide applications such as photovoltaic cells, photocatalysis, environmental purification, photoinduced superhydrophilicity as well as an ingredient in a pigment. With respect to photocatalysis, TiO₂ is close to being an ideal photocatalyst due to its properties as mentioned above. Generally, both anatase and rutile are used as photocatalysts and some research stated that anatase had higher photoactivity than rutile (Yates *et al.*, 1995). There are also other studies which claimed that mixture phases between anatase and rutile provided higher efficiency than the pure phase (Muggli *et al.*, 2001). In these different results, they should rely on the intervening effect of several factors such as specific surface areas, crystallite sizes, pore size distribution as well as preparation methods. In photocatalytic reactions, TiO₂ can degrade not only organic compounds such as hydrocarbons, chlorinated compounds and nitrogen- or sulfur-containing compounds but also inorganic compounds such as nitrogen oxide species (NO_x). Overall, photocatalytic reactions can be generally summarized as displayed in Figure 2. Initially, e⁻ and h⁺ are generated by using photon energy (hν) which has equal or higher energy than band gap energy of TiO₂. Some electrons (e_{cb}⁻) are excited into the conduction band whilst holes (h_{vb}⁺) still stay in the valence band and then both of them will move to the TiO₂ surface with a view to reducing or oxidizing. On the other hand, e⁻ and h⁺ are able to recombine again which can occur at the bulk and at the surface. The recombination process is usually considered as the deactivation process in photocatalytic reaction.

In most studies about photocatalysts, oxygen (O₂) plays a vital role in the primary electron acceptor. This step electron will transfer to oxygen and further generate H₂O₂ and ·OH. Meanwhile, h_{vb}⁺ reacts with adsorbed water molecules on the surface or surface titanol group (>TiOH) and finally hydroxyl radicals are also formed. H₂O₂ contributes to the degradation pathway by acting as an electron

acceptor or as a direct source of $\cdot\text{OH}$ due to homolytic scission. All of these reactions are summarized and illustrated in Figure 3.

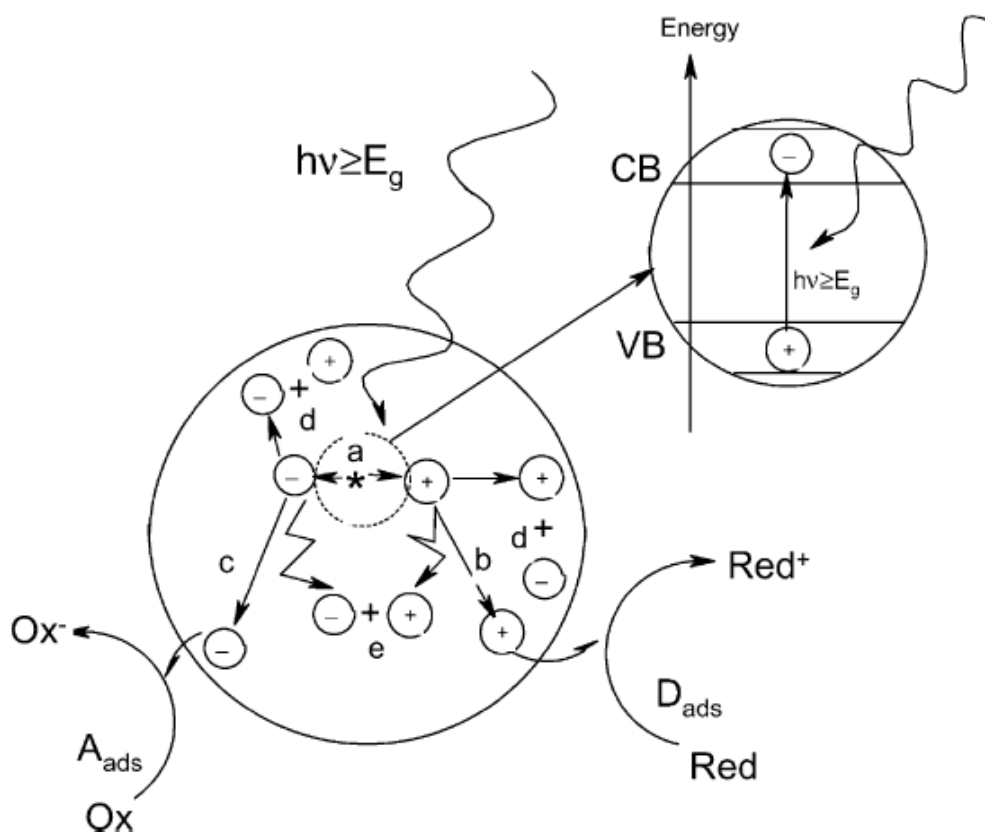


Figure 2 Principal processes on the TiO_2 particles; (a) $e^- + h^+$ generation, (b) oxidation of donors (D), (c) reduction of acceptors (A), (d) and (e) $e^- - h^+$ recombination at surface and in bulk, respectively.

Source: Mills *et al.* (1997)

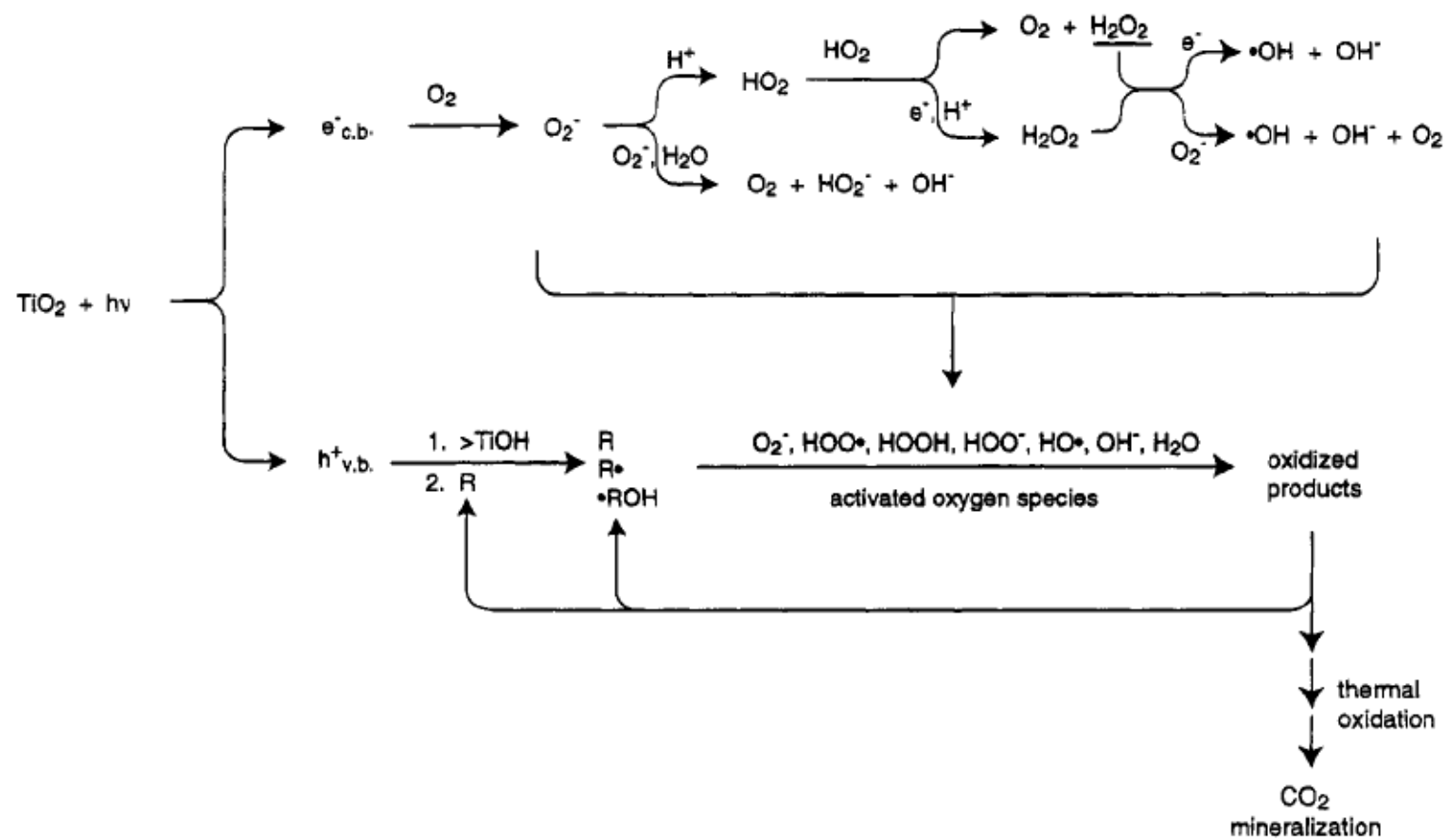


Figure 3 Secondary reactions with activated oxygen species in the photoelectronchemical mechanism.

Source: Hoffman *et al.* (1995)

3. TiO₂ modification

In order to enhance the photocatalytic activity of TiO₂, many researchers try to extend the range of photoefficiency of TiO₂ into visible light because normally TiO₂ will be active when irradiated with UV light. Moreover, there is only 3-4% of an ultraviolet part in the solar light that shines through the earth (Shifu *et al.*, 2005). One of the most applicable approaches is to doping semiconductors with various types of transition metal ions or anions species. Both of two doping species can produce the impurity states lying between valence band and conduction band, which causes the band gap narrowing. However, as previously research by Wang *et al.* (2006), they stated that anion dopants as recombination centers might be minimized as compared to cation dopants. With regard to anion dopants, although there are several kinds of anion dopants such as B, C, N, S, F as well as co-dopants, N anion dopants seem to be the most fashionable anions because its anion size closes to that of oxygen anion in TiO₂ lattice. The modified band structure of N-doped TiO₂ is shown in Figure 4. The additional states are induced to appear near the valence band of TiO₂.

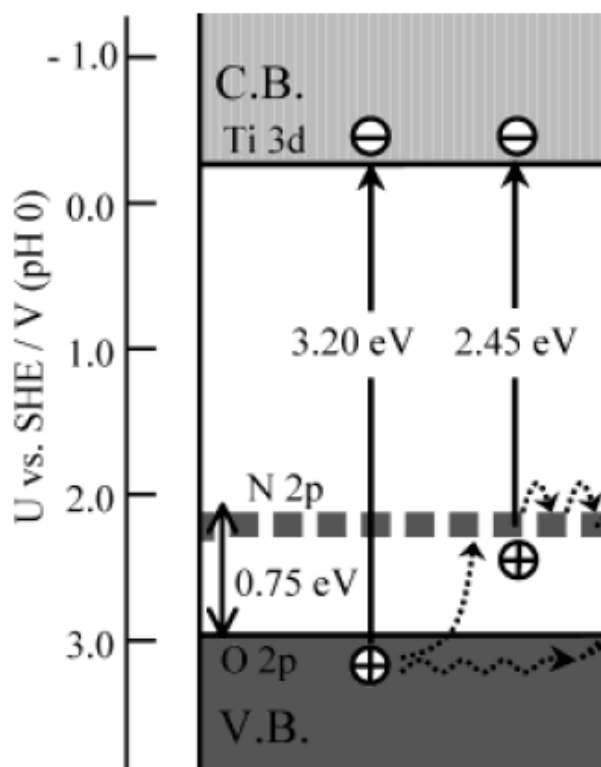


Figure 4 Schematic illustration of the expected energy bands for N-doped TiO₂ (anatase) together with some photoinduced electronic process.

Source: Nakato *et al.* (2004)

Furthermore, Valentin *et al.* (2007) added the idea that doping nitrogen species could be categorized into two main species, substitutional and interstitial nitrogen (Figure 5), which probably took place in the TiO₂ structure. Both of them gave slightly different band structures based on computational results (Figure 6). Even though we recently know that there are two types of nitrogen in TiO₂ lattice, it is very difficult to identify them. However, most researches believed that substitutional nitrogen capable of being detected by XPS at binding energy of ~397 eV (Ti-N) was the active species to photocatalytic activity.

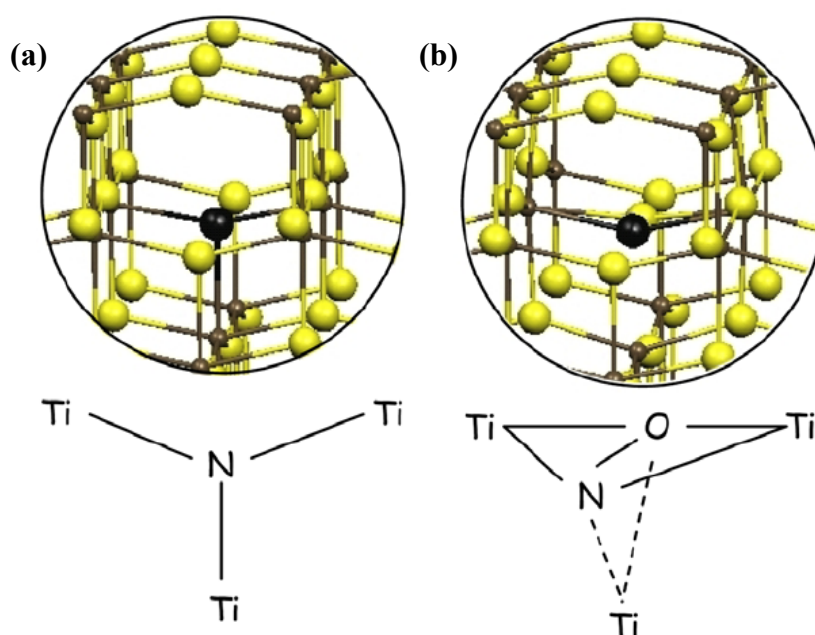


Figure 5 Model structures for (a) substitutional and (b) interstitial N-dopants in anatase TiO_2 phase.

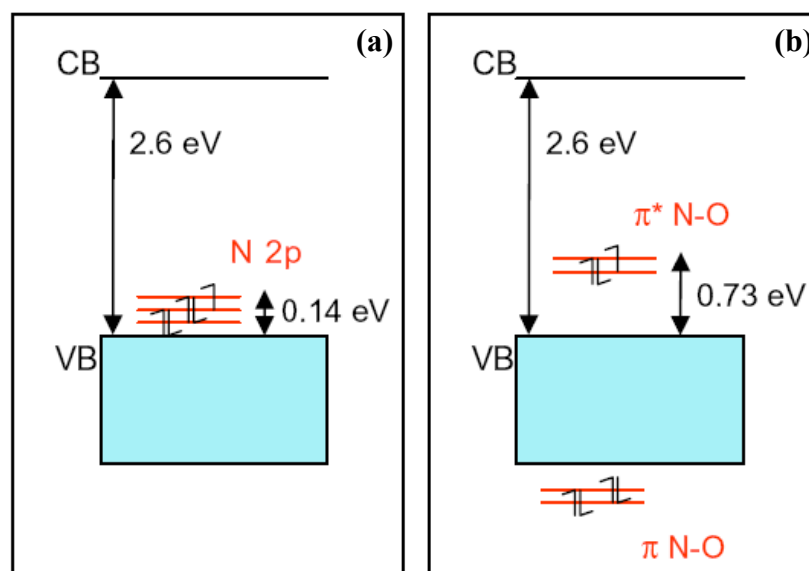


Figure 6 Electronic structures computed with PBE density function for (a) substitutional and (b) interstitial models.

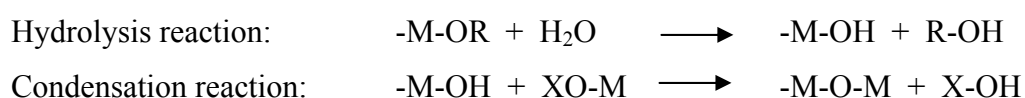
Source: Valentin *et al.* (2007)

4. Preparation method

There are diverse methods to effectively synthesize powder, thin-film and membrane TiO_2 or modified TiO_2 , namely precipitation (co-), solvothermal, sol-gel, microemulsion, electrochemical, chemical/physical vapor deposition, ion-implantation and ball milling methods. Focusing on the sol-gel method, most of recent works usually use this method. It takes many advantages over other methods in terms of purity, homogeneity, felicity and flexibility in introducing dopants in large concentrations, stoichiometric control, ease of processing and control over the composition. Generally, there are two known types of titania precursors, non-alkoxide and alkoxide, utilized in the sol-gel method. The former makes use of inorganic salts (such as chlorides, acetylacetonate, etc.), which requires the removal of the inorganic anions after preparation. In other words, the alkoxide route uses metal alkoxides as a starting material. This route has highly been used for preparing metal oxide because metal alkoxide precursors are commercially available in high purity and are easily handled at ambient temperature or under nitrogen atmosphere. Concerning preparation, the sol-gel method is composed of four key steps as follows;

4.1 Wet solution

This step focuses on gel formation, which is a diphasic material with a solid encapsulating solvent. Before gel formation occurs, a starting material will be hydrolyzed and partially condensed in order to form sol, which is liquid suspension in solid particles. After that, further condensation in three-dimension network is conducive to gel formation. In case of metal alkoxide precursors, all involving reactions are shown below.



where x is either H or R (an alkyl group).

4.2 Aging

To further complete the reaction, gel is left to continue constructing its more networks causing stronger cross-linkage. Moreover, some solvent molecules are expelled by the extensive condensation of gel. This step mainly depends on aging time, temperature as well as pH.

4.3 Drying

In order to remove organic solvent or hydrolyzed molecules, metal oxide needs to be heated at the sufficient temperature to dispose them. Additionally, this step is involved in the capillary pressure that has an effect on the pore size of metal oxide. Therefore, many factors, such as heating rate, pressure rate and time, are taken into serious consideration with a view to controlling the pore structure of metal oxide.

4.4 Calcination

This final step emphasizes on crystallization of metal oxide. Calcination is used in order to remove the dormant organic part and to crystallize phase of metal oxide. However, it will inevitably cause a decrease in surface area, loss of surface hydroxyl groups and even phase transformation.

5. Polycyclic aromatic hydrocarbons (PAHs)

Polycyclic aromatic hydrocarbon (PAH) compounds are a class of complex organic chemicals, which include carbon and hydrogen with a fused ring structure containing at least two benzene rings. Many of them have been classified as priority pollutants by US EPA (Callahan *et al.*, 1979) as shown in Figure 7. Although only at trace levels, they pose a real threat to human health because they are toxic and many of them are carcinogenic, especially high molecular weight PAHs.

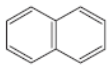
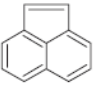
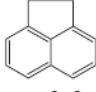
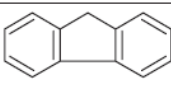
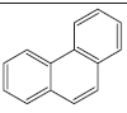
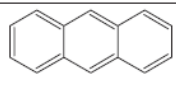
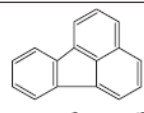
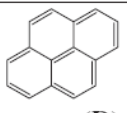
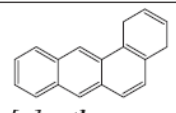
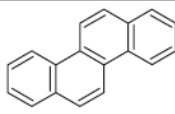
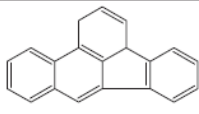
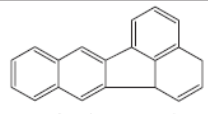
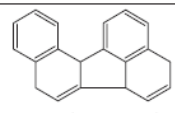
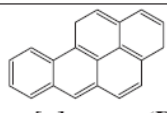
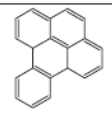
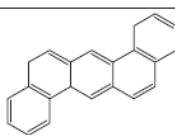
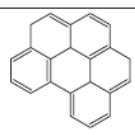
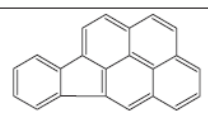
 <i>naphthalene</i> * $C_{10}H_8$	 <i>acenaphthylene</i> (D) $C_{12}H_8$	 <i>acenaphthene</i> $C_{12}H_{10}$
 <i>fluorene</i> (D) $C_{13}H_{10}$	 <i>phenanthrene</i> (D) $C_{14}H_{10}$	 <i>anthracene</i> (D) $C_{14}H_{10}$
 <i>fluoranthene</i> (D) $C_{16}H_{10}$	 <i>pyrene</i> (D) $C_{16}H_{10}$	 <i>benzo[a]anthracene</i> (B2) $C_{18}H_{12}$
 <i>chrysene</i> (B2) $C_{18}H_{12}$	 <i>benzo[b]fluoranthene</i> (B2) $C_{20}H_{12}$	 <i>benzo[k]fluoranthene</i> $C_{20}H_{12}$
 <i>benzo[j]fluoranthene</i> $C_{20}H_{12}$	 <i>benzo[a]pyrene</i> (B2) $C_{20}H_{12}$	 <i>benzo[e]pyrene</i> $C_{20}H_{12}$
 <i>dibenz[a,h]anthracene</i> (B2) $C_{22}H_{14}$	 <i>benzo[g,h,i]perylene</i> (D) $C_{22}H_{12}$	 <i>indeno[1,2,3-c,d]pyrene</i> (B2) $C_{22}H_{12}$

Figure 7 Priority listed PAHs by US EPA.

* (not included in priority list)

D (not listed as to human carcinogenicity)

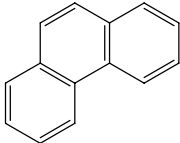
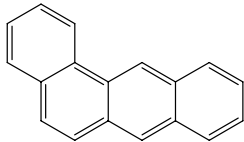
B2 (probable human carcinogen)

Source: Ravindra *et al.* (2008)

PAHs are formed from the incomplete combustion or pyrolysis of organic materials such as oil, petroleum gas, coal and wood which are usually used in energy production. They have a high tendency to be adsorbed on the solid particulates, especially on the organic fraction of the soil, because of their hydrophobic nature. Moreover, they are very persistent in the environment due to their resistance to biological degradation. Therefore, many researchers have highly paid attention to the studies on the way how to eliminate PAHs and lessen their toxicity.

First of all, focusing on phenanthrene, it is a PAH composed of three fused benzene rings (Table 2). It is found in cigarette smoke and is a known irritant, photosensitizing skin to light. Phenanthrene appears as a white powder and insoluble in water but soluble in most organic solvents. Second, regarding benz[a]anthracene, it is one of the PAHs, consisting of a consecutive four-member ring structure as shown in Table 2. It is natural products produced by the incomplete combustion of the organic material. The toxic effects of benz[a]anthracene and similar PAHs are primarily directed toward tissues that contain proliferating cells.

Table 2 The structures and general properties of phenanthrene and benz[a]anthracene.

Structure	Properties			
	Molecular formula	Molecular weight (g/mol)	Melting point (K)	Boiling point (K)
	C ₁₄ H ₁₀	178.23	372.2	613
	C ₁₈ H ₁₂	228.29	158	438

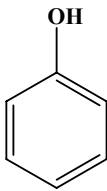
Source: Lide (1995)

6. Phenol

Phenol is categorized as one of the aromatic compounds, in which an -OH group is attached directly to a benzene ring as illustrated in Table 3. Pure phenol is a white crystalline solid, smelling of disinfectant. The crystals are often rather wet and discolored. Phenol has a limited solubility in water. It is slightly acidic. Its molecule has weak tendencies to lose the H⁺ ion from the hydroxyl group, resulting in the highly water-soluble phenoxide anion C₆H₅O⁻. Additionally, concerning natural contamination, high concentration of phenol and its derivatives are found in nature. They contaminate in wastewater derived from different chemical industries such as resin manufacturing, petrochemical, oil-refineries, paper making as well as iron smelting. However, phenol is highly corrosive and moderately toxic. It causes many effects on humans by burning the skin and other tissues that it comes into contact with. This gives severe skin burning and if inhaled serious internal corrosion. Thus,

current research aims to study how to dispose this toxic compound widespread in nature.

Table 3 The structure and general properties of phenol.

Structure	Properties			
	Molecular formula	Molecular weight (g/mol)	Melting point (K)	Boiling point (K)
	C ₆ H ₅ OH	94.11	313.5	454.7

Source: Lide (1995)

OBJECTIVES

This work aims to study the preparation with sol-gel, characterization with various techniques and photocatalytic applications of N-doped TiO₂, compared to commercial P25 TiO₂. There are five main objectives that this work focuses on.

1. To study the effect of titania precursors on the as-prepared N-doped TiO₂ in terms of its phase composition, crystallinity, surface morphology, visible absorption ability as well as the amount of doped nitrogen.
2. To study the effect of calcination temperature between 573 and 873 K on the phase transformation, crystallinity, surface morphology, visible absorption ability as well as the amount of doped nitrogen of N-doped TiO₂ compared to P25 TiO₂.
3. To use the computational calculation in order to optimize the four structures of titania precursors and compare one another.
4. To study the effect of diverse nitrogen sources on the as-prepared N-doped TiO₂ at fixed calcination temperature of 673 K in terms of its phase composition, crystallinity, surface morphology as well as the amount of doped nitrogen.
5. To make use of some of the N-doped TiO₂ in photocatalytic degradation of PAHs (phenanthrene and benz[a]anthracene) and phenol. Also, the photocatalytic activities and rate constants of each N-doped TiO₂ and P25 TiO₂ were studied.

LITERATURE REVIEW

The reviews studied the previous research on TiO_2 , P25 TiO_2 and modified TiO_2 in terms of the preparation method, the characterization techniques, the applications as well as the computational aspects on the physical properties.

1. Titanium dioxide (TiO_2)

Ireland *et al.* (1995) studied the photocatalytic degradation of a mixture of 16 polyaromatic hydrocarbons (PAHs) in aqueous suspensions of high surface area TiO_2 illuminated with 310-380 nm ultraviolet light. Triethylamine was used to increase PAH solubility in TiO_2 /water slurries. The apparent degradation rates based on a simple pseudo-first order kinetic model of the 16 individual PAHs showed measurably significant variation relative to each other. Interestingly, that the photocatalytic process was capable of generating stable intermediate oxidation by-products was demonstrated by the temporal formation of phenanthrene in the PAH mixture which reached a maximum at around 12 h irradiation time. Then, phenanthrene itself began to decompose after extended oxidation. Moreover, minimum steady-state hydroxyl radical concentrations generated during photocatalysis were also determined directly by electrospray ionization mass spectrometry analysis of the stable spin-trapped $\cdot\text{OH}$ adducts (4-POBN). The result showed that the calculated time averaged flux in the presence of 16 PAH mixture was $0.14 \mu\text{moles } \cdot\text{OH}/\text{min}$.

Zhang *et al.* (1999) studied the effect of added water and oxygen on the complete photocatalytic oxidation of C_2H_4 with O_2 into CO_2 on the powdered TiO_2 photocatalysts under UV light irradiation ($\lambda > 280 \text{ nm}$). Evidently, if TiO_2 catalysts of large surface area were used and O_2 was introduced onto photocatalysts in excess, C_2H_4 could be completely oxidized to produce only CO_2 . The addition of a constant amount of water vapor led to an increase in the yield of CO_2 , while it had no effect on the yield of CO . It was known that the adsorption of water on the TiO_2 surface caused a decrease in the upward bending of the band, resulting in the efficient recombination of the photo-generated electrons and holes. This effect will bring about the negative

impact on photocatalytic activity. On the other hand, the adsorption of H_2O resulted in the formation of surface OH groups by the reaction of H_2O with the bridging-oxygen atoms. This effect will cause the positive impact on the photocatalytic activity. Hence, these two factors might play an important role in determining the photocatalytic reactivity of TiO_2 and the contribution of these factors strongly depended on the amount of H_2O added.

Cao *et al.* (2000) investigated the effects of deactivation process, regeneration conditions and humidity on the surface and structural properties of the nanoscale TiO_2 catalysts prepared from a sol-gel process. TiO_2 was highly active catalysts for the photodegradation of toluene. Performing the reaction at room temperature resulted in rapid deactivation of TiO_2 catalysts due to the chemisorption of intermediates, such as benzaldehyde, benzoic acid. The color change of the catalysts from white to yellow was associated with the accumulation of these carbon species on the active sites. The complete recovery of catalytic activity occurred simply when the regeneration temperature was at or above 693 K burning out chemisorbed carbon species. Loading Pt on TiO_2 lowered the regeneration temperature considerably at the expense of some photocatalytic activity. High humidity in the feed stream significantly inhibited the oxidation rate of toluene since water was preferentially adsorbed on the hydrophilic surface of TiO_2 . Besides, the adsorption of intermediates was irreversible in the initial reaction stage based on kinetic studies.

Zhao *et al.* (2002) studied the affecting factors on the photocatalytic oxidation of phenanthrene in aqueous TiO_2 suspensions under UV light illumination. The pH of the dispersion, surface coverage and amount of Ph/ TiO_2 had a little effect on the photooxidation rate of phenanthrene. Moreover, some intermediate products resulted from ring-open reaction during the photooxidation of phenanthrene/ TiO_2 were detected by GC/MS and finally phenanthrene was completely mineralized to CO_2 under that condition.

Su *et al.* (2004) studied several properties of TiO_2 prepared via the sol-gel method such as crystal structure, surface area, particle size and possible reaction site

on the surface of TiO₂ on purpose. Titanium(IV) n-butoxide was used as a titania precursor in isopropyl alcohol. The result of the variation of pH showed that, for pH<3 and /or pH>9, clear sol with nanosized TiO₂ was obtained. The XRD suggested that at a calcination temperature of 673 K only anatase phase was observed. As calcination temperature was increased to 973 K, the rutile phase became the major constituent of TiO₂. The XRD data also showed that the crystal size of TiO₂ increased from 4 to 35 nm as the temperature was increased to 973 K. Simultaneously, the BET surface area recorded a decreased from 122 to 11.5 m² g⁻¹. With regard to photodegradation of salicylic acid, the calcination temperature used in sol-gel preparation of TiO₂ samples significantly affected its photocatalytic efficiency. This may be due to the aggregation and phase transformation with increasing temperature.

Chen *et al.* (2007) aimed to study the photochemical reaction of benz[a]anthracene on TiO₂ particles. They concluded that this reaction occurred on the surface of TiO₂ particles by detecting the increasing *in situ* DRIFTS peaks at wavenumber of 2697 and 3762 cm⁻¹ belonging to surface hydroxyl characteristics. Moreover, a broad band centered at 3608 cm⁻¹ and a band at 1620 cm⁻¹ gradually decreased, indicating that adsorbed H₂O dissociated to form hydroxyl. From GC/MS results, benz[a]anthracene-7,12-dione was considered as the main photoproduct.

2. Commercial P25 TiO₂

Datye *et al.* (1995) concentrated on the examination of the P25 catalyst before and after reaction by using HRTEM. They found that Degussa-P25 was characterized by individual single crystal particles of either anatase or rutile; no coexistence of more than one phase on the individual TiO₂ particles. After reaction, P25 TiO₂ particles had no change originating from use of the photocatalyst for elimination of salicylic acid. Hence, the high photocatalytic efficiency of P25 was probably a result of its crystallinity which may result in a low density of recombination centers. Other factors such as the small size of its anatase particles and the e⁻/h⁺ separation through inter-particles electron transfer may play a significant role.

Matsumura *et al.* (2001) studied the morphology of TiO₂ (Degussa, P-25), the standard material in the photocatalytic field, which consists of 75% of anatase and 25% of rutile. The results from TEM indicated that the anatase and rutile particles separately formed their agglomerates. However, under the operational conditions of the photocatalytic reactions, the agglomerates were expected to be decomposed and the anatase particles and rutile particles were in contact. This phenomenon must be the significant key to improve the photocatalytic activity of the P-25 powders.

Yu *et al.* (2006) studied the influence of hydrothermal treatment not only on the microstructures of P25 TiO₂ powders but on the photocatalytic activity evaluated by the photooxidation of acetone as well. From the XRD result, it was found that after hydrothermal treatment for 72 h, the content of rutile reached ca. 29.6% changing 7.25% from prior to hydrothermal treatment. Therefore, it was reasonable to suggest that a small amount of anatase phase was transformed into rutile TiO₂. TEM images showed that more aggregates of TiO₂ crystallites were clearly observed after hydrothermal treatment for 10 h. The formation of more aggregates might be related to the change of surface properties of the TiO₂ crystallites. Such an assumption was confirmed by XPS which indicated that the content of hydroxyl groups on the surface of the TiO₂ powders had an obvious increase after hydrothermal treatment. Compared with the P25 precursor, the S_{BET} of the hydrothermally treated TiO₂ samples slightly decreased, while the pore volume and the average pore size increased due to the formation of more aggregates of larger TiO₂ crystallites. Moreover, the photocatalytic activity of hydrothermally treated TiO₂ was also higher than that of original P25 by a factor more than two times. This could be attributed to the formation of more hydroxyl groups on the surface of TiO₂.

3. Modified TiO₂

Ihara *et al.* (2003) studied a simple wet process for synthesis of a highly vis-active and vivid yellow-colored anatase powder that contained trace amounts of nitrogen. N-doped TiO₂ was obtained by mixing between Ti(SO₄)₂ and NH₃ under the neutral pH and by calcining at 673 K. A vis-active photocatalyst was emerged in the

crystallite size D ranging between several and about 20 nm and the highest was obtained in 13 nm. Moreover, the removal of SO_4^{2-} from the hydrolysis product that left NH_4^+ adsorbed on the Brønsted acid sites by rinsing was important. This was because the presence of SO_4^{2-} inhibited the readsorption of NH_3 on the Lewis acid sites that desorbed from the Brønsted acid sites, resulting in no reaction between the nitrogen and the catalyst. With respect to N atoms, a 2.96% concentration of N atoms for the hydrolysis products and a 0.20% concentration for the calcined samples were detected. From the results of DSC measurement and heat stability, they finally concluded that oxygen-deficient sites formed in grain boundaries were important to emerge vis-activity and nitrogen doped in the part of oxygen-deficient sites were important as a blocker for reoxidation.

Yamashita *et al.* (2003) prepared Fe ion-implanted TiO_2 photocatalysts by using the ion-implantation techniques. The results could be implied that the Fe ion-implanted TiO_2 catalysts enabled the absorption of visible light up to a wavelength of 400–600 nm. EXAFS results indicated that Fe ions existed as isolated octahedrally coordinated Fe^{3+} species substituted with lattice Ti^{4+} ions in the lattice of TiO_2 . Moreover, Fe ion-implanted TiO_2 catalysts successfully enabled photocatalytic reaction of 2-propanol diluted in the liquid-phase systems. The photocatalytic reactivity under visible light increased, as increasing the amount of Fe ions implanted. However, after reaching the maximum reactivity, the photocatalytic reactivity decreased by further implantation of Fe ions. This suggested that the photoreactivity of Fe ion-implanted TiO_2 depended upon the amounts of Fe ions implanted.

Sano *et al.* (2004) developed a new preparation method of N-doped TiO_2 using a Ti^{4+} –bipyridine complex precursor. From the UV-Vis/DR, it could be implied that the further absorption by the as-prepared catalyst is explicable by assuming simultaneous incorporation of N and C atoms originating from bipyridine into the anatase lattice. The XRD results suggested that small crystallites of anatase were formed during the calcination at 573 K and that the crystallinity of the anatase phase increased during the heat treatment at 653 K. The crystallite sizes of the photocatalysts were determined to be 7.7–8.7 nm from the half width of the 101 peak

by using the Scherrer's formula. Moreover, the co-existence of N and C atoms in the anatase lattice shrank the distance between ions coordinated along the c-axis direction. The XPS spectra also showed the coexistence of N 1s and C 1s peaks at binding energy of 396 and 400 eV for N species and 283-289 eV for C species. The photocatalyst exhibited high photocatalytic activity for NO oxidation under visible light. It seems to be due to the high absorbance of visible light with long wavelengths and large relative surface area. Since NO_2 and NO_3^- were formed from NO, it was inferred that the active oxygen species were formed on the photocatalyst by visible light illumination.

Yin *et al.* (2004) prepared N-doped TiO_2 with different phases such as anatase, brookite and rutile, by a solvothermal process in TiCl_3 -hexamethylene tetramine (HMT)-alcohol solution. They found from the XRD results that anatase would formed in the existence of methanol while mixture phases between rutile and brookite was detected in the ethanol system. All prepared powders possessed well-crystallized nanocrystals with yellowish or beige color, certifying the formation of nitrogen doping. Evidently, nitrogen doping resulted in the formation of N 2p band locating above O 2p valence band in TiO_2 , which caused the observable second edge absorption around 520-535 nm in the UV-Vis/DR spectra. Besides, the XPS result supported the presence of Ti-N binding at 396 eV even though the peak intensity was not so strong. The N-doped TiO_2 anatase with high specific surface area of $201 \text{ m}^2/\text{g}$ could continuously destruct 39% and 83% of nitrogen monoxide under irradiation of light of wavelength $> 510 \text{ nm}$ and $> 290 \text{ nm}$, respectively. The visible light photocatalytic ability was more than 5 times higher than that of commercial P25 TiO_2 .

Fernandes *et al.* (2005) demonstrated a simple route for synthesis of nano-crystalline N-doped titania by calcination of acidified TiCl_3 in presence of urea and oxalic acid. While urea was used as a source of nitrogen, oxalic acid was found to be crucial in controlling the phase, porosity as well as the nitrogen content. XRD results indicated that the additional use of oxalic acid could retard phase transition from anatase to rutile, compared to the absence of oxalic acid adding. Moreover, both the surface area and porosity increased when oxalic acid was used. However, they found

that oxalic acid prevented nitrogen doping, which could be seen from the XPS and UV-Vis/DR results. Meanwhile, N-doped TiO₂ was occurred in case of the absence of oxalic acid but this sample had almost rutile structure. Concerning the photocatalytic activity in sunlight, both of these catalysts were able to completely degrade methylene blue in less than 120 minutes. In comparison, the commercial rutile TiO₂ was inactive.

Morawski *et al.* (2005) obtained the N-doped TiO₂ via direct heat treatment of TiO₂.xH₂O at temperatures of 373-1073 K under an ammonia atmosphere. The UV-Vis/DR spectra of N-doped TiO₂ catalysts showed an additional absorption edge in the visible region ($\lambda \approx 470$ nm; $E_g \approx 2.64$ eV) at temperature higher than 673 K. On the basis of XRD analysis it could be supposed that N-doping did not have an effect on the anatase-to-rutile phase transformation. The photoactivity of the modified catalysts was determined on the basis of decomposition rate of phenol and azo-dye (Reactive Red 198) under visible light. The most photoactive catalysts for the degradation of azo-dye were those calcined at 773 and 873 K (ca. 40-45%) while phenol decomposition was obtained in case of catalyst calcined at 973 K (6.55%). These might result from different mechanisms of photodegradation for the compounds.

Nosaka *et al.* (2005) tried several nitrogen-source organic compounds to prepare N-doped TiO₂ for comparison. They used commercially available TiO₂ powder mixed with organic nitrogen compounds such as urea, guanidine hydrochloride and guanidine carbonate. Guanidine carbonate is more efficient than guanidine hydrochloride and urea to prepare N-doped TiO₂ powders. The XPS result indicated that N atoms were incorporated into two different sites of the bulk phase of TiO₂ and both contributed the visible light absorbance. The intensity of XPS signal at 396 eV assigned to Ti-N, which was substituted N atom for the O site in TiO₂, correlated with the photocatalytic activity with visible light. Meanwhile, the intensity of another XPS peak at about 400 eV assigned to N-O had a negative correlation with the visible light photocatalytic activity. Regarding the photocatalytic activity for decomposition of 2-propanol in aqueous solution under visible light, it increased with

the decreased of doped N atoms in O site, while decreased with decrease of the other sites.

Sato *et al.* (2005) used the wet method to prepare N-doped TiO₂ by mixing between titanium(IV) tetraisopropoxide or TiCl₄ and ammonia solution at low temperature (273 K). The reflect spectrum of pale yellow doped sample shifted to shorter wavelength than that of anatase TiO₂ probably due to a size quantization effect. Each doped sample showed more weight loss than did a pure sample during calcination because of the desorption of ammonia. From the XPS result, it was evident that N-doped TiO₂ was less than 1.3 at.% and was not bound directly to Ti. The quantum yield for the CO photooxidation on the N-doped TiO₂ in the visible region was less than that in UV region. These results implied that the N doping by the wet method was similar to impurity doping.

Cheng *et al.* (2006) made use of a simple mechanochemical reaction for preparing TiO_{2-x}N_x. Anatase titania powder was milled in gaseous NH₃ and air. The XRD result implied that the transformation from anatase to srilankite and rutile in NH₃ was greatly delayed when titania was milled in NH₃ atmosphere compared to that in air. The interaction between fresh surfaces and NH₃ adsorbed on the surface played an important role in delaying the phase transformation. XPS spectra showed that an obvious peak at near 396 eV attributed to the formation of Ti-N bonds was observed for the samples milled in NH₃ but no similar peak appeared for the samples milled in air. UV-Vis/DR showed two absorption edges at 405-409 nm (3.03-3.06 eV) and 515-530 nm (2.34-2.41 eV) of the samples milled in NH₃ while only one edge at 410-425 nm (3.02-2.92 eV) belonged to the samples milled in air. The first and second edges are attributed to the band structure of original TiO₂ and the newly formed N p band which is located above the O 2p valence band. Besides, NH₃ had apparently effect on increasing surface area due to steric hindrance and two hours seemed to be the optimal time to obtain high surface area titania.

Khan *et al.* (2006) focused on the wet process synthesis of carbon-modified (CM)-*n*-TiO₂ nanoparticles and their photocatalytic activities. CM-*n*-TiO₂ was

prepared by hydrolysis of TiCl_4 with tetrabutylammonium hydroxide or with the sodium hydroxide in the presence of glucose as the carbon source. The XRD results demonstrated that the CM- $n\text{-TiO}_2$ nanoparticles were of anatase structure with low crystallinity and the average grain sizes were found to be 6 and 4 nm for CM- $n\text{-TiO}_2$ prepared with tetrabutylammonium hydroxide and glucose, respectively, as carbon sources. Extended aging and subsequent calcination of $n\text{-TiO}_2$ in the presence of tetrabutylammonium species or glucose contributed to the incorporation of carbon into $n\text{-TiO}_2$ lattice. These photocatalyst nanoparticles absorbed well into the visible to near infrared region up to 800 nm and exhibited enhanced photocatalytic activity for the degradation of 4-chlorophenol under visible light illumination. With glucose as a carbon source, CM- $n\text{-TiO}_2$ generated 13-fold increase in the initial rate of photodegradation compared to that by regular $n\text{-TiO}_2$. Meanwhile, CM- $n\text{-TiO}_2$ increased only 8-fold when tetrabutylammonium hydroxide was used as the carbon source.

Lee *et al.* (2006) prepared $\text{TiO}_{2-x}\text{N}_x$ by hydrolytic synthesis method (HSM) using TiCl_3 and ammonium hydroxide and calcined at 673 K. This work focused on kinetics and crystallization behaviors of $\text{TiO}_{2-x}\text{N}_x$ formation in N-doped amorphous TiO_2 powders. The XRD result suggested that corresponding crystalline phase were obtained by thermally induced transformation of these amorphous powders. From FT-IR and XPS results, it was concluded that a complex containing titanium and ammonia was formed in the precipitate stage while calcination drove weakly adsorbed ammonium species off the surface, decomposed ammonia bound on the surface of precipitated powder and led to substitution of nitrogen atom into the lattice of TiO_2 during the crystallization. The TEM image of $\text{TiO}_{2-x}\text{N}_x$ showed nanoparticles with an irregular spherical shape and a particle size of 20 nm. Moreover, UV-Vis/DR of TiO_2 anatase showed a single sharp edge, whilst $\text{TiO}_{2-x}\text{N}_x$ provided two absorption edges; the main edge due to the oxide at 390 nm and a weak shoulder due to nitrogen doping at 451 nm. This shoulder peak was responsible for the visible light catalytic activity. The activation energies required for the grain growth and phase transformation of $\text{TiO}_{2-x}\text{N}_x$ were determined to be 1.6 kJ/mol and 129.3 kJ/mol, respectively.

Shouxin *et al.* (2006) synthesized N-doped TiO₂ using TiCl₄ mixed with (NH₄)₂SO₄ under acid condition and calcined at 773 K. They found the formation of new Ti-O-N bonds on TiO₂, which was identified by FT-IR at 1060 cm⁻¹. The red shift of the absorption edge to the visible region was also observed due to the effect of the substitution oxygen by nitrogen in metal oxide structures. Moreover, they stated that nitrogen doping inhibited the phase transformation of TiO₂ and reduced crystal agglomeration. The TON photocatalysts exhibited higher activity to degrade phenol under visible light, compared to unmodified TiO₂ and P25 TiO₂. This suggested that the nitrogen doping could extend the absorption edge to the visible region and improve the photocatalytic activity of TiO₂ under visible irradiation.

Fornasiero *et al.* (2007) studied the sol-gel preparation, characterization and photocatalytic applications of TiO₂ nanopowders doped with boron, nitrogen or both species compared to undoped TiO₂. Moreover, the effect of dopants on the titania structure and texture was also studied. The obtained results indicated that N-doping did not appreciably modify the TiO₂ structure whereas B incorporation resulted in lower crystallite dimensions, a higher surface area as well as facilitation of the anatase-to-rutile transformation. A remarkable reactivity improvement with respect to pure TiO₂ was observed only in the co-doped systems while N- or B-doped TiO₂ had less photocatalytic activities compared to TiO₂. Moreover, a rational interpretation of the observed behavior was attempted by calculation based on the density functional theory (DFT). They concluded that the presence of B in molar excess with respect to N generated reactive Ti(III) sites, which might induced the formation of reactive superoxide species.

Viswanath *et al.* (2007) studied the preparation of N-doped TiO₂ via the sol-gel method by mixing between titanium isopropoxide and melamine in hot water-ethanol solution and then calcining at different temperatures. The UV-Vis/DR revealed that the N-doped TiO₂ showed the light absorption onset in the visible region. The extent of light absorption depended on the content of nitrogen in the samples, which decreased with increasing the calcination temperature. The SEM and TEM images illustrated a mixture of spherical-shaped and flake like particles with the

average size of 25-50 nm. The XRD patterns of N-doped TiO₂ confirmed the presence of crystalline anatase TiO₂ nanoparticles below 773 K. At temperature above 773 K, the less photoactive rutile crystalline phase started appearing along with the anatase phase. The XPS results indicated that the N existed as an anion, like in the doped samples and possibly the doped N occupied the oxygen position in the TiO₂ lattice. With regard to visible photocatalytic activity, N-doped TiO₂ was able to degrade methylene blue for 40% decomposition.

Huang *et al.* (2008) prepared N-doped TiO₂ via a modified sol-gel hydrothermal method by using tetrabutyl titanate as the precursor and calcined at 593 K. Clear evidence for the mixed crystal lattice structure of TiO₂ was obtained from XRD analysis. The average particle size was 13.5 nm and the narrow particle size distribution was present. UV-Vis spectra depicted the strong visible-light absorption of N-doped TiO₂, which continued above 550 nm. The FT-IR spectra revealed that Ti-O, N-H, TiO-H, H-O-H and Ti-NO_x groups existed in the as-prepared sample and the forming of -Ti-NO_x (-Ti-O-N-Ti-) might indicate that N atoms were incorporated into the TiO₂ crystal lattice, which was consistent with XPS results. The thermal analysis suggested that nitrogen atoms doped in TiO₂ could prevent phase transformation of anatase to rutile, because as far as pure TiO₂ was concerned, most TiO₂ particles were transformed into rutile at 973 K. From, all of these properties the N-doped TiO₂ (A/R = 4:1) mixed crystal sample showed the high visible-light response photocatalytic activity which was attributive to a synergistic effect among its surface acidity, effect of mixed crystal and N atoms doping. The decrease of acidic surface enhanced the adsorption of cationic organic compounds. The doping N atoms improved the visible-light absorption and the effect of mixed crystal could result in several beneficial effects upon the photocatalytic activity.

Ksibi *et al.* (2008) focused on the sol-gel preparation of N- and/or S-doped TiO₂ using a titanium(IV) (diisopropoxide)bis(2,4-pentadionate) precursor and different nitrogen and sulfur sources. The TGA-DTA data showed the weight loss in the range of 40-60%. The XRD patterns of the N- and/or S-doped TiO₂ samples revealed anatase as the predominant homogeneous crystalline phase. The absorption

profile of doped TiO_2 compared to P25 TiO_2 shifted toward visible regions (400-500 nm), originating from band gap narrowing of doped TiO_2 . Photocatalytic activities of titania powders determined by discoloration of Congo red dye were enhanced by the effect of N and/or S doping compared to pure TiO_2 under visible light. In particular, S-doped TiO_2 showed the highest activity among the doped TiO_2 because the crystallinity of anatase was improved upon S-doping. Moreover, sulfur atoms prevented phase transition from anatase to rutile.

Palgrave *et al.* (2008) applied high resolution XPS to study the electronic structure of N-doped TiO_2 prepared by annealing single crystal rutile (110) substrates in NH_3 at high temperature. The results showed that treatment by ammonia at 873 K led to the incorporation of N 2p states at the top of the valence band without concomitant reduction of Ti^{4+} to Ti^{3+} . In case of annealing at 973 K, the introduction of N 2p states was also occurred at the same position but it led to the surface reduction. This doping brought about band gap narrowing in valence region photoemission spectra.

MATERIALS AND METHODS

Materials

Reagents

1. Titanium(IV) bis(ethyl acetoacetato)diisopropoxide ($C_{18}H_{34}O_8Ti$, Lab. Grade, Aldrich, St. Louis, USA)
2. Titanium(IV) tetra-n-butoxide ($C_{16}H_{36}O_4Ti$, Lab. Grade, Merck, Hohenbrunn, Germany)
3. Titanium(IV) tetraisopropoxide ($C_{12}H_{28}O_4Ti$, Lab. Grade, ACROS, New Jersey, USA)
4. Titanium(IV) chlorine ($TiCl_4$, Lab. Grade, Merck, Hohenbrunn, Germany)
5. Ammonia solution (NH_3 , 25%, AR. Grade, Merck, Danmstadt, Germany)
6. Hydrazine hydrate ($N_2H_4 \cdot H_2O$, 98%, AR. Grade, Carlo Erba, Val de Reuil, France)
7. Ammonium chloride (NH_4Cl , AR. Grade, Ajax Finechem, Auckland, New Zealand)
8. Urea ($(NH_2)_2CO$, AR. Grade, BDH, Poole, England)
9. Methanol (CH_3OH , AR. Grade, BDH, Poole, England)
10. Hexane (C_6H_{14} , AR. Grade, Fisher, New Jersey, USA)
11. Sodium sulfate (Na_2SO_4 , AR. Grade, Merck, Hohenbrunn, Germany)
12. Phenanthrene ($C_{14}H_{10}$, HPLC Grade, Fluka, Buchs, Switzerland)
13. Benz[a]anthracene ($C_{18}H_{12}$, Lab. Grade, Fluka, Buchs, Switzerland)
14. Phenol (C_6H_5OH , AR. Grade, Carlo Erba, Van de Reuil, France)

Methods

1. Catalyst preparation

Photocatalysts, N-doped TiO_2 , were prepared by the sol-gel method. Initially, 5.00 ml of 25% ammonia solution as a nitrogen source was continually added into 10.00 ml titanium(IV) bis(ethyl acetoacetato)diisopropoxide as a titania precursor under the constantly stirring rate (400 rpm) at 303 K. In the first ten minutes of the addition, the rapid hydrolysis and condensation reactions caused more condensed solution, like colloids. This system was held for an hour at 303 K. Subsequently, yellow gel powder was obtained and then dried at 393 K in the oven for an hour to evaporate the remaining ammonia solution and some organic by-products generating from the hydrolysis reaction. Finally, as-prepared N-doped TiO_2 was calcined in the muffle furnace at various temperatures (573 K – 973 K) for an hour to bring about a thermal decomposition, phase transition and removal of a volatile fraction. The color of N-doped TiO_2 much more varied depending upon the calcination temperature.

1.1 Effect of titania precursors

The variation of different kinds of titania precursors (listed below) was studied. 10.00 ml of a titania precursor was used to prepare N-doped TiO_2 via the sol-gel method and 5.00 ml ammonia solution was specifically selected as a nitrogen source.

- a) Titanium(IV) bis(ethyl acetoacetato)diisopropoxide
- b) Titanium(IV) tetra-n-butoxide
- c) Titanium(IV) tetraisopropoxide
- d) Titanium(IV) tetrachloride

In case of TiCl_4 , however, it was difficult to handle at room temperature because TiCl_4 can easily react with water as well as water vapor in the atmosphere and it then causes white smoke. This showed that its hydrolysis reaction was out of

control under ambient condition. Therefore, this titania precursor was not suitable for synthesizing N-doped TiO₂ in this work.

1.2 Effect of nitrogen sources

N-doped TiO₂ was prepared with various types of nitrogen sources based on the mole equality of nitrogen (as shown in Table 4) and the selected 10.00 ml titanium(IV) bis(ethyl acetoacetato)diisopropoxide precursor. The sol-gel method was used as previously mentioned but the calcination step was held at 673 K for an hour.

Table 4 Different nitrogen sources which were employed with their concentrations, volumes and the mole equality of nitrogen.

Nitrogen source	Chemical formula	Volume (ml)	Concentration (M)	The amount of nitrogen (mol)
Ammonia	NH ₃	5	13.38	0.067
Hydrazine hydrate	N ₂ H ₄ .H ₂ O	5	6.70	0.067
Ammonium chloride	NH ₄ Cl	10	6.70	0.067
Urea	(NH ₂) ₂ CO	5	6.70	0.067

With regard to the preparation of each nitrogen source, 25% (13.38 M) NH₃ solution was used directly without dilution. 98% (20.16 M) N₂H₄.H₂O needed diluting with distilled water into 6.70 M, which was a half of NH₃ concentration since N₂H₄.H₂O consists of two moles of nitrogen per one molecular formula. 3.58 g NH₄Cl was dissolved by distilled water and made up the volume to 10.00 ml in order to obtain 6.70 M NH₄Cl solution. Finally, 4.02 g (NH₂)₂CO was also dissolved in distilled water and made up the volume to 10.00 ml, leading to 6.70 M urea solution.

2. Catalyst characterization

2.1 Thermal Gravimetric Analysis (TGA)

The range of calcination temperature of as-prepared catalysts was obtained from a TGA 7 Perkin Elmer analyzer. 4.000-5.000 mg of a reference material, Al_2O_3 , was loaded to protect the damaging effect of samples on an alumina pan when temperature was increased up to 1073 K. This weight was set as zero and then about 10.000 mg of the powdered sample was added into the pan. The temperature program was set up from 273 K to 1073 K with the rate of 10 K/min under nitrogen purge.

2.2 X-ray Diffraction (XRD)

2.2.1 Determination of the crystalline phase

The crystalline phase was obtained by a Philips Pw 1830 X-ray diffractometer (XRD) operated at 40 kV and 35 mA and a Philips X' Pert X-ray diffractometer operated at 40 kV and 30 mA, both of which used $\text{Cu K}\alpha$ radiation source at λ of 1.54 Å. XRD data were collected from 2θ of 20-60 degree. Each of the crushed samples was either coated on the inverse side of cello tape and made its surface smooth by pressing with a spatula or spread on a small piece of glass and pressed with another smooth-surfaced glass. The crystalline phase of all samples was identified by comparison with the Joint Committee on Powder Diffraction Standards (JCPDS) files.

2.2.2 Determination of the crystallite size

The crystallite size was also calculated applying the Sherrer's equation as shown in equation 1 (Patterson *et al.*, 1939).

$$d = \frac{k\lambda}{\beta \cos\theta_B} \quad \dots\dots(1)$$

where d is the crystallite size (nm)

k is the constant whose value is approximately 0.9

λ is the wavelength of the X-ray radiation source (0.154 nm for Cu K α)

β is the full width at half maximum intensity (FWHM) (radians)

θ_B is the Bragg angle at the position of the peak maximum

The example of the calculation is shown in the Appendix A.

2.2.3 Determination of the content of anatase

The content of anatase was also calculated applying Spurr-Myers equation as shown in equation 2 (Spurr *et al.*, 1957).

$$w_A = \frac{1}{(1 + 1.26 \frac{I_R}{I_A})} \quad \dots(2)$$

where w_A is the weight fraction of anatase in the mixture

I_R is the intensity of the diffraction peak of rutile

I_A is the intensity of the diffraction peak of anatase

The example of the calculation is shown in the Appendix A.

2.2.4 Determination of the unit cell volume

The unit cell volume was calculated from the product among three lattice parameters (a , b and c), which can be equated for the tetragonal system ($a \neq b = c$) as follows;

$$\frac{1}{d^2} = \frac{h^2 + k^2}{a^2} + \frac{l^2}{c^2} \quad \dots(3)$$

where d is a lattice spacing between the planes in the atomic lattice

h , k and l are the Miller indices

a , b and c are the lattice parameters

The example of the calculation is shown in the Appendix A.

2.3 Scanning Electron Microscopy (SEM)

The morphology of all N-doped TiO_2 catalysts was determined by SEM recorded on a JEOL JSM-5600Lv scanning electron microscope fitted with tungsten filament. Each of the powdered samples was spread on a carbon tape mounted on a SEM stub and needed to be coated with Pt/Pd particles prior to SEM operation.

2.4 Transmission Electron Microscopy (TEM)

The morphology and particle size of all catalysts were investigated by TEM recorded on a JEOL 1200 EX electron microscope fitted with a standard tungsten filament and operated at 80 keV. Images were recorded digitally using a Mega View II digital camera with Soft Imaging System GmbH analysis 3.0 image analysis software and/or on KODAK Electron Image Film SO-163. Samples diluted in ethanol solution were deposited onto Formvar-coated, carbon-reinforced, 3-mm-diameter copper electron microscope grids and left to air-dry prior to analysis.

2.5 Raman Spectroscopy

The Raman shifts of N-doped TiO_2 and P-25 TiO_2 were performed on a Renishaw Raman Imaging Microscope operated with green laser. Si plate was used to calibrate Raman, which exhibited the evident Raman shift at 520 cm^{-1} . Each of the finely-ground samples was deposited on a glass and a little acetone solution was dropped in order to make the sample tightly attach each other and be easy to smooth its surface with a spatula.

2.6 X-ray Photoelectron Spectroscopy (XPS)

The XPS technique was carried out at the Siam Photon Laboratory using a VG Scientific concentric hemispherical analyzer with an Al K α (1486.68 eV) radiation source. All samples were pressed on carbon tapes mounted on a molybdenum plate. Then they were placed on a holder in vacuum system at 10^{-4} torr using a rotary pump and a turbo pump. After that, pressure was still decreased into 10^{-8} torr using an ion pump. Eventually, the sample holder was transferred into the analysis chamber. XPS was used to detect not only the nitrogen species that was incorporated into the TiO₂ lattice in terms of substitution and interstitial but other species, such as Ti, O, C, were also analyzed at different binding energies. Peak marking and curve fitting of all elements were performed on the Advantage Program.

2.7 Elemental Analysis (EA)

The nitrogen and carbon contents were carried out on LECO CHNS-932 Elemental Analyzer. Before operating, a blank sample of which the weight was set up at 2.000 mg needed to be run for many times until the percentages of C, H, N and S were constant. About 2.000 mg standard reference, sulfamethazine, was also necessary to be operated in order to check the instrumental accuracy which shows that the percentages of C, H, N and S should be congruent with the standard values, that is, C of 51.78%, H of 5.07%, N of 20.13% and S of 11.52%. Then set blank again for one time before three-replicated samples weighted in tin capsules about 2.000 mg in each replica were run.

2.8 Diffuse Reflectance UV-Vis Spectrophotometry

Diffuse reflectance UV-Vis spectra from 200 nm to 700 nm of all catalysts with slit width of 2 nm were collected on a Perkin Elmer Lambda 650 spectrophotometer. The powdered sample was mounted on a glass by using acetone to help the sample adhere to the glass plate during running time. Then, the sample was pressed by a spatula to have a smooth surface and moved into the analysis chamber.

3. Quantum chemical calculations

To optimize molecular structures and calculate the total energy, bond length and bond angle of studied compounds, quantum chemical calculations were performed using Gaussian 03 program on a PC Intel Pentium 4, 1.8 GHz, RAM 1 GB, Hard Disk 80 GB.

4. Inventive photoreactor

The photodegradation reaction of PAHs/phenol was studied by using an inventive photoreactor (Figure 8). 90/100W of the Xe lamp as a light source has been fitted, which can be selected to operate 90W, 100W or 190W per one lamp. The current adaptor has necessarily been used for the adjustment of AC 220V to DC 12V. Inside the reactor; it contained a set of magnetic stirrer, including a 400 ml foil-covered beaker equipped with a HOYA UV 385 cutoff filter. Besides, this reactor can control the inside temperature in 303 K during 9 hours of the reaction.

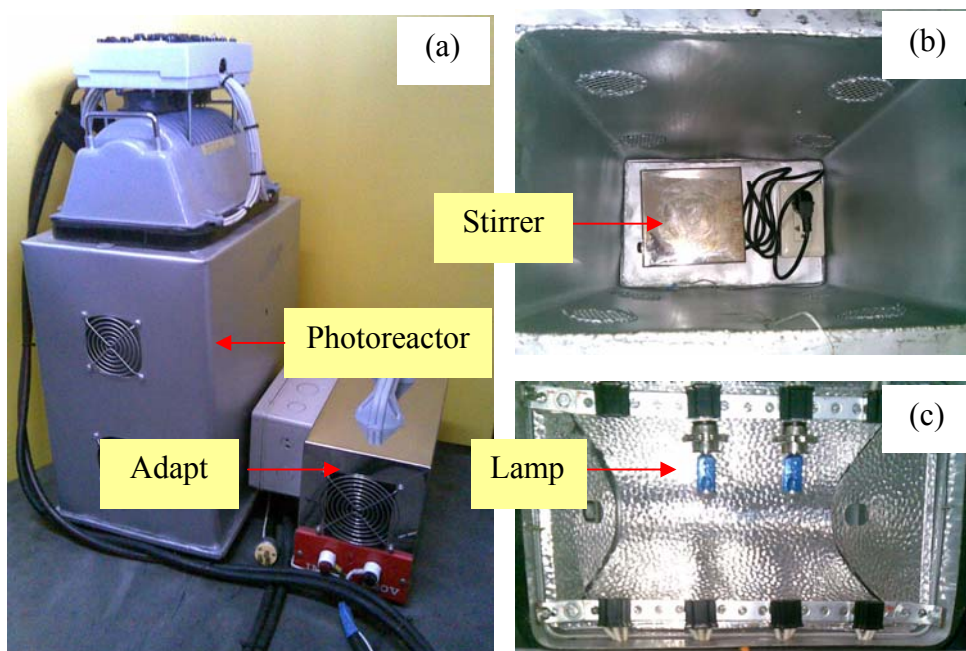


Figure 8 The graphic picture of the inventive photoreactor; (a) the photoreactor set, (b) the stirrer set and (c) the lamp set.

5. Preparation of PAHs/phenol solution for photodegradation reaction

5.1 Preparation of phenanthrene solution

25.00 ml of 1000 ppm stock phenanthrene solution was prepared by weighing 0.0250 g standard phenanthrene and then it was dissolved in pure methanol solvent with a certain volume in a 25 ml volumetric flask.

10.00 ml of 1000 ppm phenanthrene solution was measured out and diluted into 500.00 ml of 20 ppm with distilled water and methanol in the volumetric ratio of 3:1. Concomitantly, the solution was sonicated in water bath in order to enhance the solubility of phenanthrene and the homogeneity of solution.

5.2 Preparation of benz[a]anthracene solution

25.00 ml of 1000 ppm stock benz[a]anthracene solution in pure methanol solvent was prepared by dissolving 0.0250 g standard benz[a]anthracene with a certain volume in a 25 ml volumetric flask.

500.00 ml of 20 ppm benz[a]anthracene solution was prepared by diluting 10.00 ml of stock benz[a]anthracene solution with distilled water and methanol in the volumetric ratio of 1:3. Concurrently, benz[a]anthracene solution was also sonicated, which was similar in case of preparation of phenanthrene solution.

5.3 Preparation of phenol solution

25.00 ml of 1000 ppm stock phenol solution in distilled water solvent was prepared by dissolving 0.0250 g standard phenol with a certain volume in a 25 ml volumetric flask.

500.00 ml of 20 ppm phenol solution was prepared by diluting 10.00 ml of stock phenol solution with distilled water. Simultaneously, phenol solution was also sonicated, which was similar in case of preparation of phenanthrene solution.

6. Preparation of PAHs/phenol solution for linear calibration curves

6.1 The calibration curve of phenanthrene solution

Firstly, the series of phenanthrene concentrations, 2, 4, 6, 8 and 10 ppm, were prepared by diluting from 20 ppm of phenanthrene solution (as prepared in section 5.1) with the volume of 1.00, 2.00, 3.00, 4.00 and 5.00 ml, respectively. Secondly, diluted solution was made up the volume to 10 ml by distilled water and, finally, it was ready to measure the absorption using a Perkin Elmer Lambda 35 UV-Vis spectrophotometer.

6.2 The calibration curve of benz[a]anthracene solution

Initially, the series of benz[a]anthracene concentrations, 1, 2, 3, 4 and 5 ppm, were prepared by diluting from 20 ppm of benz[a]anthracene solution (as prepared in section 5.2) with the volume of 0.50, 1.00, 1.50, 2.00 and 2.50 ml, respectively. After that, diluted solution was made up the volume to 10 ml by distilled water and, finally, it was ready to measure fluorescence emission using a Perkin Elmer Lambda 35 luminescence spectrophotometer.

6.3 The calibration curve of phenol solution

At the beginning, the series of phenol concentrations, 5, 10, 15 and 20 ppm, were prepared by diluting from 20 ppm of phenol solution (as prepared in section 5.3) with the volume of 2.50, 5.00, 7.50 and 10.00 ml, respectively. Then, diluted solution was made up the volume to 10 ml by distilled water except the last phenol concentration. Finally, it was ready to measure the absorption using a Perkin Elmer Lambda 35 UV-Vis spectrophotometer.

7. Photocatalytic study

The general procedure used to study the photocatalytic activity of each photocatalyst is as follows;

Initially, 125.00 ml of 20 ppm PAHs/phenol divided from 500 ml of 20 ppm PAHs/phenol was poured into a 400 ml foil-covered beaker equipped with a UV cutoff filter. Then 0.1000 g (0.8000 g/l) of the photocatalyst was added. The degradation reaction was operated under dark reaction for an hour and then under artificial light reaction with 190 W of the Xe-lamp. The dark reaction was done in order to make the system reach the equilibrium point before degradation. In this condition, solution was stirred under the constant temperature (303 K) in the photoreactor during the period of degradation.

To follow the reaction, sampling by hypodermic syringes was used to measure the amount of initial (before adding the photocatalyst) and remaining concentration of PAHs/phenol in each period of time. Before samples were picked up, the stirrer was switched off by 15 min in order to abate the suspension of the catalyst in solution. All of collected samples were left overnight in dark and then centrifuged about 30 min to reduce the distribution of the fine-powdered catalyst again. After that, the centrifugate was transferred using a dropper into a vial. Finally, all samples were diluted with distilled water at a certain volume and their concentrations were measured with an appropriate technique as will be discussed below.

7.1 Photodegradation of phenanthrene

Based on the general procedure, the period of time for phenanthrene photodegradation was set on nine hours consisting of one hour in dark reaction and eight hours in photoreaction. The sample collection was handled initially before adding the catalyst and after mixing with the catalyst in every hour. 3 ml of a sample were pipetted from the centrifuged sample and made up the volume by distilled water in a 10 ml volumetric flask. The photocatalytic activity was determined by measuring

the reduction of phenanthrene concentration in terms of UV absorption at wavelength of 251 nm. In case of phenanthrene, besides, the measuring of its concentration, some intermediate products originating from degradation of phenanthrene were also investigated by GC/MS. All samples were conducted in three replicates.

7.2 Photodegradation of benz[a]anthracene

Five hours consisting of one hour in dark reaction and four hours in photoreaction were set up for benz[a]anthracene degradation. Under the photoreaction, the sample was collected every 30 min until 90 min of degradation. After that, the sample was continually collected every hour. All of samples were taken by passing the general process as mentioned above. Then, only 1 ml of a sample was picked up using an autopipette from the centrifuged sample and made up the volume by distilled water in a 10 ml volumetric flask. Fluorescent measurement at λ_{em} of 527 nm was applied to detect the concentration of each sample. All samples were also conducted in three replicates.

7.3 Photodegradation of phenol

Photodegradation of phenol was studied under eight hours after one hour in dark reaction. The sample was collected in every hour. After all samples were left overnight and centrifuged, the centrifugate parts of all samples were separated by using a dropper. After that, their concentrations were measured directly without dilution, using the UV-Vis spectrophotometer at λ_{max} of 271 nm. All samples were conducted in three replicates.

8. Concentration measurement of PAHs, phenol and intermediate products from degradation

8.1 UV-vis Spectrophotometry

The decreasing concentration of phenanthrene or phenol was followed by measuring the absorption on a Perkin Elmer Lambda 35 spectrophotometer operated from 500 nm to 200 nm with slit width 2 nm. Distilled water was considered as a blank setup.

8.2 Luminescence Spectrophotometry

The decreasing concentration of reactants namely benz[a]anthracene was followed by measuring the absorption on a Perkin Elmer Lambda 35 spectrophotometer. To get an obvious spectrum, emission slit width or excitation slit width should be also adjusted to find the appropriate condition. Eventually, for benz[a]anthracene, the optimized condition was λ_{ex} at 287.0 nm, excitation slit width of 10.0 nm and emission slit width of 2.5 nm with scan speed of 1000 nm/min.

8.3 Gas Chromatography/Mass Spectrometry (GC/MS)

Some intermediate products from photodegradation reaction were analyzed by using a gas chromatograph HP 5890 series II (column HP-5MS; 30 m x 0.25 mm (i.d.), film thickness 0.25 μm) with a mass spectrometric detector HP 5989B. The optimized GC condition was set up by initial temperature of 373 K with rate of 15 K/min, final temperature of 573 K and solvent delay time of 5 min. The optimized MS condition was at mass range of 50-390, source temperature of 473 K and quadrupole temperature of 373 K. All centrifuged samples were extracted with 5 ml of hexane in a separating funnel for two times and the upper part of solution was kept into a vial. A little amount of Na_2SO_4 as a desiccant was added to the vial in order to eliminate water molecule that has a severe effect on HP5 column. 2 μl of each extracted sample was injected into GC/MS with the splitless mode.

RESULTS AND DISCUSSION

1. Catalyst characterization

1.1 Effect of titania precursors

1.1.1 Thermal Gravimetric Analysis (TGA)

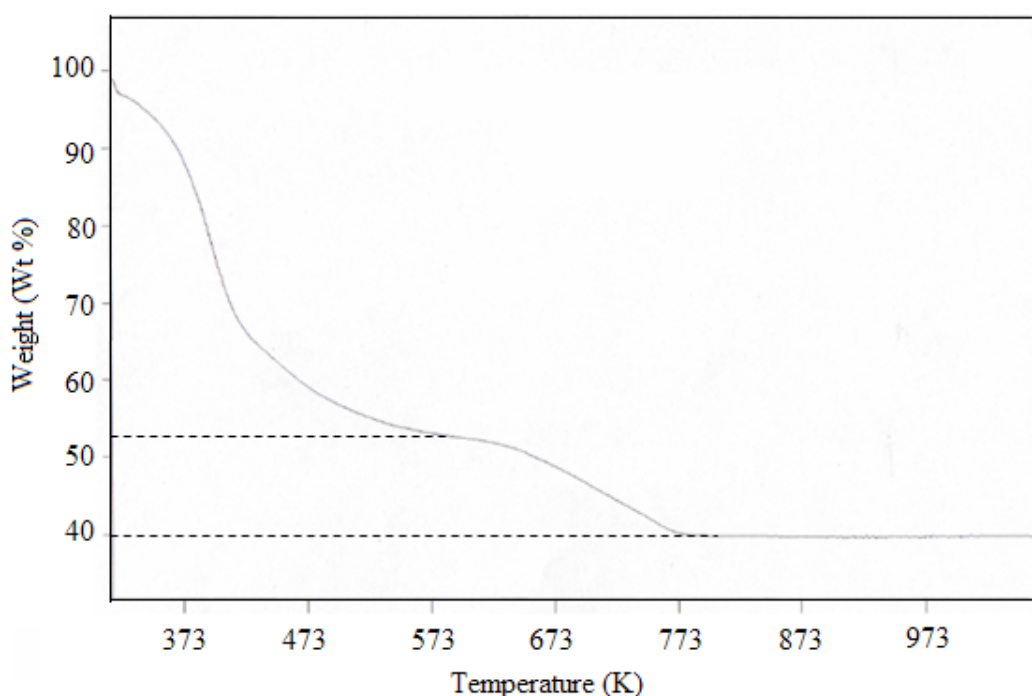


Figure 9 The TG curve of as-prepared N-doped TiO_2 using titanium(IV) bis(ethyl acetoacetato)diisopropoxide as a titania precursor.

The TG curve (Figure 9) of the as-prepared N-doped TiO_2 using titanium(IV) bis(ethyl acetoacetato)diisopropoxide after dried at 393 K presents two main stages of weight loss. The first weight loss of 48% at 573 K was presumably ascribed to the removal of weakly-adsorbed water molecules (H_2O), nitrogen species (NH_3) as well as organic molecules. The second weight loss of 12% at 773 K resulted from the removal of tightly-entrapped organic residuals or nitrogen species.

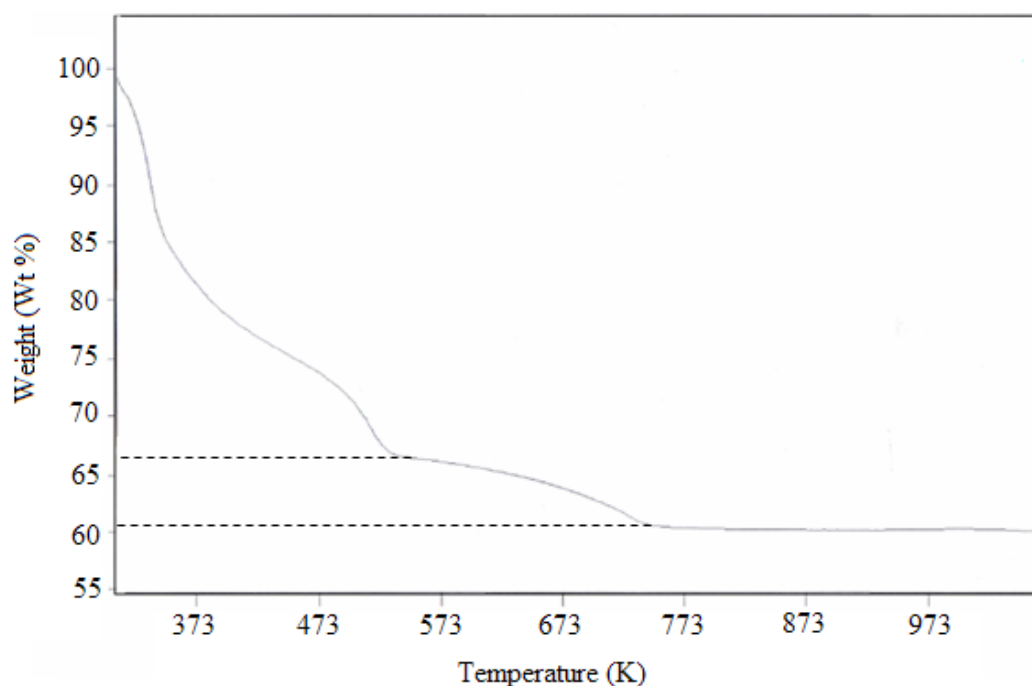


Figure 10 The TG curve of as-prepared N-doped TiO_2 using titanium(IV) tetra-n-butoxide as a titania precursor.

The TG curve (Figure 10) of the as-prepared N-doped TiO_2 using titanium(IV) tetra-n-butoxide after dried at 393 K also illustrates two significant stages of weight loss. First, 33% weight loss at 573 K was attributed to the elimination of loosely-adsorbed species on the surface of as-prepared N-doped TiO_2 such as H_2O , NH_3 and organic molecules resulting from the hydrolysis reaction. Second, about 6% weight loss at 773 K indicates that a small number of organic contents, including nitrogen species, were still entrapped in the N-doped TiO_2 structure.

Both TG curves of as-prepared N-doped TiO_2 show that at high temperature (>573 K) there were still weight loss observed at the high extent. This suggests that both titania precursors were hydrolyzed incompletely during preparation process therefore they needed to be eliminated at higher temperature. The evidence that supported this idea will be shown in the Elemental Analysis results which will be discussed later.

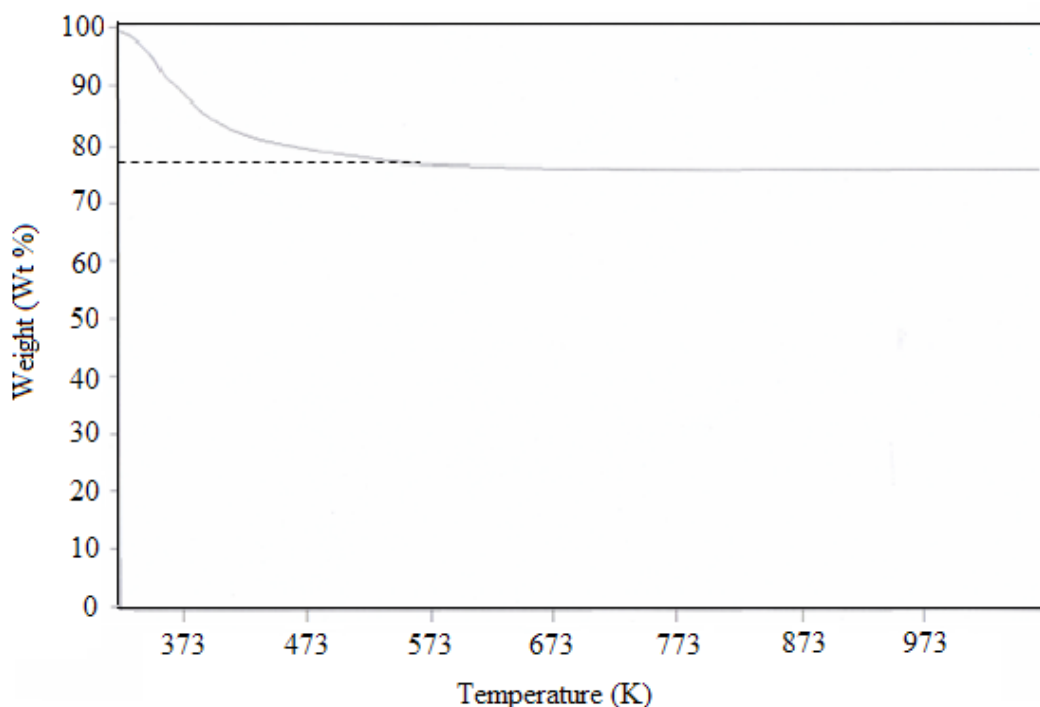


Figure 11 The TG curve of as-prepared N-doped TiO_2 using titanium(IV) tetraisopropoxide as a titania precursor.

The TG curve (Figure 11) of as-prepared N-doped TiO_2 using titanium(IV) tetraisopropoxide after dried at 393 K exhibits one apparent stage of 22% weight loss at 573 K. This originated from the disposal of weakly-adsorbed species on the surface of N-doped TiO_2 namely H_2O , NH_3 and organic molecules. The TG curve is different from the first two TG curves as already shown in Figure 9 and 10, respectively, in terms of one-stage decomposition and the lower percentage of the overall weight loss.

The presence of one-stage decomposition indicates that the hydrolysis of Ti-O-R (R = isopropoxide) was quite complete. No organic residuals were further released after 600 K. Therefore, weight loss was not clearly observed at higher temperature (>573 K). Moreover, the percentage of weight loss between 273 and 573 K is lower than any other that of N-doped TiO_2 using titanium(IV) bis(ethyl acetoacetato)diisopropoxide or N-doped TiO_2 titanium(IV) tetra-n-butoxide. The

appropriate reason used to elaborate this phenomenon is to the boiling points of each organic species from the hydrolysis reactions.

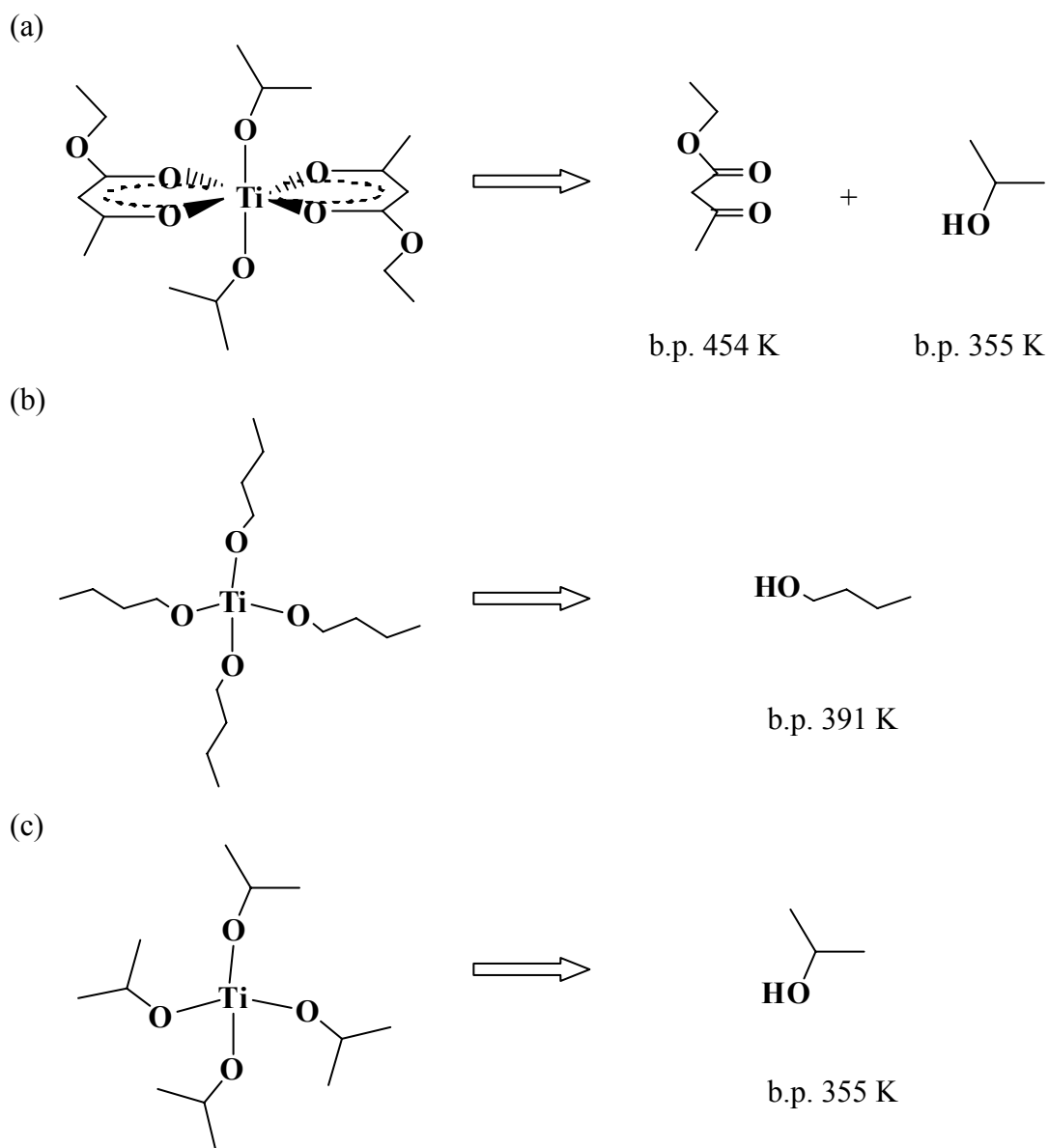


Figure 12 Expected products from the hydrolysis reaction of (a) titanium(IV) bis(ethyl acetoacetato)diisopropoxide, (b) titanium(IV) tetra-n-butoxide and (c) titanium(IV) tetraisopropoxide.

From Figure 12a, titanium(IV) bis(ethyl acetoacetato) diisopropoxide gave ethyl acetoacetate and isopropanol after hydrolysis reaction. The boiling points of ethyl acetoacetate and isopropanol are 454 and 355 K, respectively, indicating that the former was very difficult to be removed at 393 K under the drying step. It, therefore, adsorbed on the surface of as-prepared N-doped TiO₂ and caused high percentage of weight loss (47%) between 273 and 573 K in the TG curve. Meanwhile, the hydrolysis of titanium(IV) tetra-n-butoxide provided n-butanol (Figure 12b) of which boiling point is 391 K. Under the drying step at 393 K, therefore, n-butanol was evaporated at the small extent and still adsorbed on the surface of the catalyst. Thus, the TG result of as-prepared N-doped TiO₂ using titanium(IV) tetra-n-butoxide showed 33% weight loss between 273 and 573 K but its weight loss is less than that of as-prepared N-doped TiO₂ using titanium(IV) bis(ethyl acetoacetato)diisopropoxide. In other words, the hydrolysis of titanium(IV) tetraisopropoxide gave rise to isopropanol (Figure 12c) of which the boiling point is 355 K. In drying step, isopropanol was considerably evaporated at 393 K. As a result, only 22% of weight loss was observed between 273 and 573 K in the TG curve.

In addition, as previously studied by Fornasiero *et al.* (2007), Temperature-Programmed Oxidation experiments (TPO) was used to study the presence of carbon and nitrogen-containing species on as-prepared N-doped TiO₂ which the results are shown in Figure 13. They found that weakly-adsorbed carbon and nitrogen-containing species were eliminated in forms of CO, CO₂, NO_x, NH₃, NH₂ etc. at lower temperature. Meanwhile, at higher temperature the high amount of nitrogen was still detected by TPO, which resulted from the oxidation of strongly-bonded nitrogen species. This could be implied that nitrogen anions were able to incorporate with the strong bonds in the TiO₂ structure and were hardly disposed. On the other hands, carbon species was rapidly reduced to the infinitesimal amounts. This could be assumed that no strong bonds took place in the TiO₂ structure so the high amount of carbon was easy to be annihilated at lower temperature.

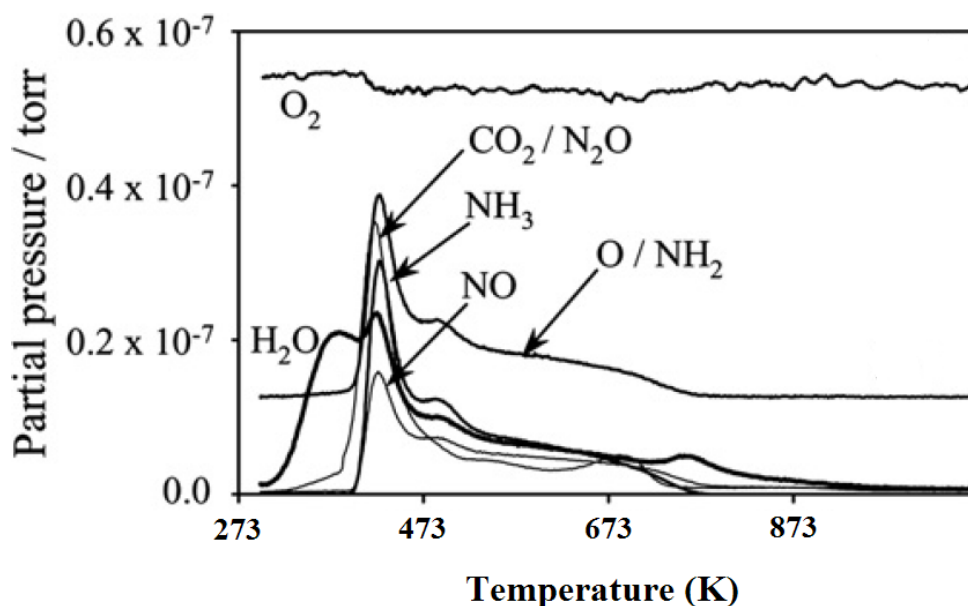


Figure 13 Temperature-Programmed Oxidation (TPO) of as prepared N-doped TiO₂.

Source: Fornasiero *et al.* (2007)

In comparison with Fornasiero *et al.* (2007), TG results may be confirmed that the first stage of weight loss was related to the evolution of weakly-adsorbed species namely H₂O, NO_x, NH₃, NH₂, CO, CO₂ etc. The second stages were presumably concerned with the tightly-adsorbed species, both carbon and nitrogen, as shown in case of as-prepared N-doped TiO₂ using titanium(IV) bis(ethyl acetoacetato) diisopropoxide and N-doped TiO₂ using titanium(IV) tetra-n-butoxide. However, as-prepared N-doped TiO₂ using titanium(IV) tetraisopropoxide shows that the organic contamination nearly ran out in the N-doped TiO₂ structure at the calcination temperature higher than 673 K. Hence, it can be assumed that only strongly-bonded nitrogen was latent in the TiO₂ structure. The supportive results from the EA technique will be shown later.

1.1.2 X-ray Powder Diffraction (XRD)

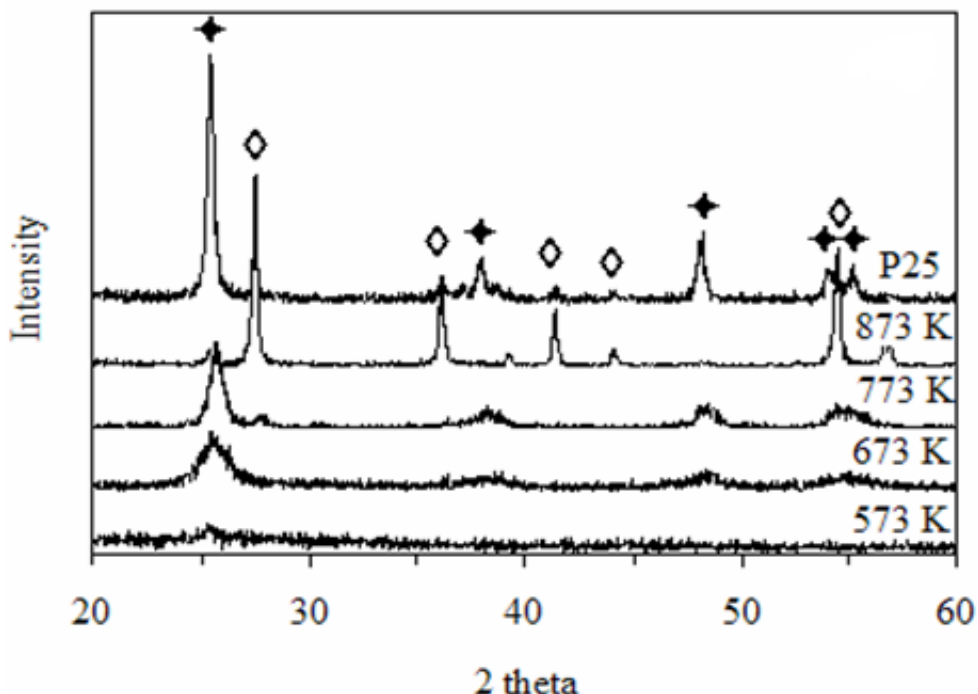


Figure 14 The XRD patterns of N-doped TiO_2 using titanium(IV) bis(ethyl acetoacetato)diisopropoxide as a titania precursor with different calcination temperatures and P25 TiO_2 . (◆ for the anatase phase and ◇ for the rutile phase)

The XRD patterns in Figure 14 indicate that the structure of N-doped TiO_2 was amorphous at 573 K. Then, it changed into the anatase phase which is firstly seen at 673 K. The anatase phase was identified at 2θ of 25.4° , 38.1° , 48.2° , 53.9° and 55.1° , respectively, corresponding with the standard XRD pattern (JCPDS files No. 21-1272). At 773 K, the characteristic peak of anatase is sharper and clearer to observe, in particular, at 2θ of 25.4° . Moreover, the presence of the rutile peak at 2θ of 27.5° indicates that phase transformation occurred with increasing temperature. Rutile phase was also identified at 2θ of 27.5° , 36.1° , 41.3° , 44.2° and 55.5° , respectively, corresponding with the standard XRD pattern (JCPDS files No. 21-1276). At 873 K, the rutile phase is very prominent with high intensity which

meant high crystallinity. Additionally, phase components of this catalyst at 873 K are 92.7% for rutile and 7.3% for anatase as shown in Table 5.

Regarding the crystallite size of N-doped TiO₂ using titanium(IV) bis(ethyl acetoacetato)diisopropoxide (Table 5), its crystallite size is considerably increased from 9 to 51 nm with elevating temperature in case of the anatase structure. This suggests that the higher calcination temperature caused the agglomeration of N-doped TiO₂ particles. Surprisingly, the crystallite size of its rutile structure is 31.5 nm three times as large as that of its anatase calcined at 673 K. Nevertheless, its surface area (S_{BET}) was drastically changed from 254 m²/g to 4.84 m²/g with increasing calcination temperature.

P25 TiO₂ as shown in Figure 14 consists of mixed phases in the ratio of 75% anatase to 25% rutile. The XRD peaks at 2θ of 25.4° and 27.6° show the predominant characteristics of the anatase and rutile phases, respectively. The crystallite size of anatase P25 TiO₂ (Table 5) differs from N-doped TiO₂ since it was synthesized via the different process and had no nitrogen-doping effect on its structure.

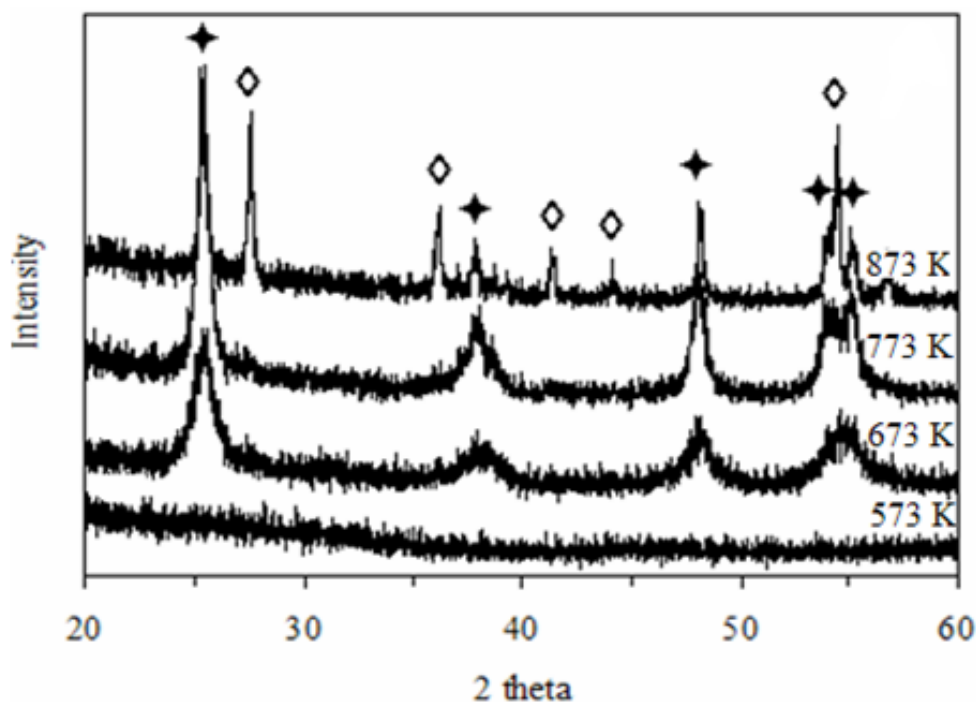


Figure 15 The XRD patterns of N-doped TiO₂ using titanium(IV) tetra-n-butoxide as a titania precursor with different calcination temperatures. (◆ for the anatase phase and ◇ for the rutile phase)

The XRD patterns in Figure 15 illustrate that at lower temperature the structure of N-doped TiO₂ was amorphous; no XRD diffraction peaks were detected at any diffraction angles. However, with higher temperature the XRD diffraction pattern identified as an anatase phase occurs especially at 2θ of 25.4° and gradually increases the intensity. When the calcination temperature was raised up to 873 K, the rutile XRD pattern starts appearing at 2θ of 27.6° , 36.2° , 41.5° , 44.2° and 55.6° , respectively. All of XRD patterns are matched with the standard XRD patterns of TiO₂, both anatase (JCPDS files No. 21-1272) and rutile phases (JCPDS files No. 21-1276). Besides, the phase ratio of rutile to anatase is 51.7 % to 48.3% as shown in Table 5.

Furthermore, the tendency of particle growth of anatase is that the higher the calcination temperature, the larger the crystallite size of N-doped TiO₂.

Interestingly, the crystallite size of rutile is 35.6 nm at 873 K which is also three times as large as that of anatase at 673 K.

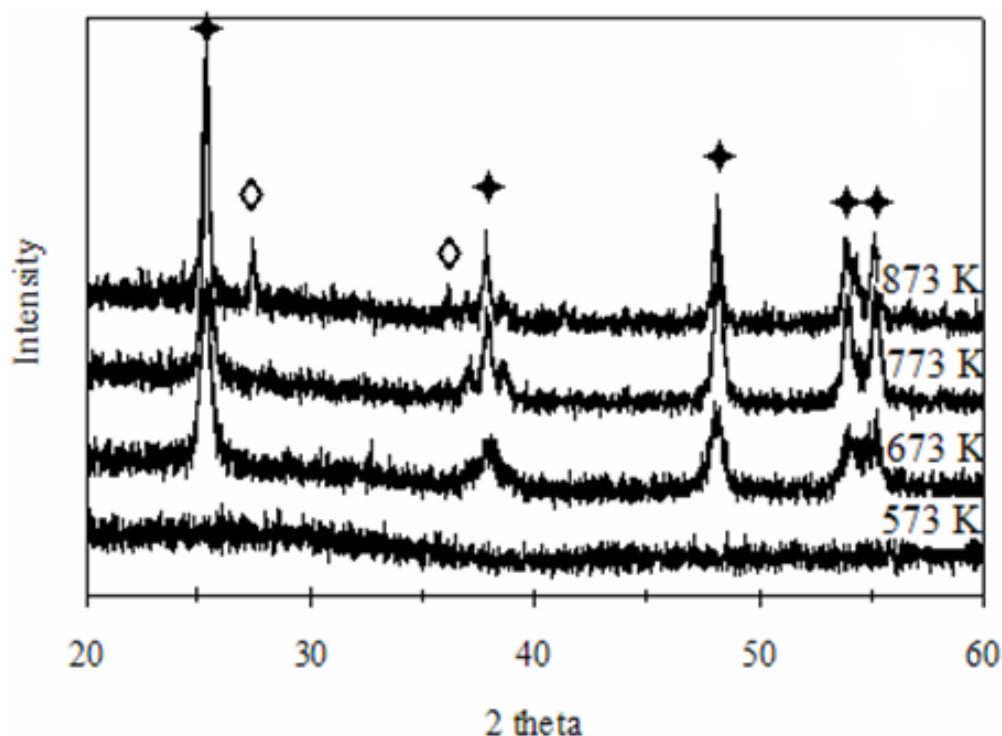


Figure 16 The XRD patterns of N-doped TiO₂ using titanium(IV) tetraisopropoxide as a titania precursor with different calcination temperatures. (◆ for the anatase phase and ◆ for the rutile phase)

The XRD patterns in Figure 16 exhibit amorphous, anatase and rutile phases, depending on temperature. At 573 K, there is no diffraction pattern occurred, which shows the amorphous structure of N-doped TiO₂. After the temperature was raised up to 673 K, all peaks ($2\theta = 25.4^\circ, 38.1^\circ, 48.4^\circ, 53.9^\circ, 55.2^\circ$) which are regarded as an attributive indicator of the anatase phase of titania (JCPDS files No. 21-1272) are clearly presented. Then, at 873 K the characteristic peak of rutile is emerged at 2θ of 27.5° and 36.1° , respectively (JCPDS files No. 21-1276). Focusing on anatase at 2θ of 25.4° , when calcination temperature was elevated, the crystallinity of N-doped TiO₂ continually increased with the higher and sharper peak.

Moreover, at 873 K phase composition of N-doped TiO₂ is 32.1% of rutile and 67.9% of anatase as shown in Table 5.

The crystallite size of N-doped TiO₂ is 16.3 nm for the anatase structure at 673 K and gradually increases to 28.1 nm at 873 K because of the particle agglomeration. Moreover, the crystallite size of rutile is 51.1 nm at 873 K three times as large as that of anatase at 673 K.

In comparison with XRD patterns of N-doped TiO₂ using three different types of titania precursors, there are three main aspects having to be discussed such as crystallinity, anatase-to-rutile phase transformation and crystallite sizes.

First, N-doped TiO₂ using titanium(IV) bis(ethyl acetoacetato) diisopropoxide and N-doped TiO₂ using titanium(IV) tetra-n-butoxide provided less crystallinity than N-doped TiO₂ using titanium(IV) tetraisopropoxide at 673 K because of latent organic residuals (Ti-O-R) in the structure which prevented the formation of Ti-O-Ti. Thus, their characteristic peaks at 2θ of 25.5° are very broad at 673 K. However, they gradually sharpen with elevating temperature. This suggests that the higher the calcination temperature, the higher the crystallinity of N-doped TiO₂.

Second, N-doped TiO₂ using titanium(IV) bis(ethyl acetoacetato)diisopropoxide starts phase change at 773 K in which rutile was initially detectable. Meanwhile, N-doped TiO₂ using titanium(IV) tetra-n-butoxide and N-doped TiO₂ using titanium(IV) tetraisopropoxide shows phase changes at 873 K. Furthermore, N-doped TiO₂ using titanium(IV) tetraisopropoxide has the lowest rutile fraction at 873 K about 32.1%, suggesting that the structure of N-doped TiO₂ using titanium(IV) tetraisopropoxide was retarded to transform into rutile with increasing temperature. This can be assumed that nitrogen doping caused the retardation of phase change. Additionally, nitrogen doping has a few effects on the other two N-doped TiO₂ because a smaller amount of nitrogen (will be discussed later) still remained in

the TiO_2 lattice at high temperature. Again, focusing on anatase-to-rutile phase transformation, the unit cell volume of N-doped TiO_2 is extremely changed more than 50% (Table 6). These results demonstrate that high temperature (873 K) brought about the more closely packing lattice structure beside phase transformation.

Third, the crystallite sizes of N-doped TiO_2 using titanium(IV) bis(ethyl acetoacetato)diisopropoxide and N-doped TiO_2 using titanium(IV) tetra-n-butoxide are smaller than that of N-doped TiO_2 using titanium(IV) tetraisopropoxide at 673 K because the remaining organic contents blocked particle agglomeration of N-doped TiO_2 . However, with increasing temperature, the crystallite sizes of all N-doped TiO_2 were increased. Moreover, it is obvious that the crystallite size of rutile at 873 K is usually three times as large as that of anatase at 673 K. This result is in good agreement with previous research by Kumar (1995), stating that the critical nucleus size of rutile crystallites was at least three times larger than that of anatase.

As all mentioned above, it can be implied that N-doped TiO_2 using titanium(IV) tetraisopropoxide provided both higher characteristics and crystallinity of anatase in spite of its larger crystallite size when compared to the other two N-doped TiO_2 photocatalysts.

Table 5 Effect of titania precursors and calcination temperatures on the crystallite sizes and phase content of N-doped TiO₂ and P25 TiO₂.

Titania precursor	Calcination temperature (K)	Phase ^a	2θ (degree)	Cosθ	β (degree)	β (radian)	Crystallite size (nm) ^b	Intensity (A)	Intensity (R)	% A ^c	% R ^d
Titanium(IV) bis(ethyl acetoacetato) diisopropoxide	673	A	25.490	0.975	0.89	0.0155	9.15			100	0
	773	A	25.670	0.975	0.71	0.0124	11.5			100	0
	873	A	25.410	0.976	0.16	0.00279	50.9	23	231	7.32	92.7
		R	27.550	0.971	0.26	0.00506	31.5				
Titanium(IV) tetra-n-butoxide	673	A	25.440	0.975	0.86	0.0151	9.41			100	0
	773	A	25.375	0.976	0.51	0.00894	15.9			100	0
	873	A	25.375	0.976	0.30	0.00524	27.1	362	308	48.3	51.7
		R	27.565	0.971	0.23	0.00489	35.6				
Titanium(IV) tetraisopropoxide	673	A	25.355	0.976	0.50	0.00873	16.3			100	0
	773	A	25.395	0.976	0.33	0.00576	24.7			100	0
	873	A	25.365	0.976	0.29	0.00506	28.1	538	202	67.9	32.1
		R	27.495	0.971	0.16	0.00541	51.1				
P25 TiO ₂	-	A	25.430	0.975	0.36	0.00628	22.6	296	79	74.9	25.1
		R	27.610	0.971	0.18	0.00314	45.5				

^aA stands for anatase and R stands for rutile.

^cThe anatase content was calculated by applying Spurr-Myers equation.

^bThe crystallite size was calculated by using Sherrer' s equation.

^dThe rutile content was calculated by 100% - Anatase%.

Table 6 Effect of calcination temperatures on the unit cell volume of N-doped TiO₂ and P25 TiO₂.

Titania precursor	Calcination temperature (K)	Phase	Lattice parameters (nm)			Unit cell volume (nm ³)
			a	b	c	
Titanium(IV) bis(ethyl acetoacetato) diisopropoxide	673	A	0.3764	0.3764	0.9312	0.1320
	773	A	0.3718	0.3718	0.9412	0.1301
	873	A	-	-	-	-
		R	0.4576	0.4576	0.2953	0.06183
Titanium(IV) tetra-n-butoxide	673	A	0.3783	0.3783	0.9404	0.1346
	773	A	0.3776	0.3776	0.9448	0.1347
	873	A	0.3766	0.3766	0.9488	0.1345
		R	0.4574	0.4574	0.2966	0.06206
Titanium(IV) tetraisopropoxide	673	A	0.3780	0.3780	0.9452	0.1350
	773	A	0.3769	0.3769	0.9496	0.1349
	873	A	0.3774	0.3774	0.9496	0.1352
		R	-	-	-	-
P25 TiO ₂	-	A	0.3758	0.3758	0.9588	0.1354
		R	0.4569	0.4569	0.2984	0.06230

1.1.3 Raman Spectroscopy

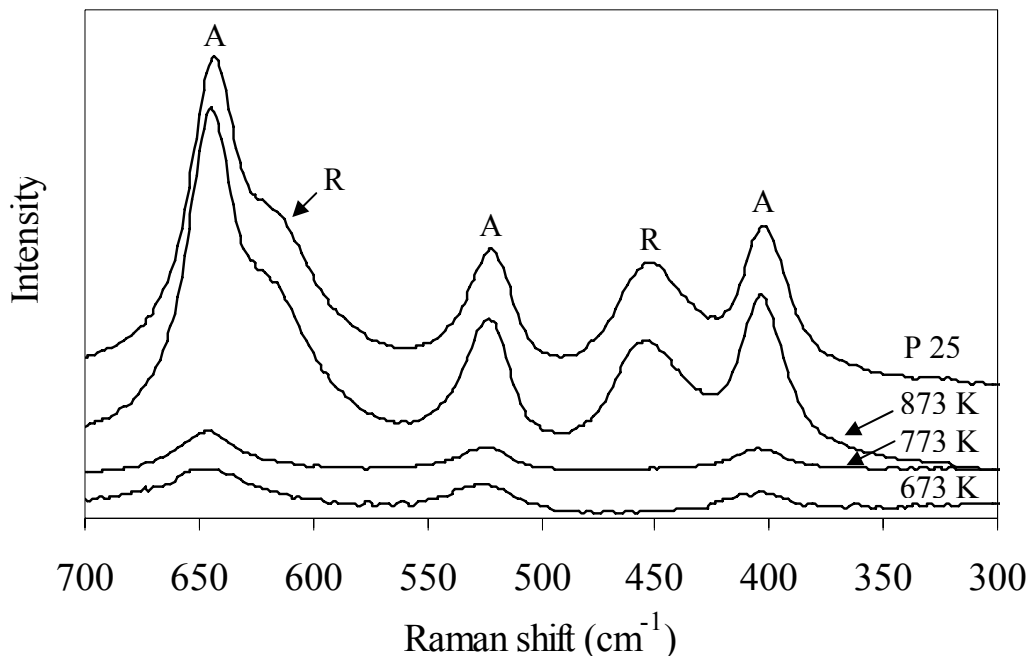


Figure 17 Raman spectra of N-doped TiO₂ using titanium(IV) bis(ethyl acetoacetato) diisopropoxide as a titania precursor with different calcination temperatures.
 (“A” for anatase phase and “R” for rutile phase)

In Figure 17, it can be obviously seen that at lower calcination temperature (673 and 773 K) the eminent phase at Raman shifts of 399 cm⁻¹, 519 cm⁻¹ and 639 cm⁻¹ was considered as anatase phase (Gnaser *et al.*, 2007). With increasing temperature, the anatase phase abruptly changed into the rutile phase, which could be identified at Raman shift of 447 cm⁻¹ and 612 cm⁻¹ (Gnaser *et al.*, 2007). This Raman result is in quite good agreement with the XRD result that phase transformation was evidently occurred in the temperature interval between 773 and 873 K.

As regards to P25 TiO₂ (Figure 17), the Raman spectrum shows mixed composition phases. It exhibits anatase at 399 cm⁻¹, 519 cm⁻¹ and 639 cm⁻¹ and rutile at 447 cm⁻¹ and 612 cm⁻¹, respectively. The positions of both anatase and rutile phases quite resemble with N-doped TiO₂ calcined at 873 K.

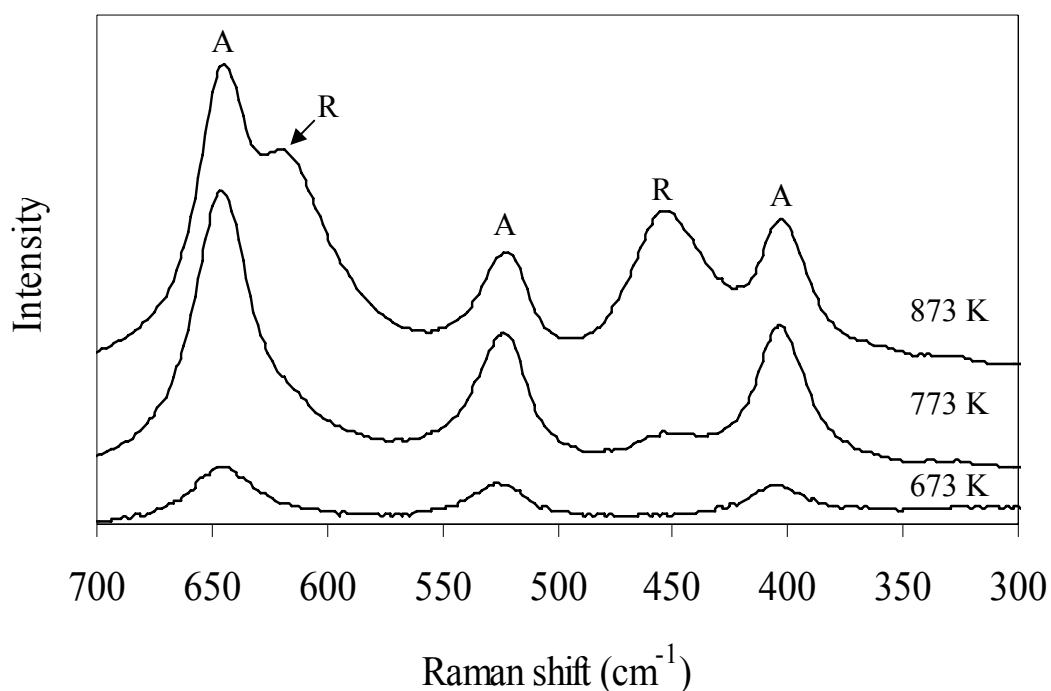


Figure 18 Raman spectra of N-doped TiO₂ using titanium(IV) tetra-n-butoxide as a titania precursor with different calcination temperatures. (“A” for anatase phase and “R” for rutile phase)

As shown in Figure 18, N-doped TiO₂ shows anatase phase at 673 K and 773 K which can be confirmed by the presence of Raman shifts at 399 cm⁻¹, 519 cm⁻¹ and 639 cm⁻¹, respectively. After calcined at higher temperature (873 K), the N-doped TiO₂ structure was transformed into the rutile structure, which is seen at the additional Raman shifts of 447 cm⁻¹ and 612 cm⁻¹, respectively. When compared to the XRD data, the Raman results also provided the significant data as to the phase identification and phase transformation between 673 and 873 K very well.

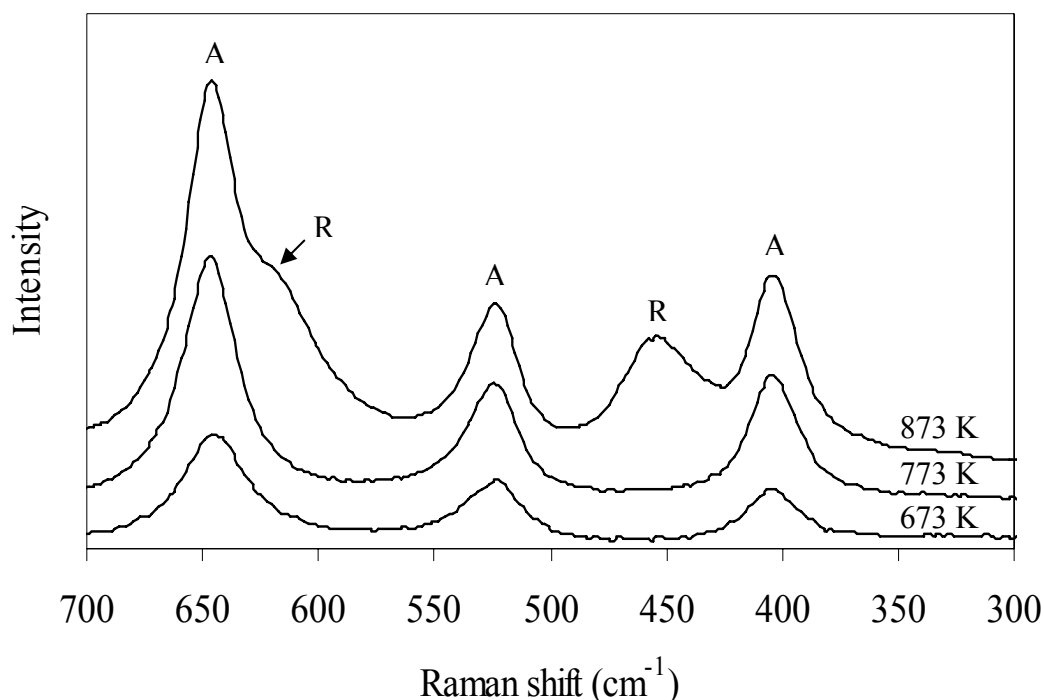


Figure 19 Raman spectra of N-doped TiO_2 using titanium(IV) tetraisopropoxide as a titania precursor with different calcination temperatures. (“A” for anatase phase and “R” for rutile phase)

The Raman spectra of N-doped TiO_2 in Figure 19 demonstrate that the anatase phase prevails over the rutile phase at lower temperature. However, the rutile phase was much more clearly detected with elevating temperature to 873 K. Anatase phase was identified with a set of Raman shifts at 399 cm^{-1} , 519 cm^{-1} and 639 cm^{-1} , respectively. The rutile phase was also identifiable at 447 cm^{-1} and 612 cm^{-1} , respectively. Hence, in analogy with the XRD data, also the Raman results confirm the anatase-to-rutile phase transformation between 773 and 873 K.

Again comparison was made to the three types of N-doped TiO_2 . According to the Fornasiero’s statement, the band broadening was ascribed to both the co-presence of different titania polymorphs and the low crystallite size. Therefore, N-doped TiO_2 using titanium(IV) tetraisopropoxide should have the biggest crystallite size at 673 K based on band broadening. However, phase transformation of N-doped TiO_2 using titanium(IV) tetraisopropoxide was slower than

any other that of two different N-doped TiO₂, which can be considered in terms of peak intensity at Raman shifts of 447 cm⁻¹ and 612 cm⁻¹. If the presence of peaks at those Raman shifts is observed with high intensity, it can be implied that there are the high amounts of rutile components predominant in N-doped TiO₂. Comparatively, all of these Raman results are in good agreement with the XRD results.

1.1.4 Scanning Electron Microscopy (SEM) and Transmission Electron Microscopy (TEM)

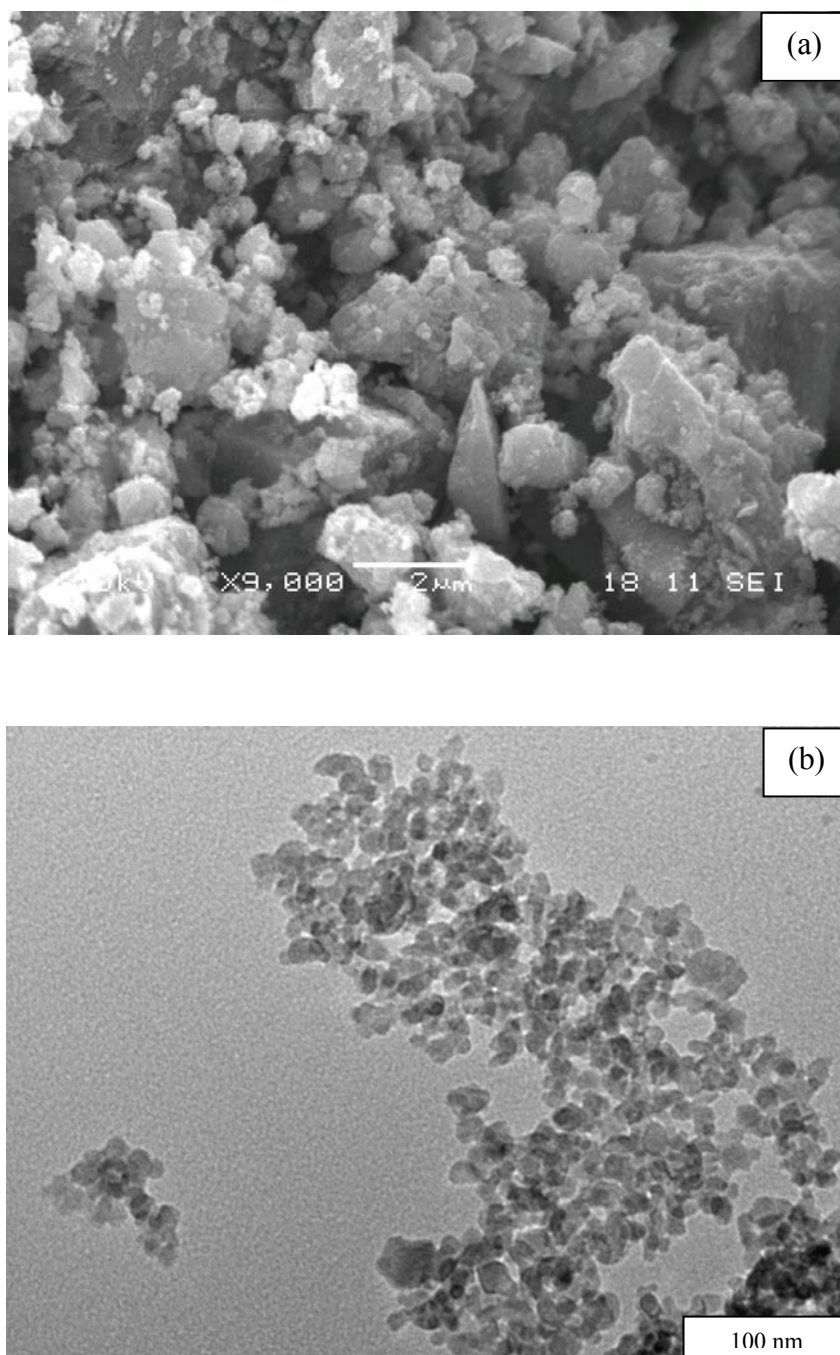


Figure 20 (a) SEM and (b) TEM images of N-doped TiO₂ using titanium(IV) bis(ethyl acetoacetato)diisopropoxide as a titania precursor and calcined at 673 K.

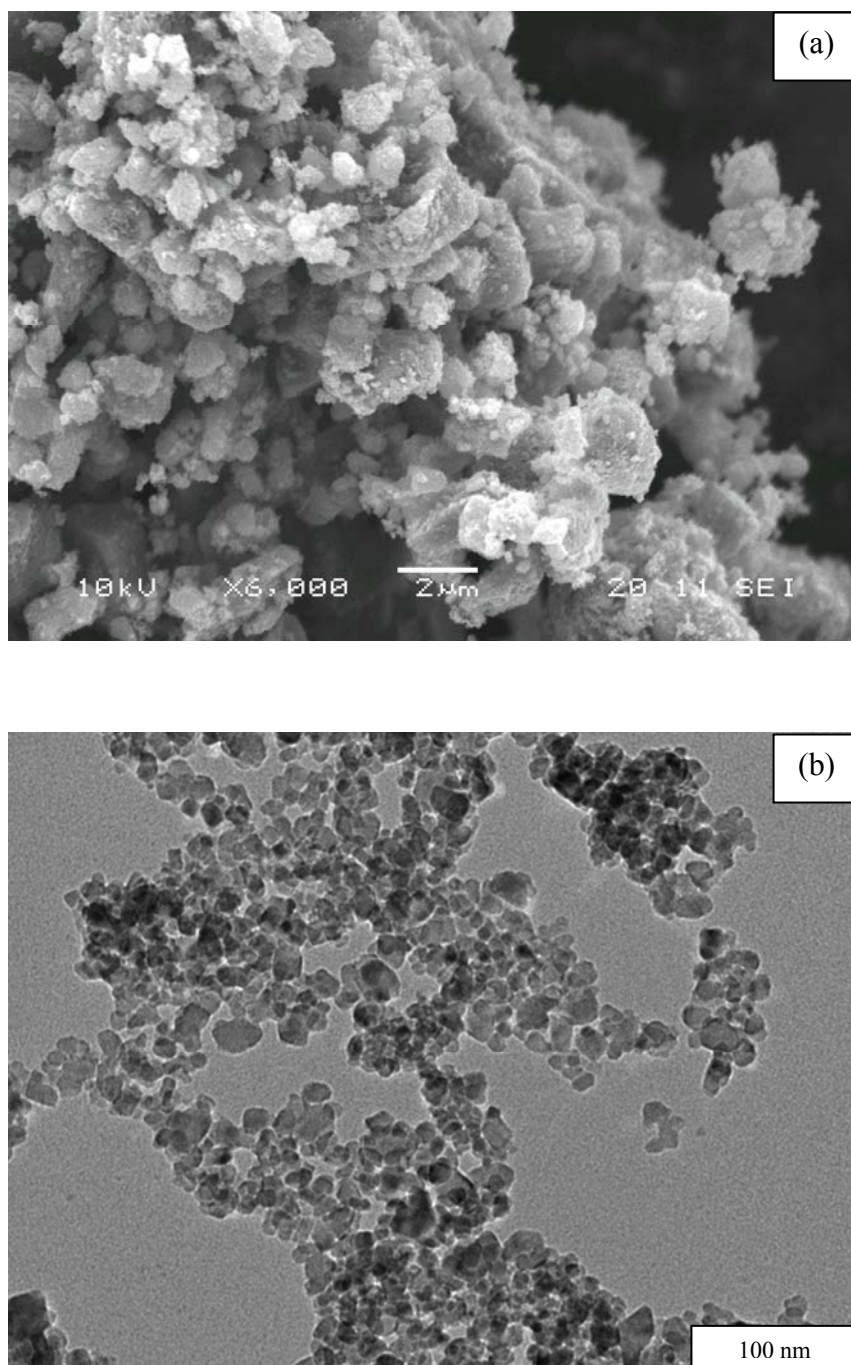


Figure 21 (a) SEM and (b) TEM images of N-doped TiO₂ using titanium(IV) bis(ethyl acetoacetato)diisopropoxide as a titania precursor and calcined at 773 K.

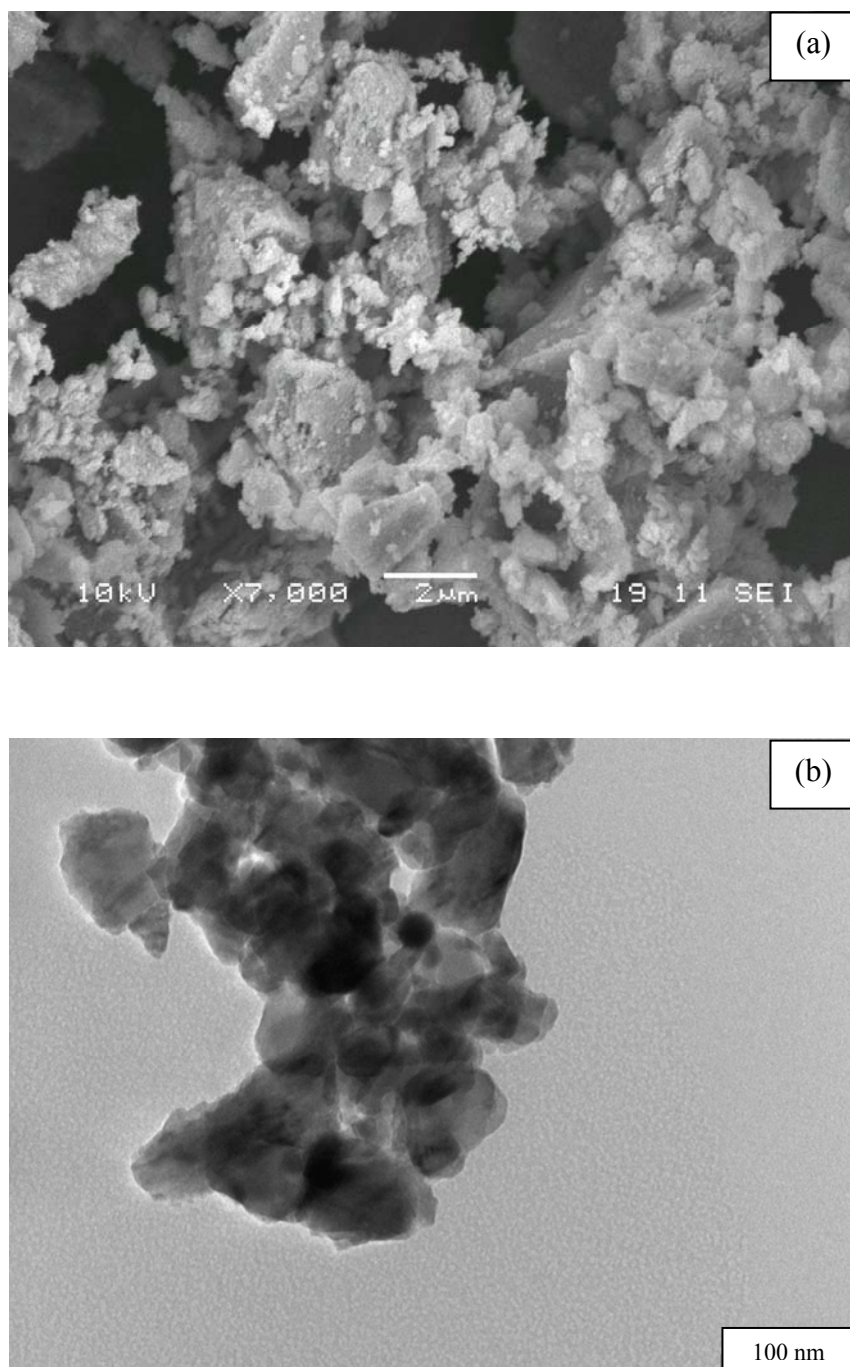


Figure 22 (a) SEM and (b) TEM images of N-doped TiO₂ using titanium(IV) bis(ethyl acetoacetato)diisopropoxide as a titania precursor and calcined at 873 K.

The surface morphology by SEM of the N-doped TiO₂ using titanium(IV) bis(ethyl acetoacetato)diisopropoxide is presented in Figure 20a, 21a and 22a. The growth of the mixture of spherical particles and flakes like semi-solid brown mass of N-doped TiO₂ can be clearly seen from these SEM images. The different morphology of the observed N-doped TiO₂ particles was described in the decomposition of the Ti-O-R precursor in accordance with the previous study (Viswanath *et al.*, 2007). This indicates that most of the titania precursor was hardly hydrolyzed under this preparation condition. Thus, the remaining Ti-O-R was necessarily decomposed at high calcination temperature and N-doped TiO₂ would be finally obtained.

In addition, the presence of most spherical type particles also can be evidently seen for the N-doped TiO₂ using titanium(IV) bis(ethyl acetoacetato) diisopropoxide, especially the ones calcined at 673 K and 773 K, from the TEM images (Figure 20b and 21b). The average sizes of the first two N-doped TiO₂ are 8.91 nm and 12.84 nm, respectively, as determined from the diameters of randomly selected 50 particles. In other words, the TEM image (Figure 22b) of N-doped TiO₂ calcined at 873 K shows the agglomeration of the particles which might be due to the calcination effect and might be related to the phase transformation itself. The particle size of this N-doped TiO₂ sample is in the range of 32-58 nm, based on the calculation from the diameters of randomly selected 25 particles.

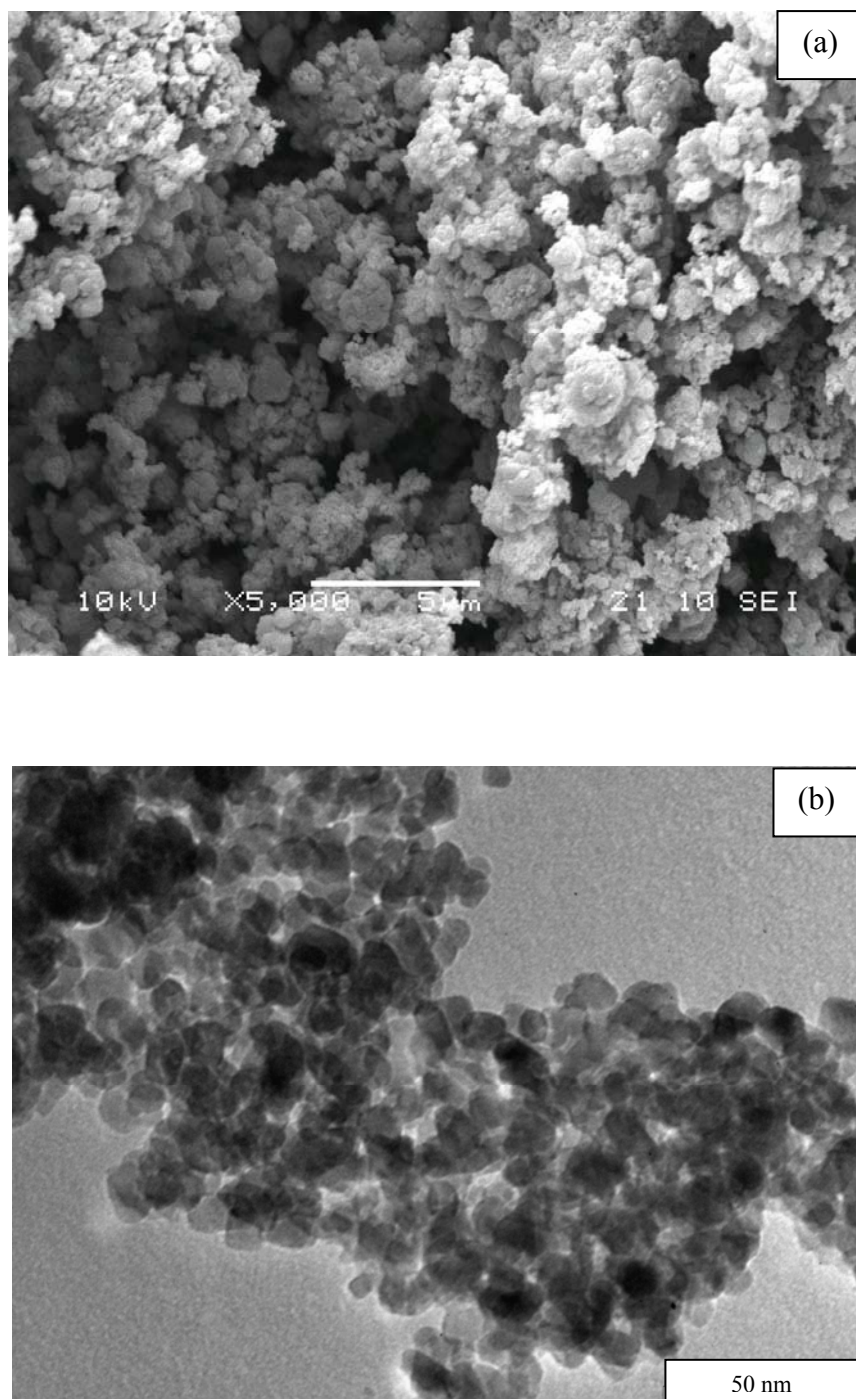


Figure 23 (a) SEM and (b) TEM images of N-doped TiO₂ using titanium(IV) tetra-n-butoxide as a titania precursor and calcined at 673 K.

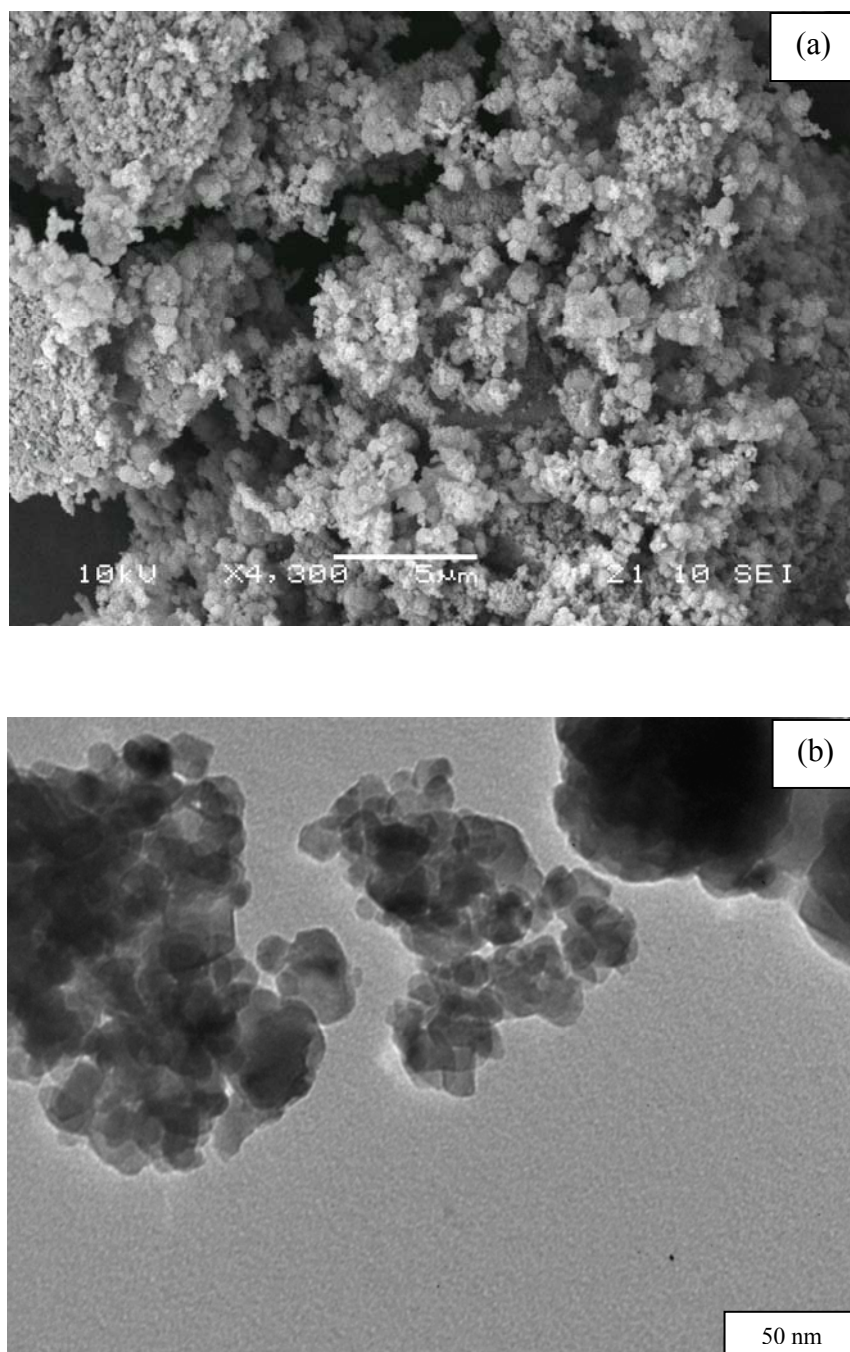


Figure 24 (a) SEM and (b) TEM images of N-doped TiO₂ using titanium(IV) tetra-n-butoxide as a titania precursor and calcined at 773 K.

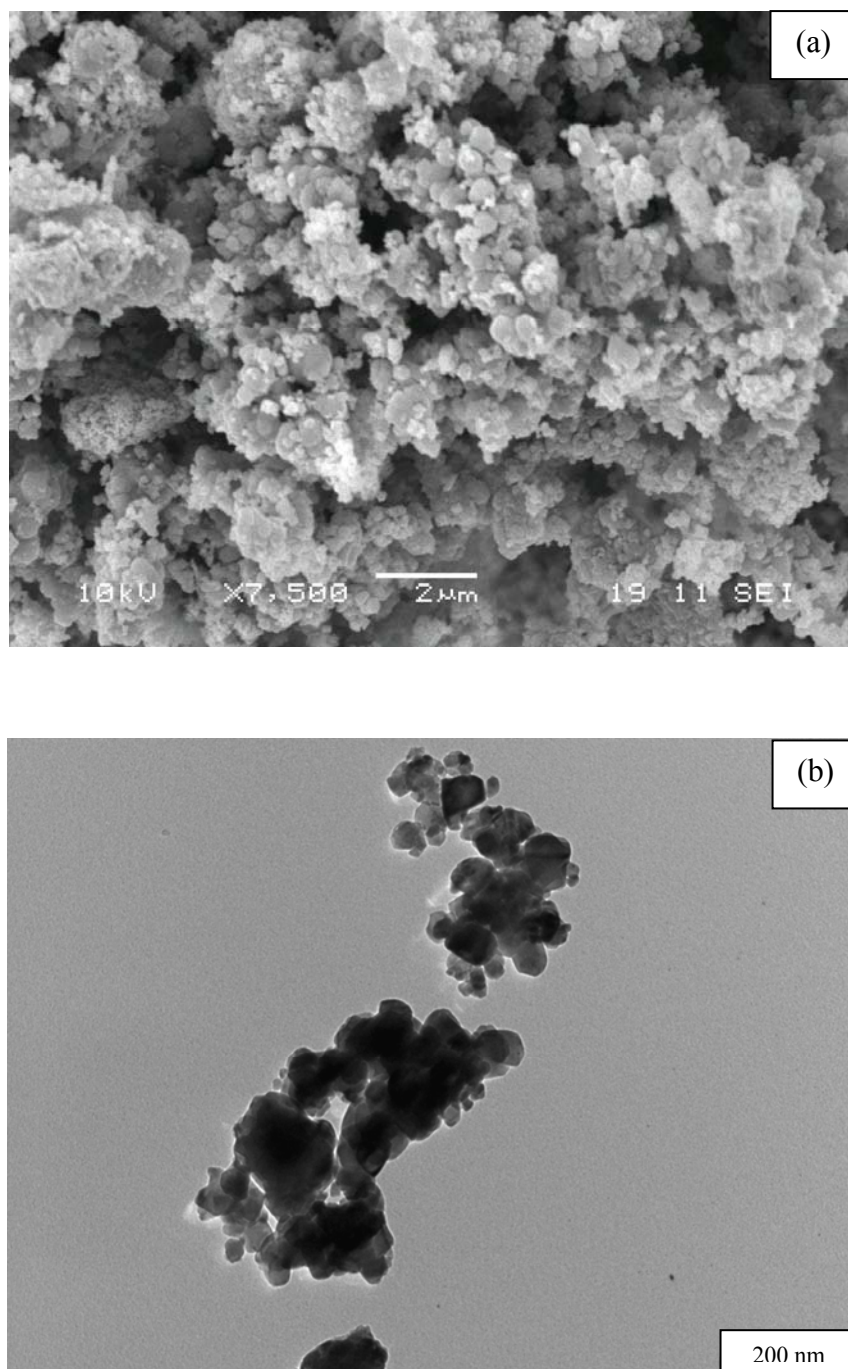


Figure 25 (a) SEM and (b) TEM images of N-doped TiO₂ using titanium(IV) tetra-n-butoxide as a titania precursor and calcined at 873 K.

The surface morphology from SEM images of N-doped TiO₂ using titanium(IV) tetra-n-butoxide seems to be the fluffy powders as shown in Figure 23a, 24a and 25a. SEM observation reveals that the particles are roughly monodispersed and assume round morphology, especially the N-doped TiO₂ calcined at 673 K. Moreover, the TEM image (Figure 23b) support that N-doped TiO₂ using titanium(IV) tetra-n-butoxide and calcined at 673 K contains the spherical monodispersed particles. The average particle size is 9.20 nm, determined from the diameters of randomly selected 50 particles. Regarding N-doped TiO₂ calcined at 773 K and 873 K, the TEM images (Figure 24b and 25b) illustrate that the more aggregate particles were obtained with increasing calcination temperature. The average particle size of N-doped TiO₂ calcined at 773 K is 18.20 nm, based on randomly selected 50 particles. However, the particle size of N-doped TiO₂ calcined at 873 K was hardly specified in terms of the average value because it is a wide range of particle size distribution between 23 and 50 nm, as determined from the diameters of randomly selected 30 particles.

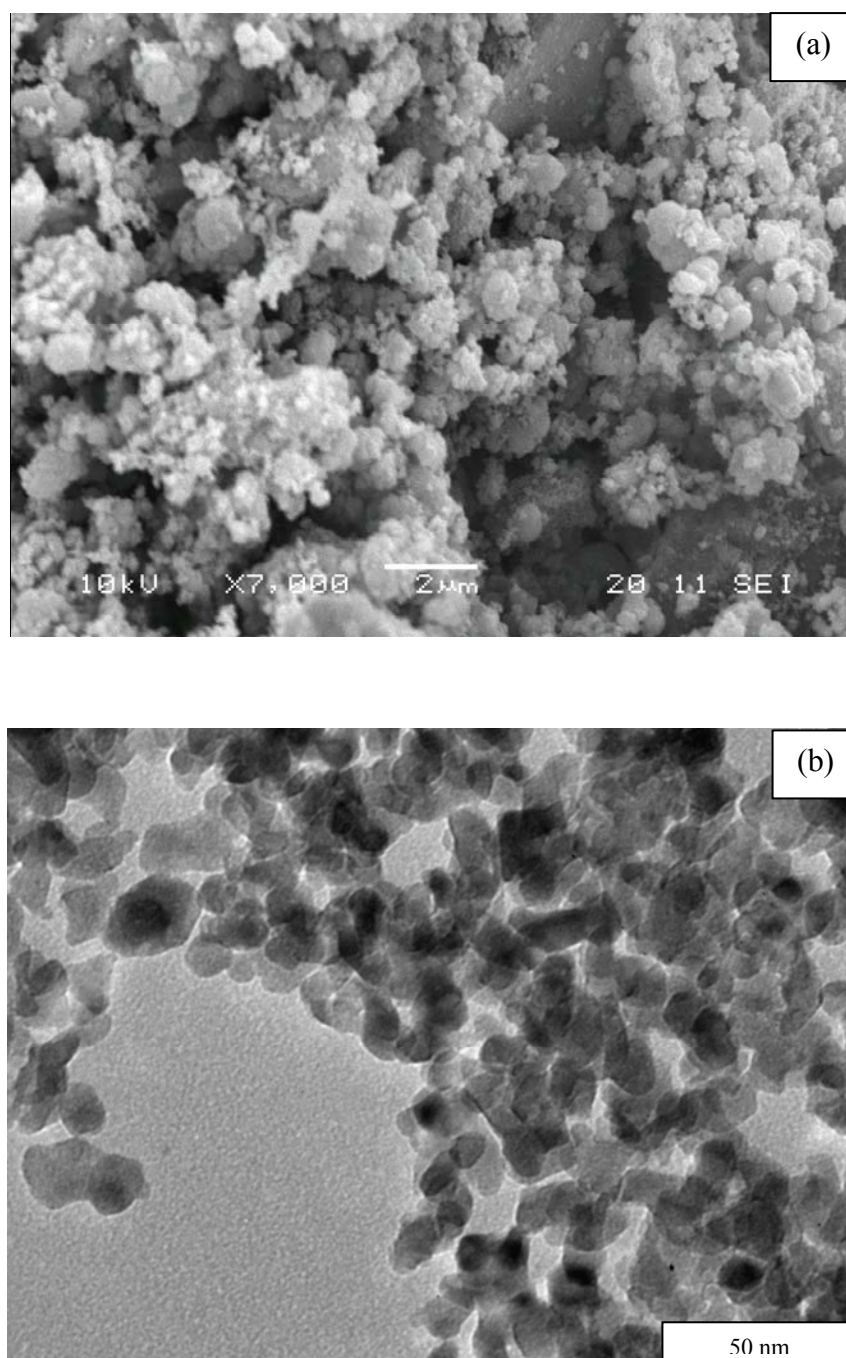


Figure 26 (a) SEM and (b) TEM images of N-doped TiO₂ using titanium(IV) tetraisopropoxide as a titania precursor and calcined at 673 K.

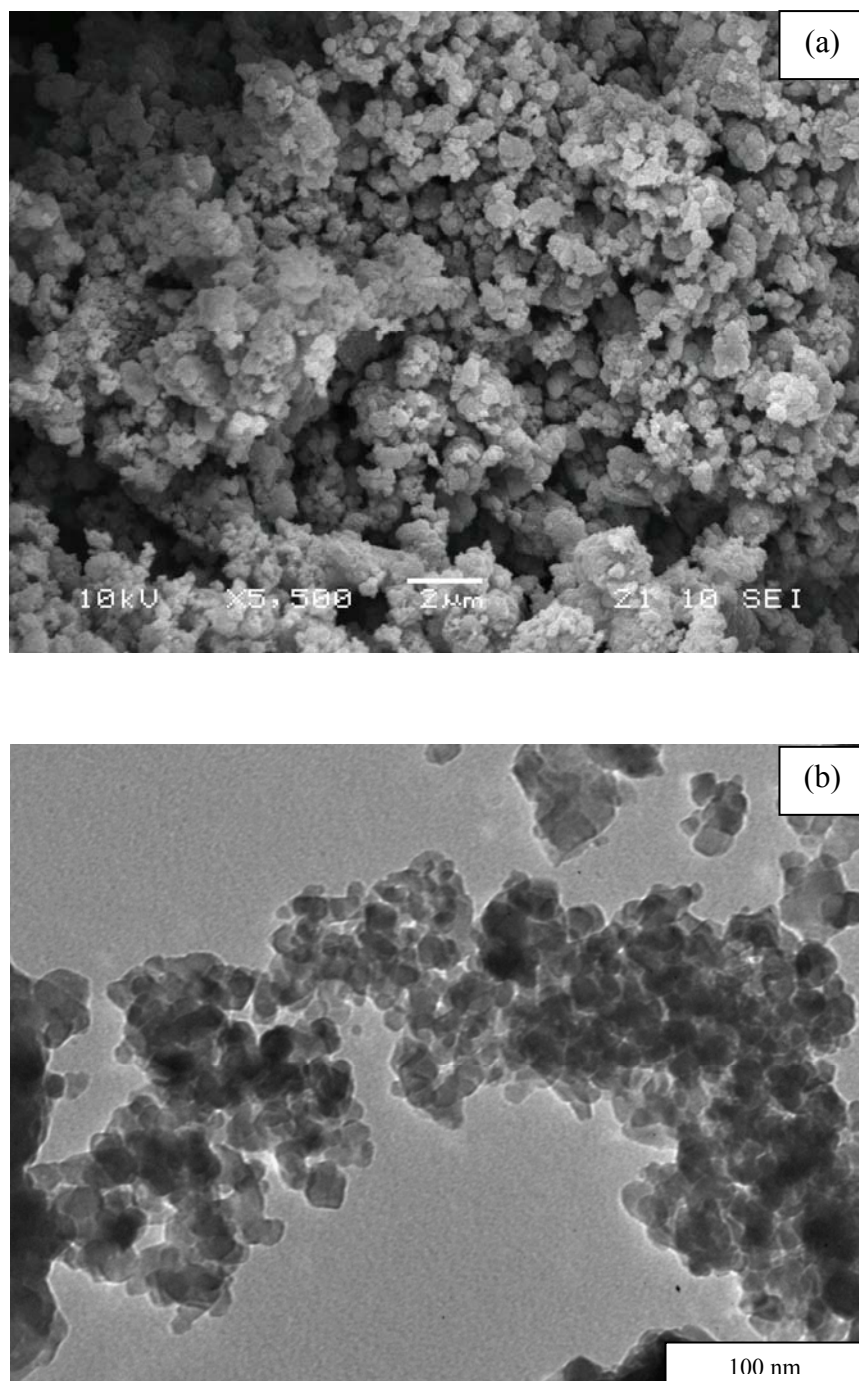


Figure 27 (a) SEM and (b) TEM images of N-doped TiO₂ using titanium(IV) tetraisopropoxide as a titania precursor and calcined at 773 K.

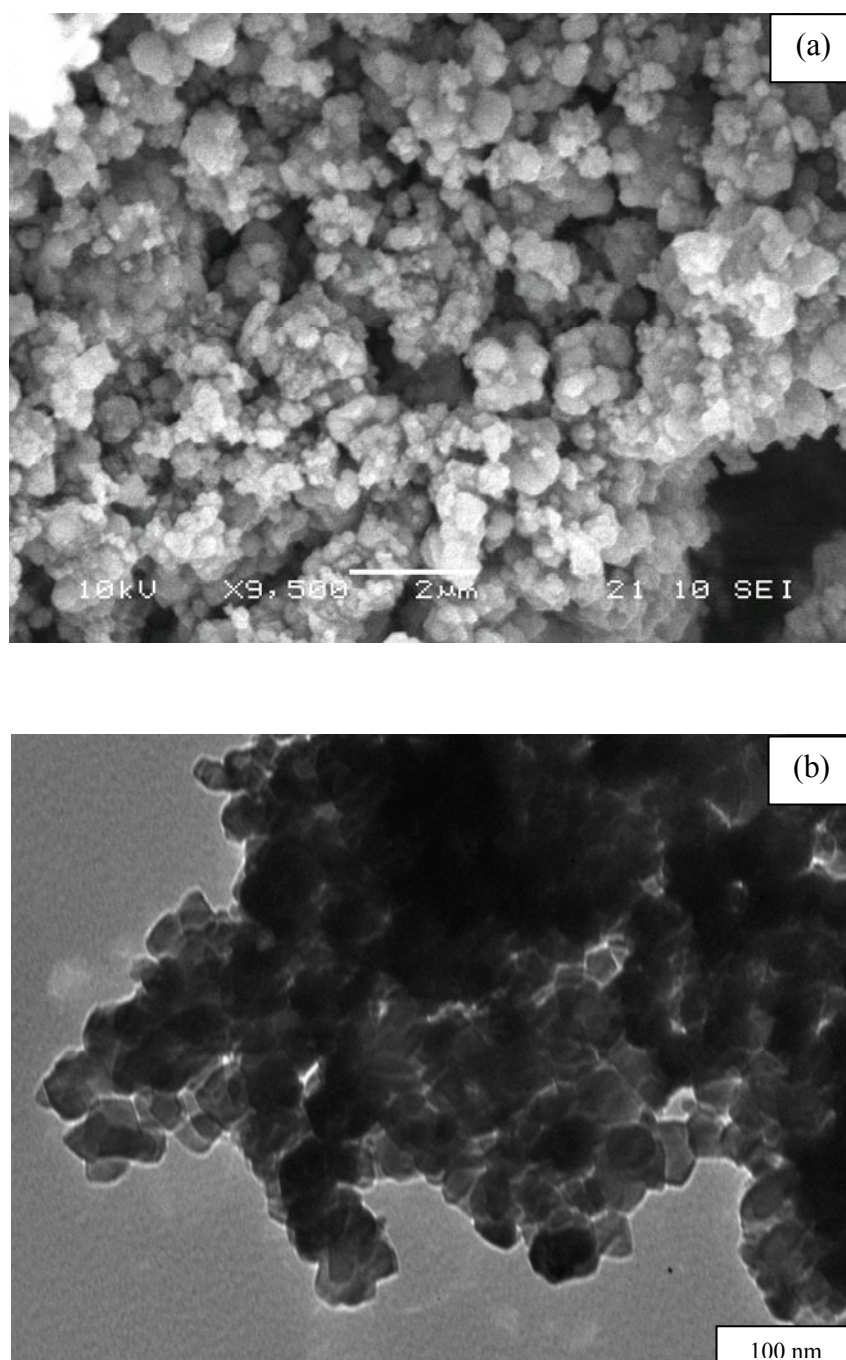


Figure 28 (a) SEM and (b) TEM images of N-doped TiO_2 using titanium(IV) tetraisopropoxide as a titania precursor and calcined at 873 K.

The SEM images (Figure 26a, 27a and 28a) exhibit that the surface morphology of N-doped TiO₂ using titanium(IV) tetraisopropoxide is mainly like fluffy grains. These results are in good agreement with TEM images (Figure 26b, 27b and 28b) for the N-doped TiO₂ samples that the particle morphology is somewhat spherical in both the analysis. Furthermore, the average sizes of N-doped TiO₂ calcined at 673 K and 773 K are 15.03 nm and 21.12 nm, respectively, based on the diameter calculation of randomly selected 50 particles. The densification phenomenon was occurred when the N-doped TiO₂ sample was calcined at 873 K as clearly displayed in the TEM image. This effect brings about the increase of particle size (30-59 nm), as determined from the randomly selected 30 particles.

When the comparison was made to each types of N-doped TiO₂, there are two significant points of view. First, the surface morphology of each N-doped TiO₂ is rather different in case of N-doped TiO₂ using titanium(IV) bis(ethyl acetoacetato)diisopropoxide, which depicts the mixture between sphere and flakes like semi-solid mass. On the other hand, N-doped TiO₂ using titanium(IV) tetra-n-butoxide and N-doped TiO₂ using titanium(IV) tetraisopropoxide provided their morphology like fluffy powders. Second, all N-doped TiO₂ has the bigger particle sizes with increasing calcination temperature even though it prepared from the different kinds of titania precursors. In each calcination temperature, the particle size from the TEM analysis is quite as equal as that from the XRD result.

Besides, the SEM and TEM images of P25 TiO₂ are also presented in Figure 29a and 29b. The surface morphology of P25 TiO₂ is spherical and looks like fluffy powders. However, P25 TiO₂ has the polydispersed round particles which can be obviously seen in the TEM image.

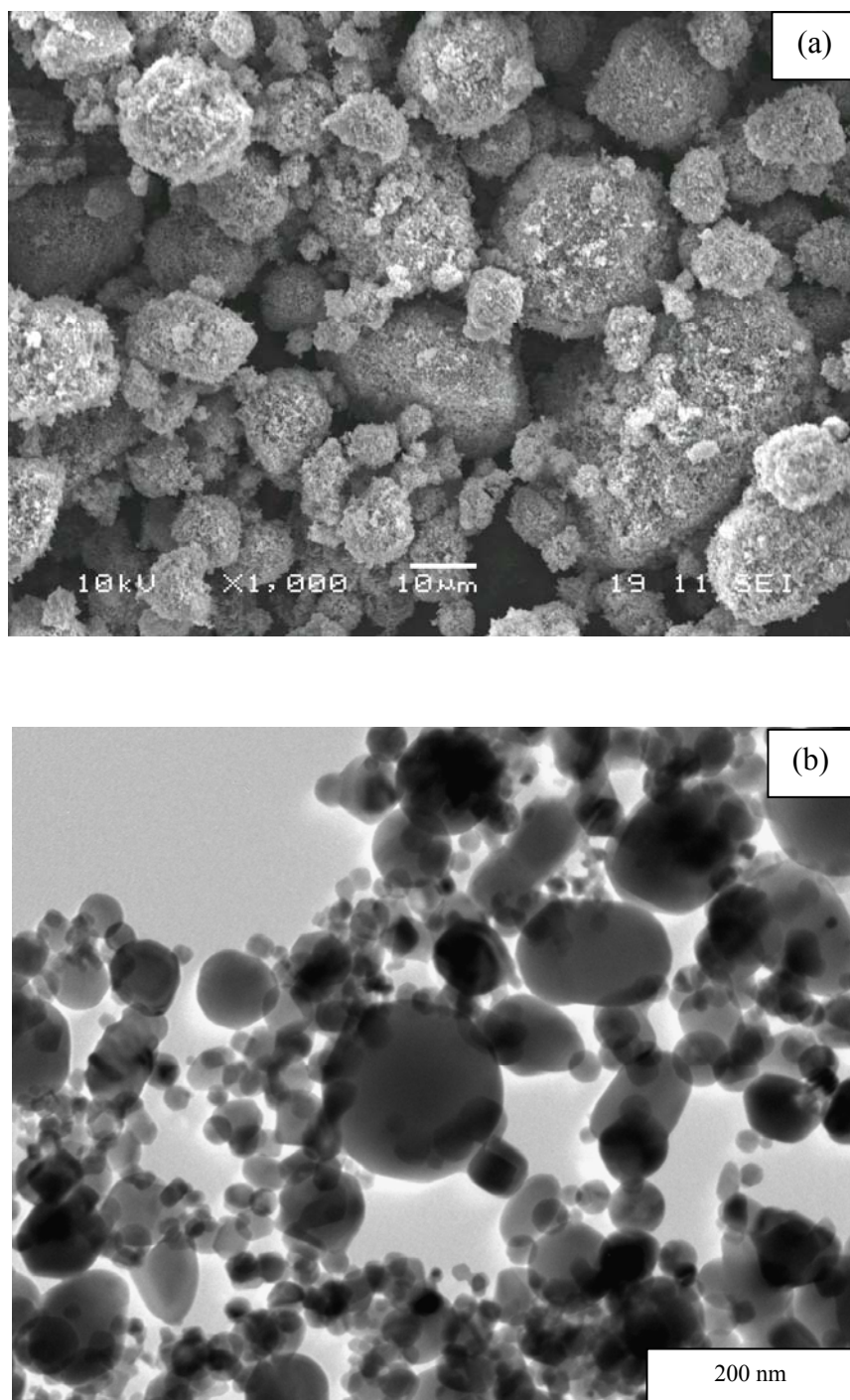


Figure 29 (a) SEM and (b) TEM images of P25 TiO₂.

1.1.5 Diffusion Reflectance UV-Vis Spectroscopy (UV-Vis/DR)

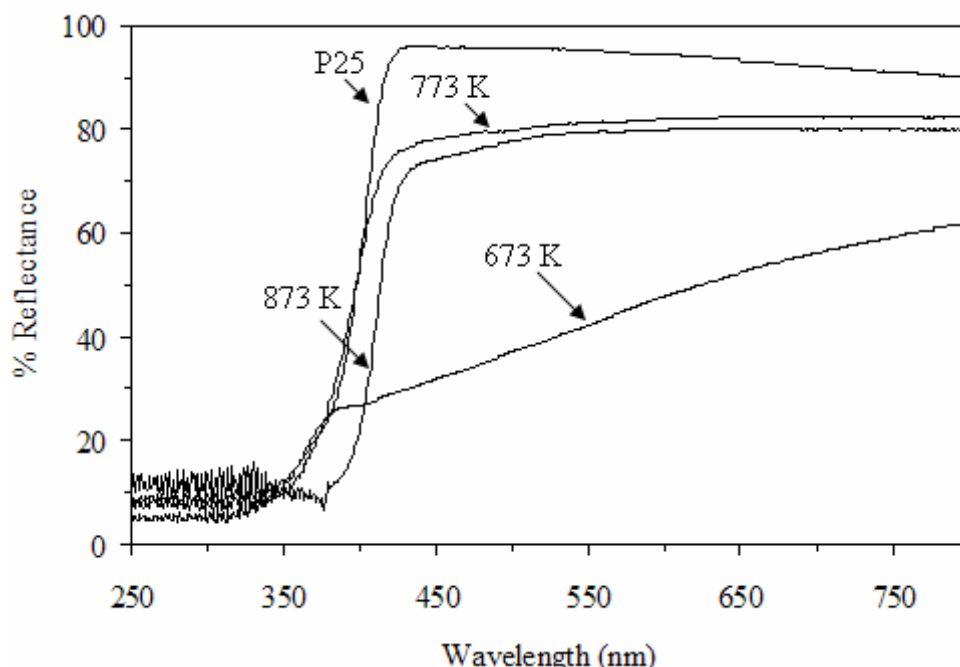


Figure 30 UV-Vis/DR spectra of N-doped TiO_2 using titanium(IV) bis(ethyl acetoacetato)diisopropoxide as a titania precursor and P25 TiO_2 .

The UV-Vis/DR spectrum in Figure 30 of brown N-doped TiO_2 calcined at 673 shows the first absorption edge around 374 nm which is relevant to the band gap of anatase TiO_2 (the procedure for the determination of the absorption edge will be shown in Appendix B). There is no second absorption edge clearly observed in visible region but N-doped TiO_2 calcined at 673 can absorb visible light because of being brown of its color. Then, N-doped TiO_2 calcined at 773 K, of which color is pale ash, shows first absorption edge around 397 nm (Figure 30) related to the band structure of anatase phase. In addition, white-powdered N-doped TiO_2 calcined at 873 K depicts higher wavelength for the first absorption edge at 415 nm (Figure 30) corresponding to the band gap of the rutile phase. Both of N-doped TiO_2 calcined at 773 K and 873 K do not show any prominent absorption edge in the visible range. Moreover, the UV-Vis/DR spectrum (Figure 30) of white P25 TiO_2 shows simply one absorption edge at 405 nm which is also related to its band structure.

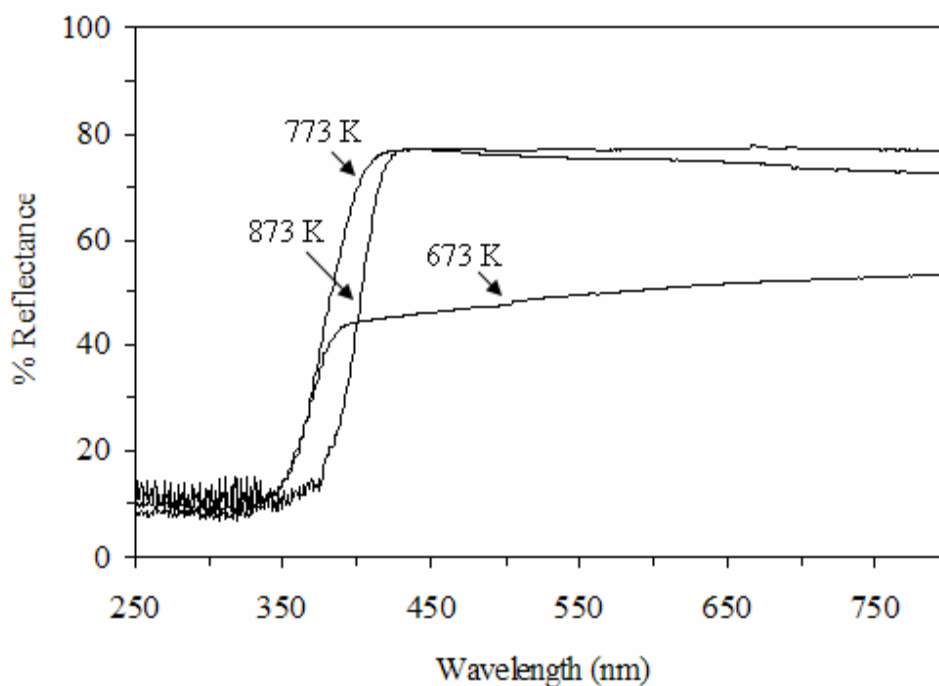


Figure 31 UV-Vis/DR spectra of N-doped TiO₂ using titanium(IV) tetra-n-butoxide as a titania precursor.

UV-Vis/DR spectra in Figure 31 illustrate that ashen N-doped TiO₂ calcined at 673 K shows the absorption edge around 375 nm based on its band gap of anatase. Also, the appearance of absorption edge of N-doped TiO₂ calcined at 773 K is observed at 395 nm consistent with the anatase structure. Furthermore, the anatase-to-rutile phase transformation caused the red shift of the absorption edge of N-doped TiO₂. This can be seen in case of N-doped TiO₂ calcined at 873 K, which shows the absorption edge at 414 nm.

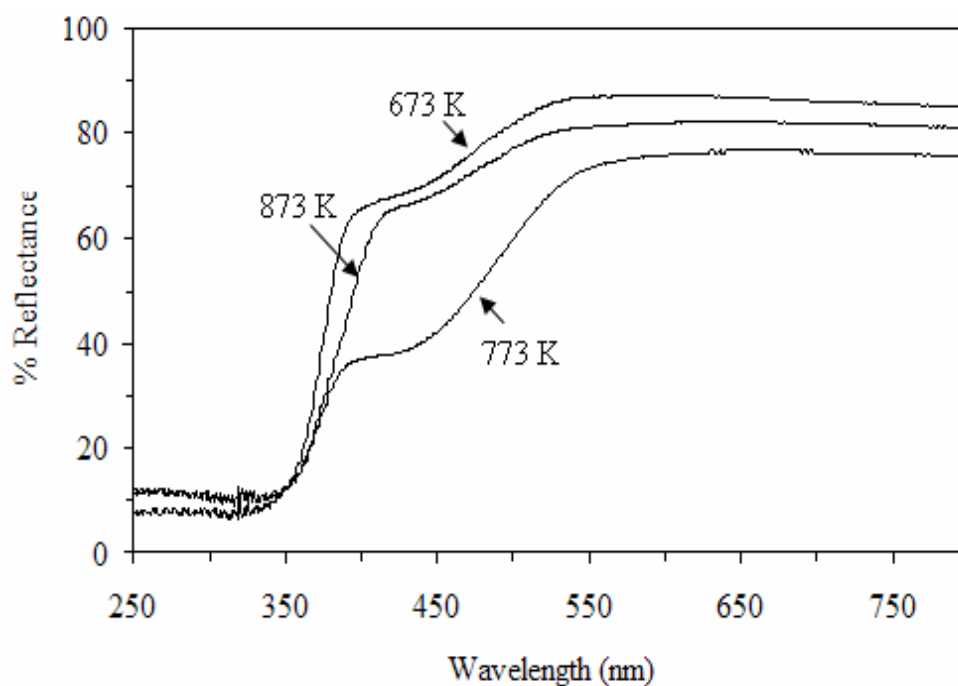


Figure 32 UV-Vis/DR spectra of N-doped TiO₂ using titanium(IV) tetraisopropoxide as a titania precursor.

UV-Vis/DR spectra in Figure 32 exhibit two-step absorption edges of yellow N-doped TiO₂ calcined between 673 and 873 K. The first edges are located between 390 and 415 nm, depending on the band structure of N-doped TiO₂ in each calcination temperature. Theoretically speaking, the anatase band structure provided absorption edge at lower wavelength than that of rutile. Besides, the second edges are apparently shown between 490 and 530 nm. These edges indicate that nitrogen doping had a significant impact on the band structure of TiO₂, which is not clearly discernible in case of N-doped TiO₂ using titanium(IV) bis(ethyl acetoacetato) diisopropoxide and N-doped TiO₂ using titanium(IV) tetra-n-butoxide.

Additionally, Table 7 summarizes the absorption edges (λ) and energy gap values (E_g) of all catalysts. The band energy could be calculated by the equation as follows (Fernandes *et al.*, 2005);

$$E_g = \frac{1239.8}{\lambda} \quad \text{.....(3)}$$

where E_g is band gap energy (eV)

λ is wavelength (nm)

Table 7 Energy gap (E_g) values of all N-doped TiO₂ and P25 TiO₂.

Titania precursors	Calcination temperature (K)	λ_1 (nm)	E_{g1} (eV)	λ_2 (nm)	E_{g2} (eV)
Titanium(IV) bis(ethyl acetoacetato) diisopropoxide	673	374	3.31	-	-
	773	397	3.12	-	-
	873	415	2.99	-	-
Titanium(IV) tetra-n-butoxide	673	375	3.31	-	-
	773	395	3.14	-	-
	873	414	2.99	-	-
Titanium(IV) tetraisopropoxide	673	392	3.16	507	2.45
	773	390	3.18	528	2.35
	873	410	3.02	494	2.51
P25	-	408	3.04	-	-

All of the first observed absorption edges can be elaborated in terms of charge transition corresponding to the excitation of electrons from the valence band (O 2p) to the conduction band (Ti 3d). Meanwhile, the second absorption edges originated from the excitation of electrons from N 2p located above valence band O 2p to conduction band Ti 3d. Therefore, having the nitrogen content in TiO₂ lattice will improve the absorption ability of photocatalysts in the visible region.

1.1.6 Elemental Analysis (EA)

In this characterization technique, it focused on measuring the amount of both nitrogen and carbon. Nitrogen contents originated from the release of remaining NH_3 from hydrolysis reaction or nitrogen species in TiO_2 lattice. Carbon contents stemmed from the decomposition of unhydrolyzed organic species of titania precursors or hydrolyzed organic species adsorbed on the TiO_2 surface.

N-doped TiO_2 using titanium(IV) bis(ethyl acetoacetato) diisopropoxide shows high nitrogen and carbon contents at 573 K (Table 8). This suggests that there were high organic contents after drying process at 393 K because the titania precursor was very difficult to be hydrolyzed with ammonia solution. However, with elevating temperature both nitrogen and carbon contents dramatically decreased due to the decomposition of unhydrolyzed organic species in titanium alkoxide chains, of hydrolyzed organic species adsorbed on TiO_2 surface and of remaining NH_3 . Focusing on the abrupt change of nitrogen contents, it can be assumed that most of nitrogen contents were in the NH_3 solution or weakly-bonded nitrogen species in TiO_2 lattice, all of which tended to be easily terminated. Therefore, the very small amount of nitrogen was detected at 873 K.

N-doped TiO_2 using titanium(IV) tetra-n-butoxide (Table 8) provided 5.35% of carbon and 0.56% of nitrogen at 573 K. This suggests that heating at 393 K was not enough to evaporate the hydrolyzed organic species at the high extent. In other words, the amount of organic species still remained as alkoxides. Nevertheless, the amounts of carbon and nitrogen decreased with increasing calcination temperature, especially carbon contents which were dramatically reduced from 5.35% at 573 K to 0.08% at 873 K. This result demonstrates the presence of weakly-adsorbed carbon and nitrogen species in TiO_2 lattice, all of which were not capable of existing with high temperature.

N-doped TiO_2 using titanium(IV) tetraisopropoxide (Table 8) gave rise to the small amount of nitrogen and carbon at 573 K. This suggests that the

titania precursor was hydrolyzed with NH_3 effectively, and the hydrolyzed organic species could be easily evaporated by preliminarily drying at 393 K because of their low molecular weight. In addition, focusing on the amount of nitrogen, there was a little change with increasing temperature. This indicates that nitrogen was strongly-bonded in TiO_2 lattice so the reduction of nitrogen contents was not observed.

From all EA data, it can be implied that titanium(IV) tetraisopropoxide was easier hydrolyzed with ammonia solution than other titania precursors such as titanium(IV) bis(ethyl acetoacetato)diisopropoxide or titanium(IV) tetra-n-butoxide. As a consequence, nitrogen was able to be doped into TiO_2 lattice with strong bonds, like Ti-N. This idea has been supported from the result that N-doped TiO_2 using titanium(IV) tetraisopropoxide succeeded in maintaining the amount of nitrogen at the high extent with elevating temperature.

Table 8 The amount of nitrogen and carbon of N-doped TiO₂ with various types of titania precursors.

Titania precursor	Calcination temperature (K)	Nitrogen content (%)			Average nitrogen content (%)	Carbon content (%)			Average carbon content (%)
		N ₁	N ₂	N ₃	N _{ave}	C ₁	C ₂	C ₃	C _{ave}
Titanium(IV) bis(ethyl acetoacetato) diisopropoxide	573	3.767	3.786	3.710	3.754	15.97	15.96	15.17	15.70
	673	0.238	0.217	0.255	0.236	0.504	0.514	0.505	0.507
	773	0.043	0.032	0.033	0.036	0.125	0.125	0.098	0.116
	873	0.024	0.017	0.018	0.021	0.112	0.086	0.079	0.093
Titanium(IV) tetra-n-butoxide	573	0.563	0.563	0.555	0.560	5.362	5.328	5.363	5.351
	673	0.082	0.084	0.081	0.083	0.396	0.408	0.411	0.405
	773	0.030	0.028	0.021	0.026	0.085	0.091	0.078	0.085
	873	0.022	0.028	0.030	0.026	0.081	0.080	0.085	0.082
Titanium(IV) tetraiso-propoxide	573	0.060	0.060	0.080	0.066	0.105	0.112	0.099	0.105
	673	0.059	0.054	0.048	0.054	0.085	0.083	0.090	0.086
	773	0.086	0.054	0.059	0.067	0.076	0.064	0.069	0.069
	873	0.084	0.094	0.078	0.085	0.045	0.045	0.046	0.045

In order to investigate all components in N-doped TiO₂ lattice, The XPS technique was adopted by measuring the binding energy of Ti 2p, O 1s and N 1s. The XPS result of N-doped TiO₂ using titanium(IV) bis(ethyl acetoacetato) diisopropoxide exhibits Ti 2p_{3/2} and Ti 2p_{1/2} located in 458.6 eV and 464.1 eV as shown in Figure 33a. These binding energies are the characteristic of Ti⁴⁺ in TiO₂. Next, O 1s peaks are situated at 529.7 eV and 533.6 eV (Figure 33b). The former suggests the presence of Ti-O bonds and the latter indicates the surface adsorbed species such as OH. Last, the N 1s peak at 396.9 eV represents the occurrence of Ti-N bonds and N 1s at 398.6 eV is referred to N-N, N-O or N-C bonds (Figure 33c). According to previous study (Asahi *et al.*, 2001), the active sites of N for photodegradation under visible light were Ti-N states at 396.6 eV. Therefore, this previous result confirms that nitrogen was able to be incorporated by substituting oxygen atoms in TiO₂ lattice.

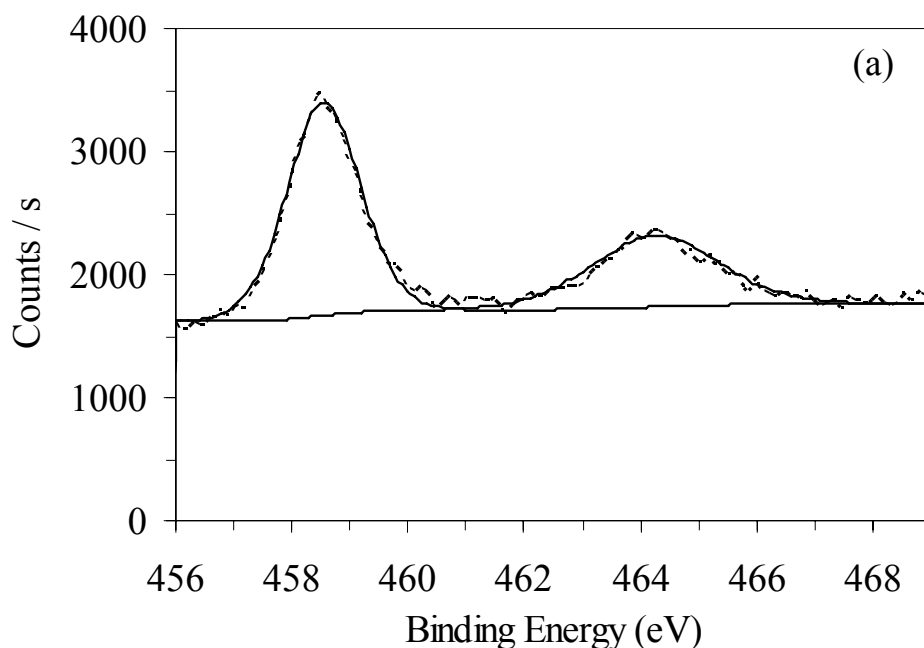


Figure 33 XPS spectra of N-doped TiO₂ using titanium(IV) bis(ethyl acetoacetato) diisopropoxide as a titania precursor with binding energy of (a) Ti 2p, (b) O 1s and (c) N 1s.

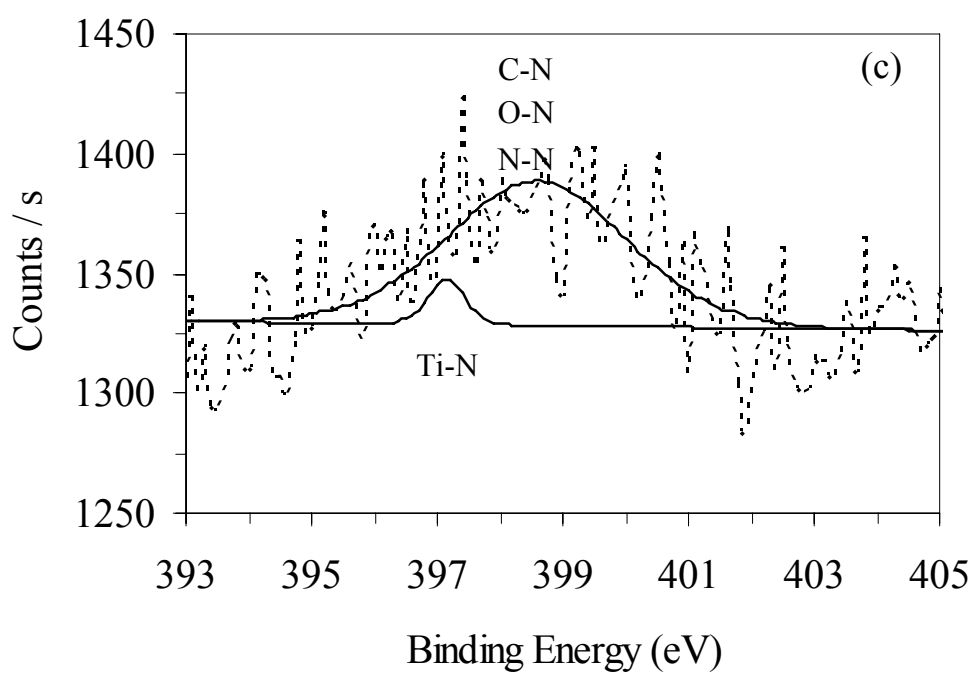
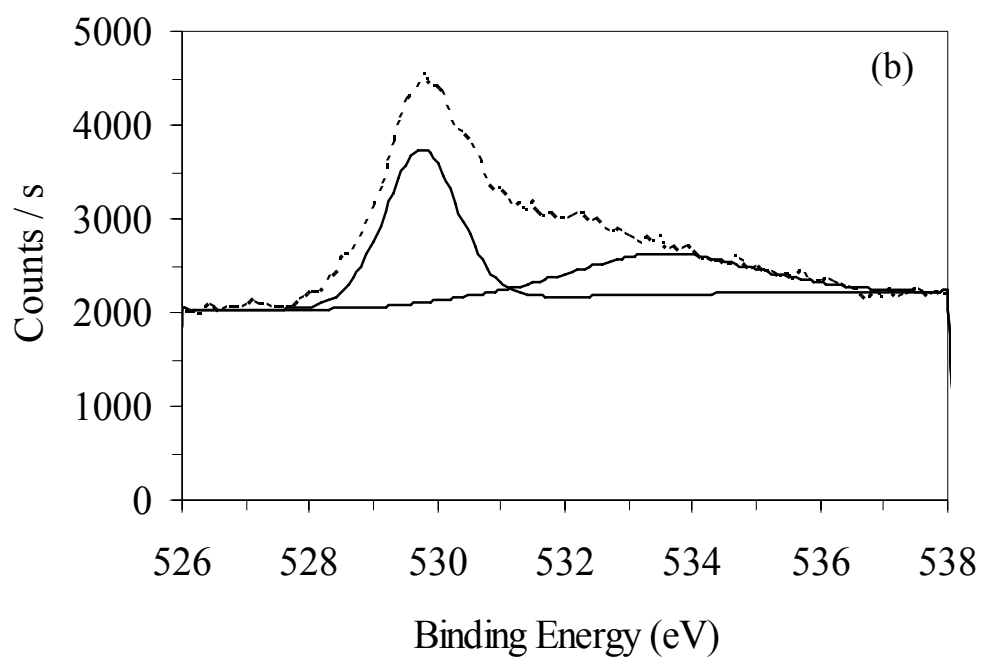


Figure 33 (Continued)

1.1.7 Structural Determination

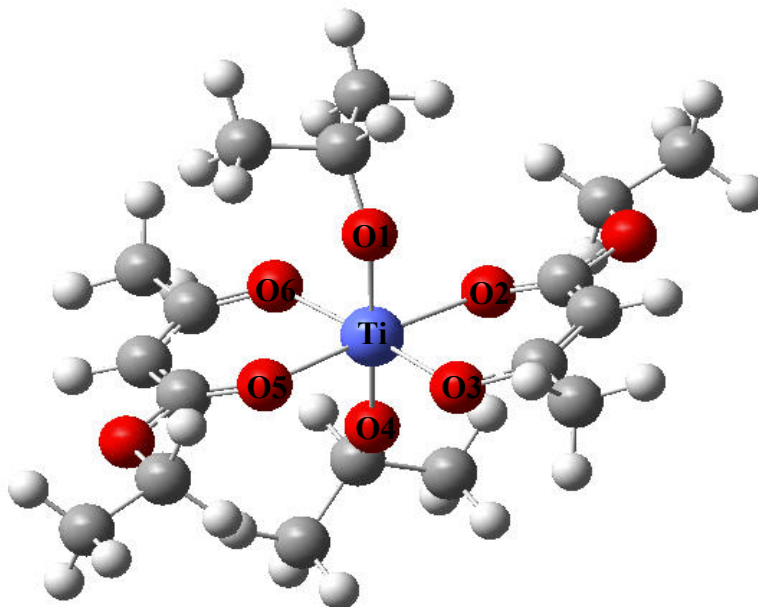


Figure 34 The optimized structure of titanium(IV) bis(ethyl acetoacetato) diisopropoxide.

The structural optimization of each titania precursor by using the Gaussian 03 program suggests that titanium(IV) bis(ethyl acetoacetato) diisopropoxide has a six-coordinate octahedral geometry (Figure 34) even though titanium(IV) coordination compounds have typically a four-coordinate tetrahedral geometry. The two additional bonds of titanium(IV) bis(ethyl acetoacetato) diisopropoxide originated from two carbonyl groups by coordinating via lone pair electrons of oxygen atoms along the equatorial position. The resonant structure with the six-member ring was finally generated. Additionally, isopropoxide groups lie in two axial positions with shorter bond length than equatorial positions. The data of total energy, bond lengths as well as bond angles will be shown in Appendix C.

Figure 35 shows the tetrahedral structure of titanium(IV) tetra-*n*-butoxide. Oxygen atoms serve as the coordinating atoms and butyl groups stretch

out far from oxygen atoms. The whole data of total energy, bond lengths and bond angles will be also shown in Appendix C.

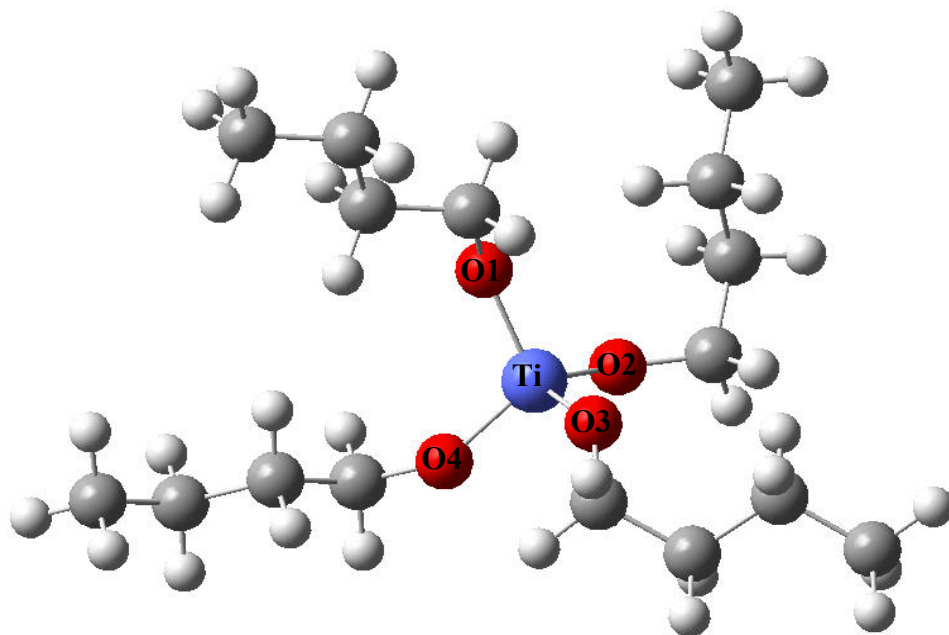


Figure 35 The optimized structure of titanium(IV) tetra-n-butoxide.

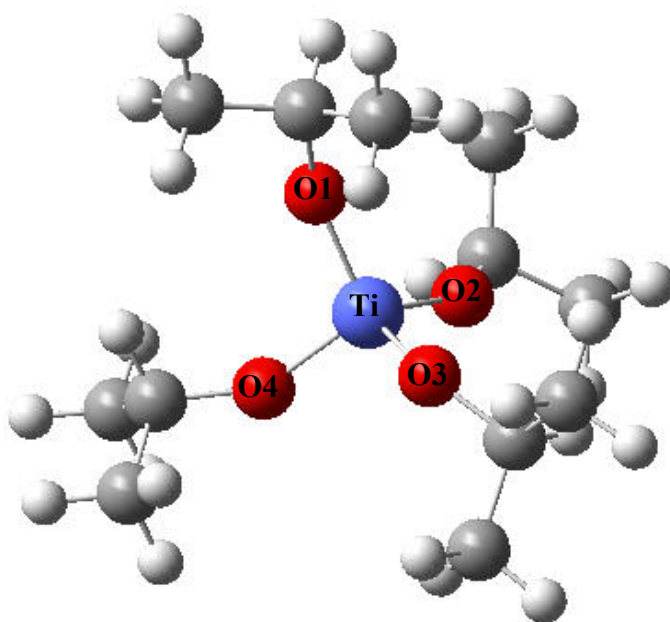


Figure 36 The optimized structure of titanium(IV) tetraisopropoxide.

In Figure 36, the structure of titanium(IV) tetraisopropoxide is the tetrahedral structure with O-coordinate covalent bonds. Meanwhile, isopropyl groups are extended from oxygen atoms. All data of total energy, bond lengths as well as bond angles will be shown in Appendix C. Comparatively, titanium(IV) tetraisopropoxide and titanium(IV) tetra-n-butoxide have lower steric hindrance than titanium(IV) bis(ethyl acetoacetato)diisopropoxide because of their geometry. Thus, they might have much more spatial areas to be attacked with water or ammonia molecules during hydrolysis reaction.

From all characterization techniques, it can be concluded that titanium(IV) tetraisopropoxide is the most appropriate titania precursor for preparing N-doped TiO₂ with ammonia solution. There are many sensible reasons to explicate this conclusion as follows;

- it provided a low percentage of overall weight loss between 273 and 973 K, indicating that nearly all organic contents were eliminated during preliminarily drying process at 393 K. Obviously, titanium(IV) tetraisopropoxide has a high ability to be hydrolyzed with ammonia solution therefore nitrogen was able to incorporate into TiO₂ lattice with Ti-N bonds.
- titanium(IV) tetraisopropoxide provided the highest crystallinity of N-doped TiO₂, especially anatase phase at 673 K. Even though N-doped TiO₂ using titanium(IV) tetraisopropoxide has a large crystallite size, its phase transformation with increasing temperature was retarded by the effect of nitrogen doping. Moreover, its surface morphology is spherical like fluffy powders.
- the effect of nitrogen doping on the absorption ability of TiO₂ was evidently seen in the occurrence of the second edge absorption in visible region which showed the ability of absorbing the visible light. Moreover, the amount of nitrogen was not decreased with increasing calcination temperature, suggesting that nitrogen stayed in TiO₂ as strong bonds with Ti (Ti-N).

1.2 Effect of nitrogen sources

1.2.1 Thermal Gravimetric Analysis (TGA)

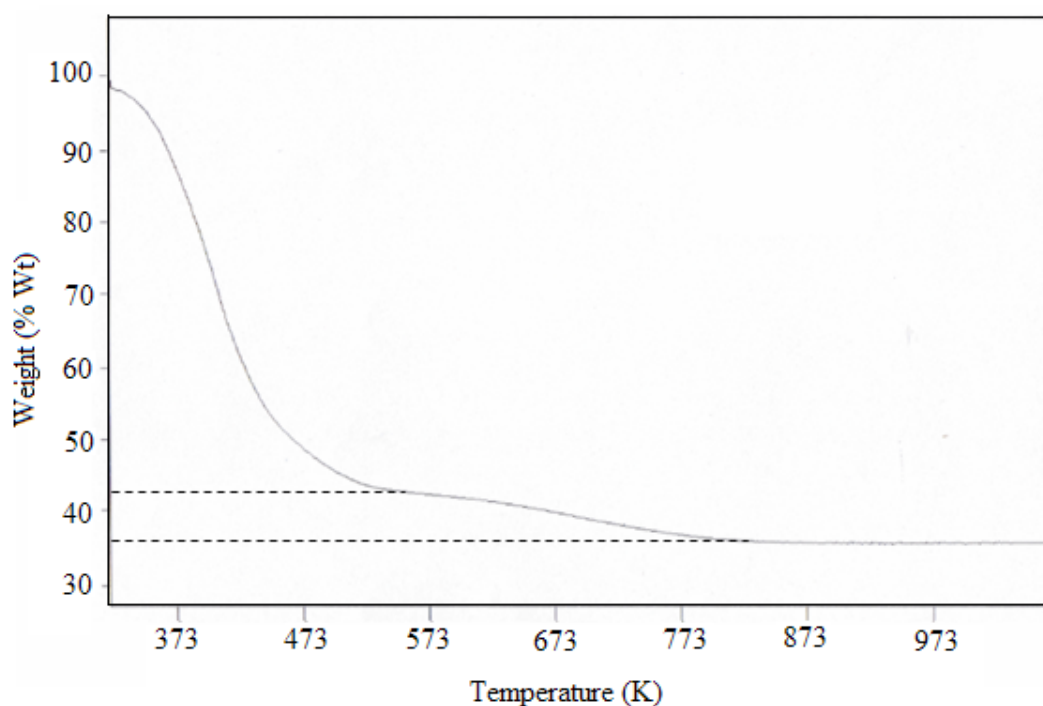


Figure 37 The TG curve of as-prepared N-doped TiO_2 using $(\text{NH}_2)_2\text{CO}$ as a nitrogen source.

Figure 37 illustrates two steps of weight loss in the TG curve of N-doped TiO_2 . The first step between 273 and 563 K is about the 57% weight loss of loosely-bound species on the surface of TiO_2 . The second step between 563 and 823 K shows 9% weight loss resulting from the tightly-bound species in the TiO_2 structure.

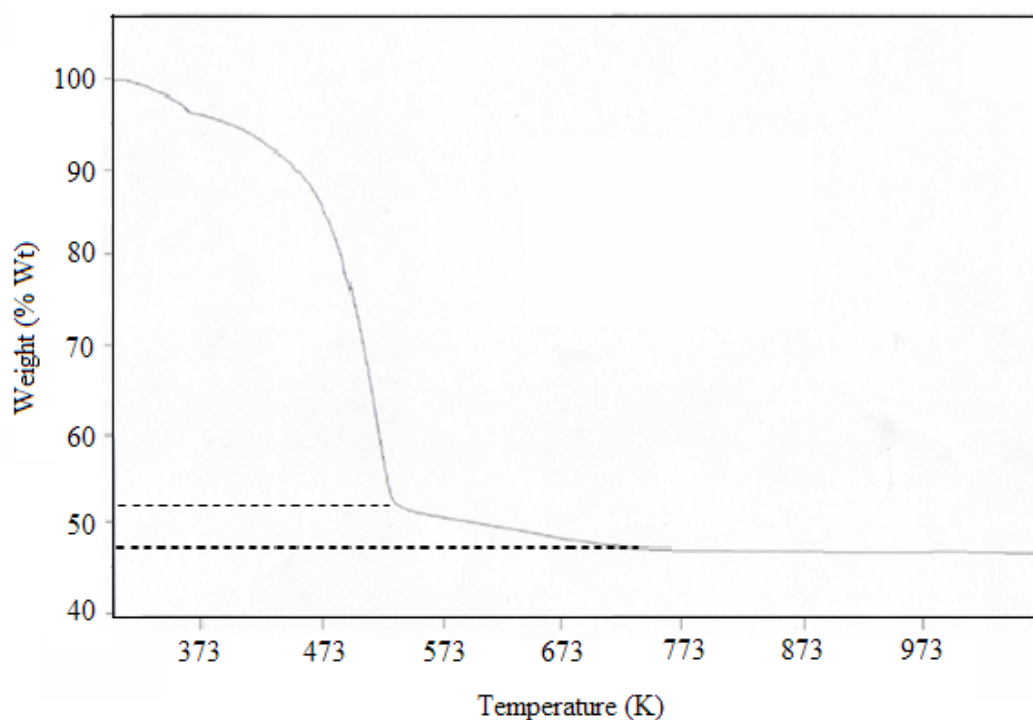


Figure 38 The TG curve of as-prepared N-doped TiO_2 using NH_4Cl as a nitrogen source.

The TG curve as shown in Figure 38 also exhibits two main steps of weight loss. Firstly, a high amount of weight loss around 48% was detected between 273 and 500 K, suggesting the removal of weakly-adsorbed species on TiO_2 surface. Secondly, between 500 and 753 K, 6% weight loss was attributed to the elimination of latent species in the TiO_2 structure.

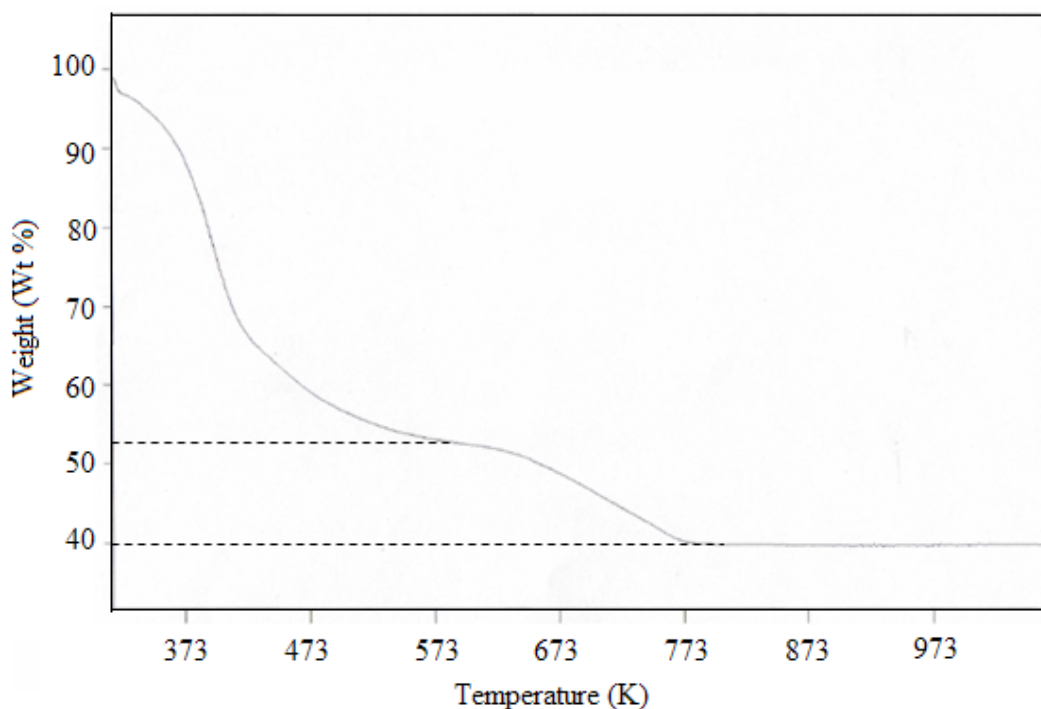


Figure 39 The TG curve of as-prepared N-doped TiO_2 using NH_3 as a nitrogen source.

The TG curve of N-doped TiO_2 in Figure 39 shows two clear steps of weight loss. First, between 273 and 573 K, 48% weight loss originated from the release of weakly-adsorbed species on the surface of TiO_2 . Second, 12% weight loss between 573 and 773 K resulted from the removal of strongly-adsorbed species in the TiO_2 structure.

Compared to previous study, like in the Section 1.1.1, all TG curves of three N-doped TiO_2 can be implied that the first step of weight loss was associated with hydrolyzed organic species that were weakly adsorbed on the surface and the rest of the nitrogen source. The second step of weight loss was involved in dormant organic molecules as alkoxide chains (Ti-O-R) of titania precursors difficult to be hydrolyzed. Moreover, NH_4Cl seems to be the best nitrogen source for preparing N-doped TiO_2 because the amount of overall weight loss (54%) is less than that of other nitrogen sources. This indicates that NH_4Cl has the higher ability to hydrolyze

the titania precursor so most organic molecules were evaporated by preliminarily drying process at 393 K. However, it is cautious that chloride anions might cause a negative impact on the formation of N-doped TiO₂ by blocking nitrogen doping.

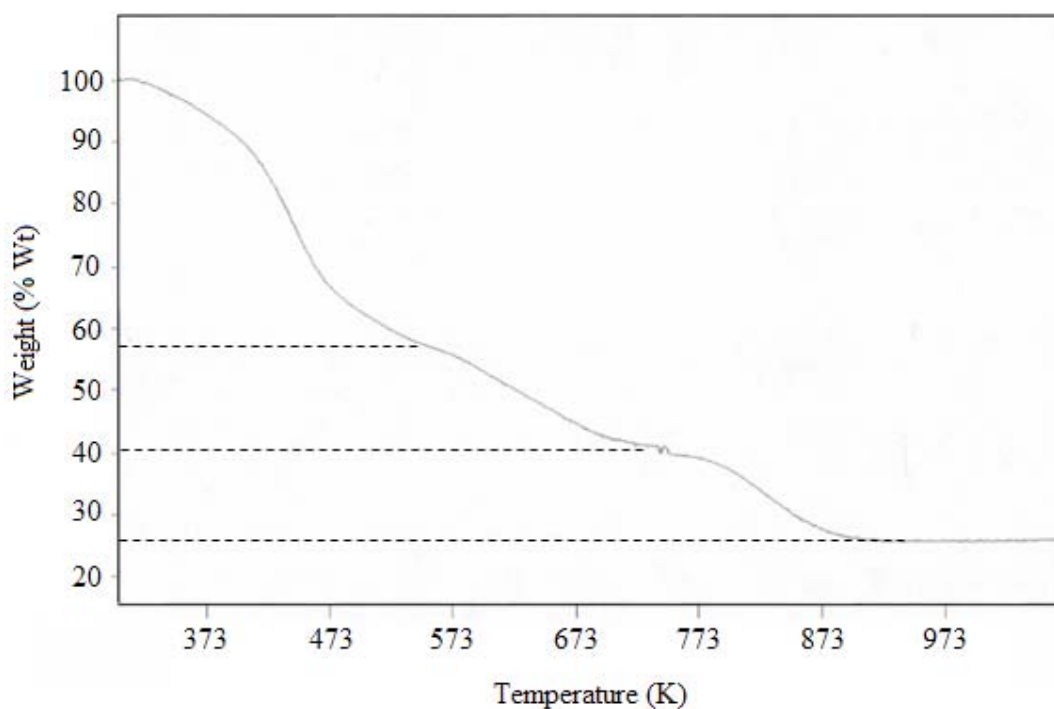


Figure 40 The TG curve of as-prepared N-doped TiO₂ using N₂H₄.H₂O as a nitrogen source.

In other words, the TG curve of N-doped TiO₂ using hydrazine hydrate (Figure 40) is somewhat different from the first three TG curves as mentioned above. It provided three steps of weight loss between 273 and 973 K. The first two steps of weight loss (42% and 17%) between 273 and 730 K originated from the removal of weakly- and hardly-adsorbed species. Additionally, the TG curve of N-doped TiO₂ using N₂H₄.H₂O shows further 15% weight loss between 730 and 913 K. This suggests that almost all titania precursors were not hydrolyzed by N₂H₄.H₂O because hydrazine is an active chemical which was burned in air at a relative low temperature (Li *et al.*, 2007). Therefore, most organic species as Ti-O-R groups needed to be terminated at very high temperature.

In comparison with each nitrogen source, NH_3 and $(\text{NH}_2)_2\text{CO}$ seem to be the good candidates for preparing N-doped TiO_2 because they did not have any interference from chloride anions. Moreover, they also were able to hydrolyze the titania precursor at the certain extent, unlike $\text{N}_2\text{H}_4\cdot\text{H}_2\text{O}$.

1.2.2 X-ray Diffraction (XRD)

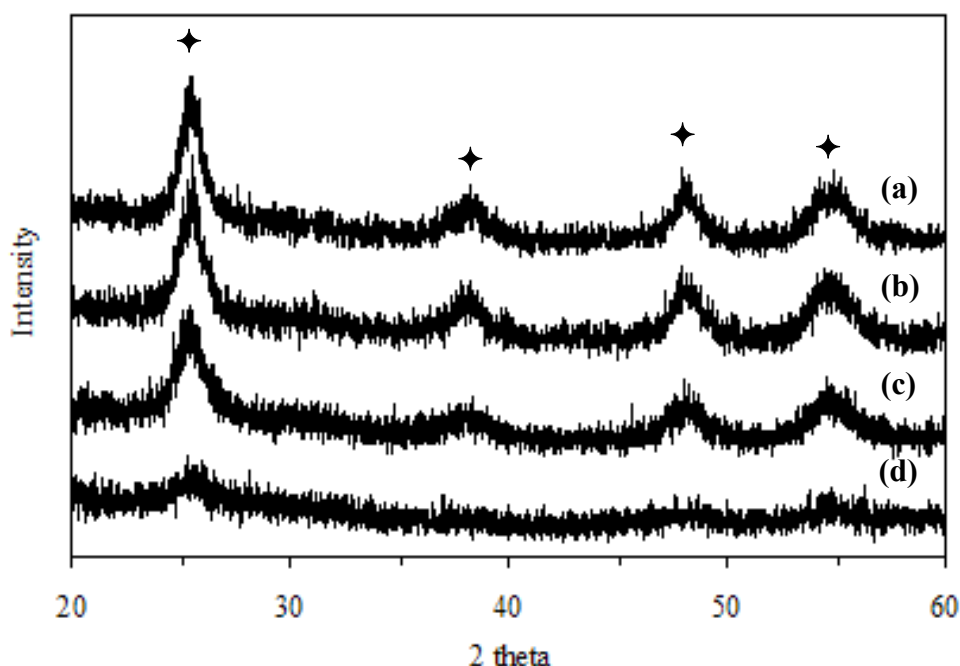


Figure 41 The XRD patterns of N-doped TiO_2 using various types of nitrogen sources; (a) $(\text{NH}_2)_2\text{CO}$, (b) NH_4Cl , (c) NH_3 and (d) $\text{N}_2\text{H}_4\cdot\text{H}_2\text{O}$ with fixed calcination temperature at 673 K.
(◆ for the anatase phase)

From the XRD patterns, it is evidently seen that N-doped TiO_2 using $(\text{NH}_2)_2\text{CO}$, NH_3 or NH_4Cl (Figure 41a-c) shows diffraction angles at 2θ of 25.5° , 38.2° , 48.2° and 55.1° which were ascribed to the anatase structure. However, there is no the presence of rutile phase. Regarding $\text{N}_2\text{H}_4\cdot\text{H}_2\text{O}$, N-doped TiO_2 did not give any apparent peaks at any diffraction angles (2θ), indicating that its structure is amorphous. Furthermore, with respect to the crystallite size of all N-doped TiO_2 as

shown in Table 9, NH_3 provided the smaller crystallite size of N-doped TiO_2 around 9.05 nm with calcination temperature at 673 K. Meanwhile, N-doped TiO_2 using $(\text{NH}_2)_2\text{CO}$ and N-doped TiO_2 using NH_4Cl had quite similar crystallite sizes, 9.93 and 9.81 nm, respectively.

Table 9 Effect of the nitrogen sources on the crystallite size and phase composition of N-doped TiO₂.

Nitrogen source	Calcination temperature (K)	Phase ^a	2 θ (degree)	Cos θ	β (degree)	β (radian)	Crystallite size (nm) ^b
Ammonia	673	A	25.455	0.975	0.90	0.0157	9.05
Urea	673	A	25.455	0.975	0.82	0.0143	9.93
Ammonium chloride	673	A	25.335	0.976	0.83	0.0145	9.81
Hydrazine hydrate	673	-	-	-	-	-	-

^aA stands for anatase.

^bThe crystallite size was calculated by using Sherrer's equation.

1.2.3 Raman Spectroscopy

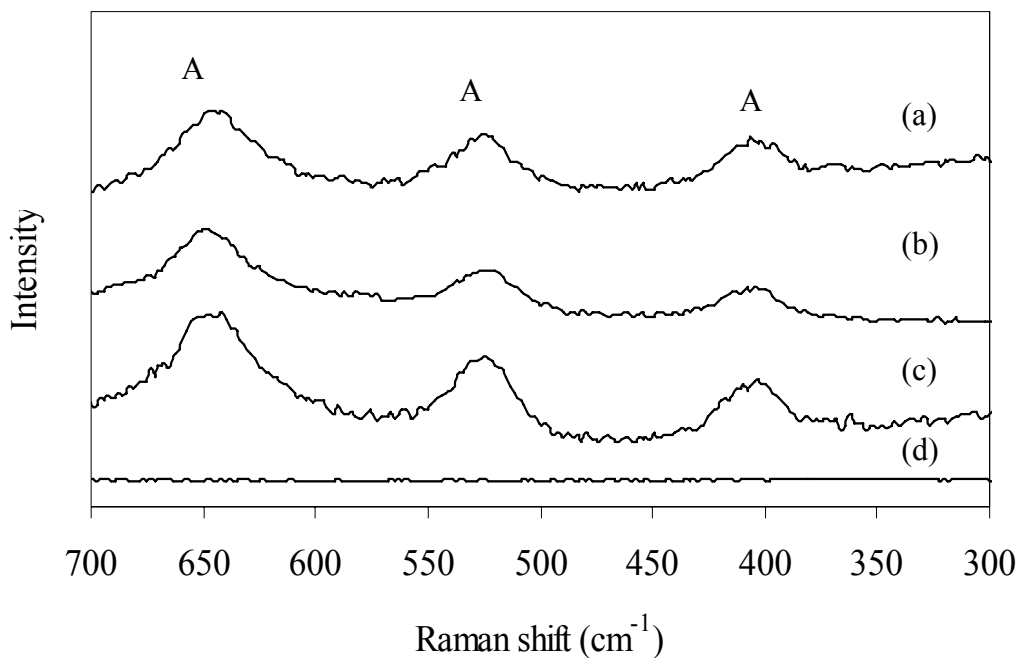


Figure 42 Raman spectra of N-doped TiO₂ using various types of nitrogen sources; (a) (NH₂)₂CO, (b) NH₄Cl, (c) NH₃ and (d) N₂H₄.H₂O with fixed calcination temperature at 673 K. (“A” for anatase phase)

Raman spectra of N-doped TiO₂ in Figure 42 suggest that N-doped TiO₂ using (NH₂)₂CO, NH₄Cl or NH₃ provided the anatase phase at calcination temperature of 673 K which occurs at Raman Shift of 399 cm⁻¹, 519 cm⁻¹ and 639 cm⁻¹, respectively. On the other hand, N-doped TiO₂ using N₂H₄.H₂O does not show any Raman shifts, indicating that it is amorphous. Comparatively, all of these Raman results are in good agreement with the XRD results.

1.2.4 Scanning Electron Microscopy (SEM) and Transmission Electron Microscopy (TEM)

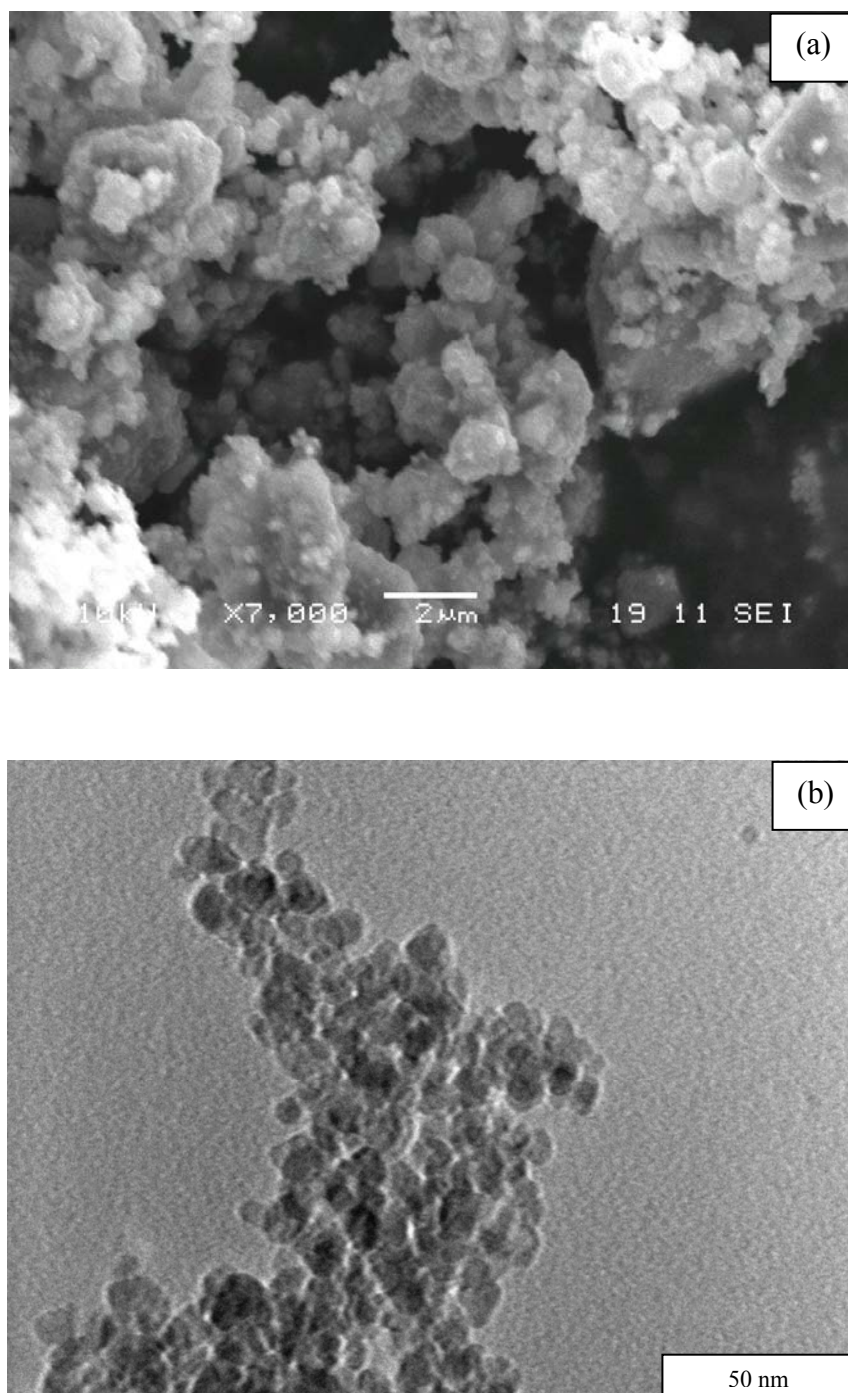


Figure 43 (a) SEM and (b) TEM images of N-doped TiO₂ using (NH₂)₂CO as a nitrogen source and calcined at 673 K.

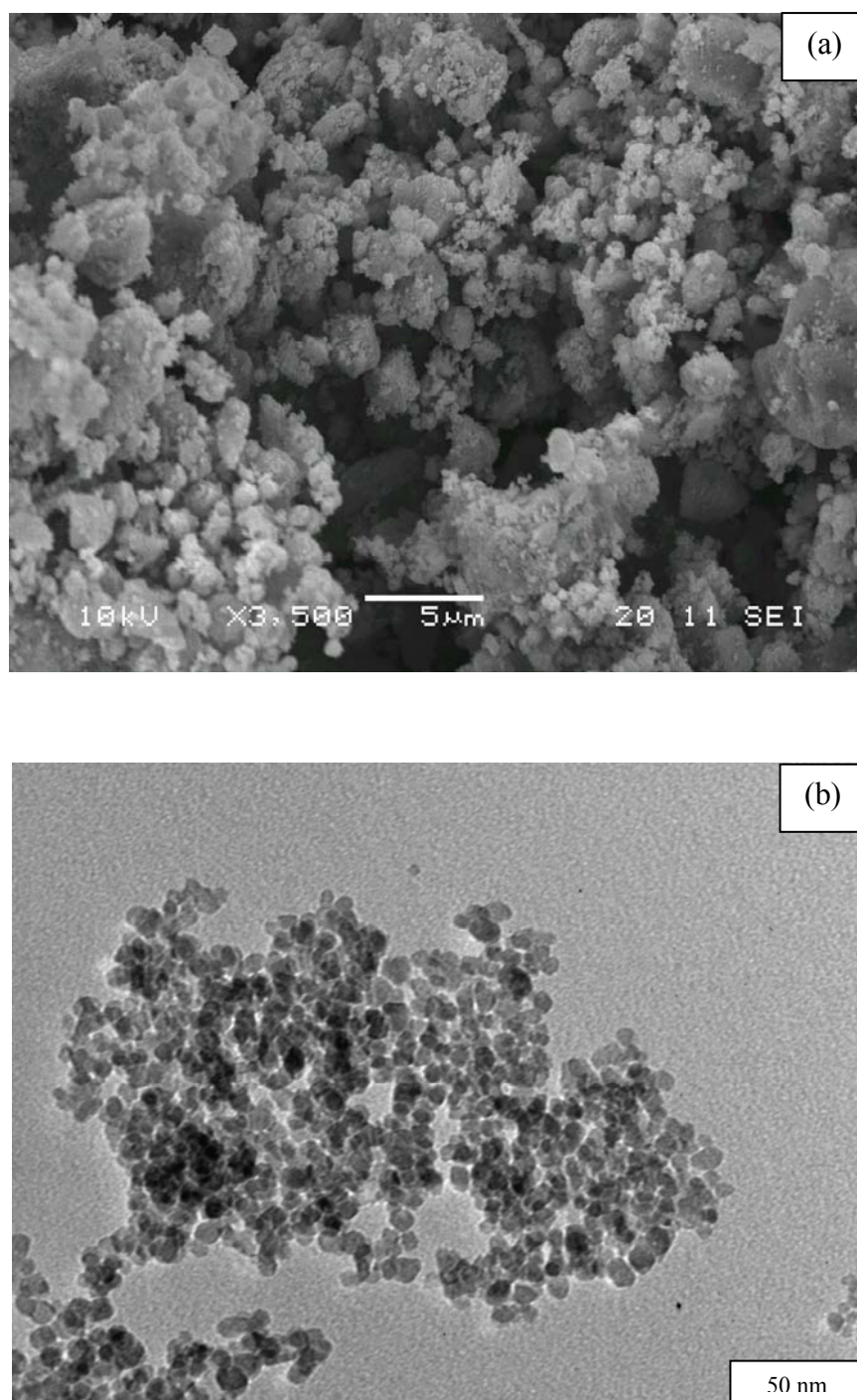


Figure 44 (a) SEM and (b) TEM images of N-doped TiO₂ using NH₄Cl as a nitrogen source and calcined at 673 K.

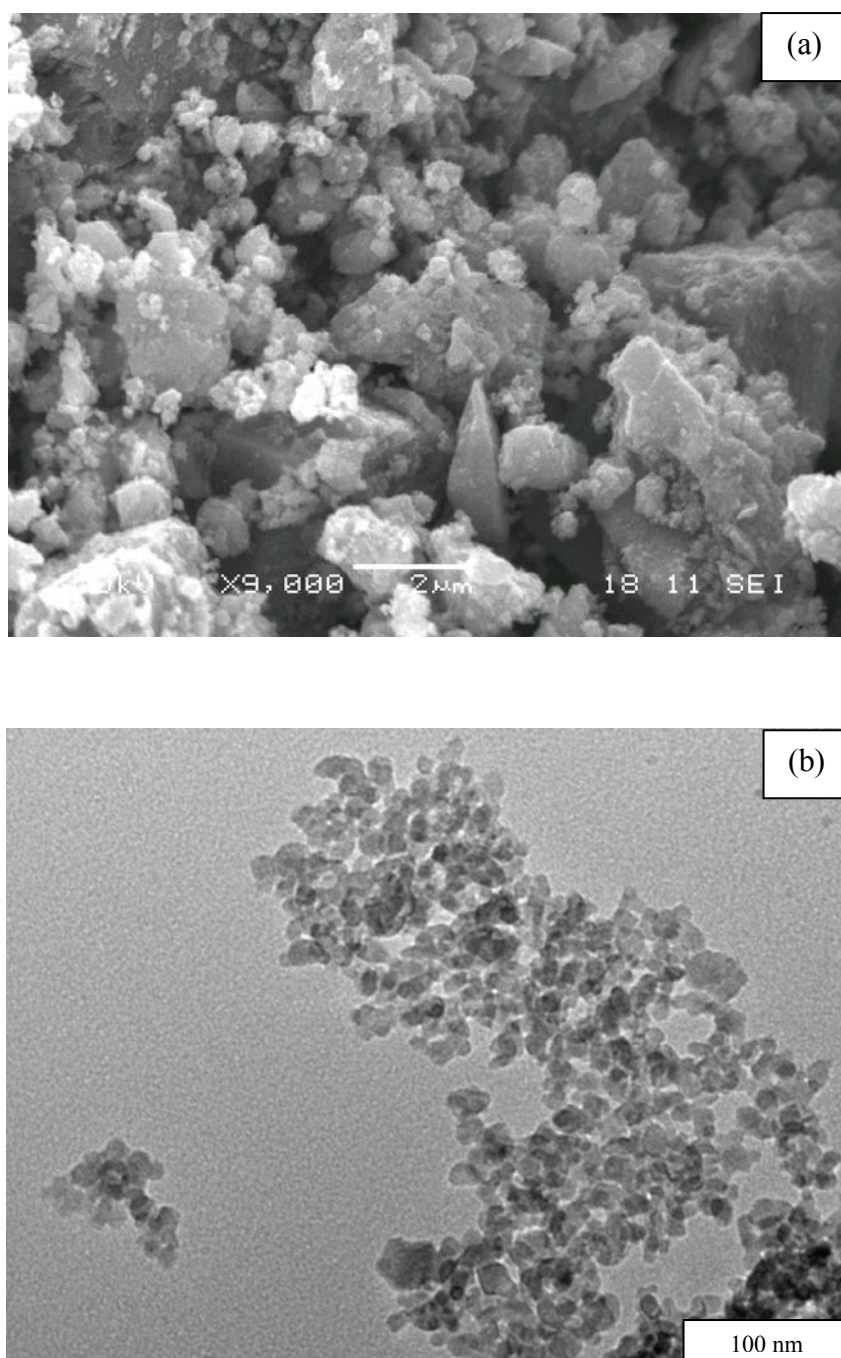


Figure 45 (a) SEM and (b) TEM images of N-doped TiO₂ using NH₃ as a nitrogen source and calcined at 673 K.

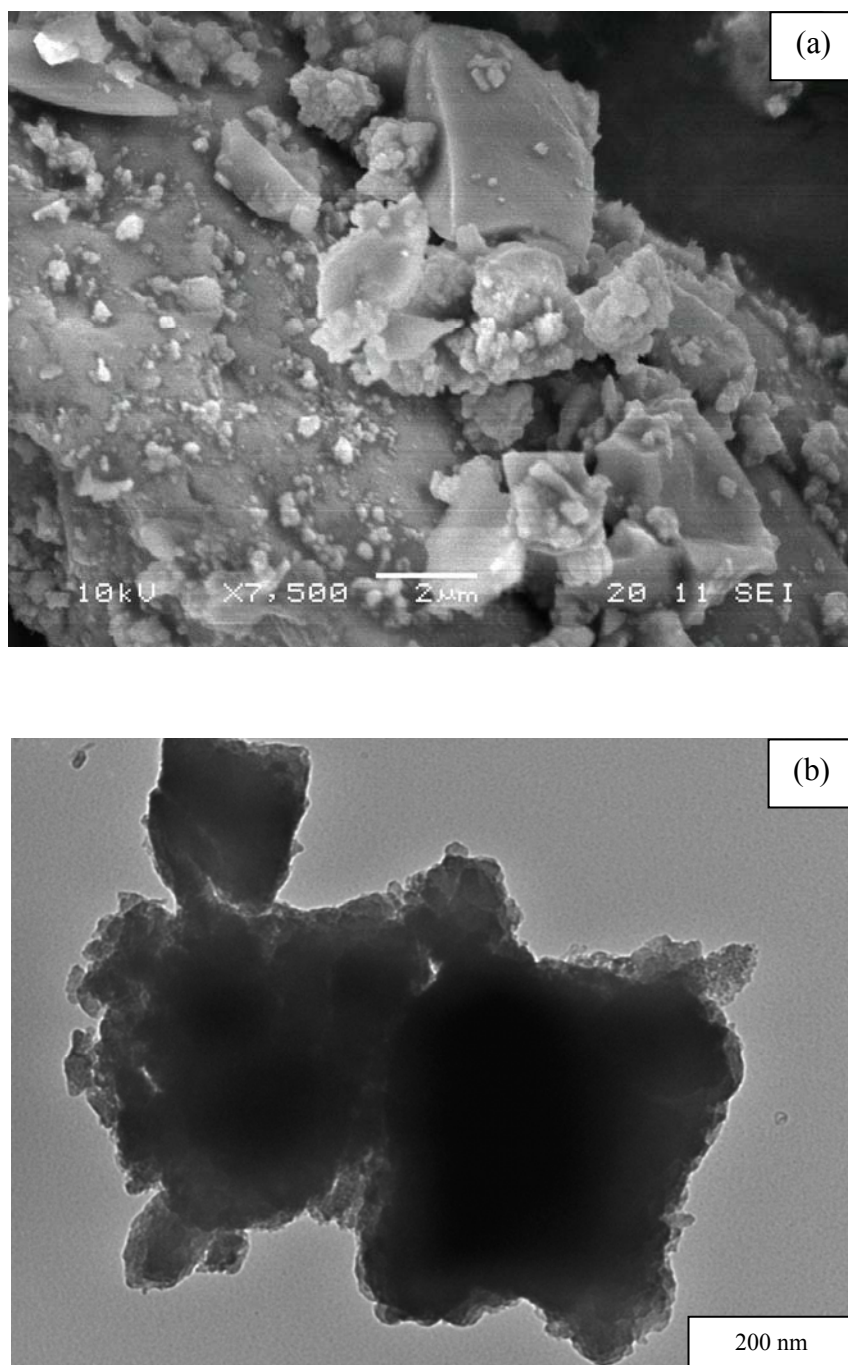


Figure 46 (a) SEM and (b) TEM images of N-doped TiO_2 using $\text{N}_2\text{H}_4\cdot\text{H}_2\text{O}$ as a nitrogen source and calcined at 673 K.

The SEM images (Figure 43a, 44a and 45a) of the first three types of N-doped TiO₂ show that there are the mixture of surface morphology between fluffy grains and semi-solid mass. This phenomenon originated from using the inappropriate titania precursor, titanium(IV) bis(ethyl acetoacetato) diisopropoxide, which was difficult to be hydrolyzed by each type of N sources, (NH₂)₂CO, NH₄Cl and NH₃. Hence, remaining Ti-O-R groups were necessarily decomposed at high temperature and finally forced the occurrence of the two different morphologies. However, the morphology of the first three types of N-doped TiO₂ differs from that of N-doped TiO₂ using N₂H₄.H₂O (Figure 46a). The surface morphology of N-doped TiO₂ using N₂H₄.H₂O looks only semi-solid black mass because almost all Ti-O-R changed into TiO₂ via the decomposition reaction.

From the TEM results (Figure 43b, 44b and 45b), the first three types of N-doped TiO₂ samples provided the spherical and quite roughly monodispersed particles. The average particles, determined from the diameters of randomly selected 50 particles, are 9.59 nm for N-doped TiO₂ using (NH₂)₂CO, 9.15 nm for N-doped TiO₂ using NH₄Cl, 8.91 nm for N-doped TiO₂ using NH₃, respectively. In case of N-doped TiO₂ using N₂H₄.H₂O, the TEM image (Figure 46b) shows the big particle of the sample. On the edge of the particle, there are some small powders attached to its surface. In this case, its particle size was unlikely to be measured.

1.2.5 Elemental Analysis (EA)

At 673 K, the amount of nitrogen found in each N-doped TiO₂ with numerous types of nitrogen sources is 3.315% for N₂H₂.H₂O, 0.236% for NH₃, 0.131% for (NH₂)₂CO and 0.062% for NH₄Cl, respectively (Table 10). From these results, N-doped TiO₂ using N₂H₂.H₂O has the highest amount of nitrogen. However, its nitrogen contents were assumed to be a weakly-adsorbed species on the TiO₂ particles because it is amorphous in the Ti-O-R form. Moreover, the EA result of carbon contents may support the fact that there were still most Ti-O-R or organic residuals because of a high amount of carbon detected at calcination temperature of 673 K. In case of N-doped TiO₂ using NH₄Cl, the lowest amount of nitrogen, it is important to point out that Cl⁻ might block nitrogen to incorporate into TiO₂ lattice. Therefore, NH₃ and (NH₂)₂CO seem to be reasonable to be used in the preparation of N-doped TiO₂. In addition, the example of the formation of Ti-N bonds in N-doped TiO₂ using NH₃ via the XPS technique was shown in Section 1.1.5 as well.

From all characterization techniques, it can be implied that NH₃ was supposed to be the best nitrogen source for preparing N-doped TiO₂ with titanium(IV) bis(ethyl acetoacetato)diisopropoxide. There are many compelling reasons to support this assumption as follows;

- although NH₃ provided the remaining of strongly-bonded organic species in the N-doped TiO₂, it was able to maintain a higher amount of nitrogen in TiO₂ lattice as Ti-N bonds, compared to (NH₂)₂CO or NH₄Cl except for N₂H₄.H₂O.
- in particular, it has the smaller crystallite size around 9 nm with the anatase structure at calcination temperature of 673 K. Despite of the fact that its surface morphology is composed of the fluffy powders and semisolid mass.

Table 10 The amount of nitrogen and carbon of N-doped TiO₂ with various types of nitrogen sources.

Nitrogen source	Calcination temperature (K)	Nitrogen content (%)			Average nitrogen content (%)	Carbon content (%)			Average carbon content (%)
		N ₁	N ₂	N ₃	N _{ave}	C ₁	C ₂	C ₃	C _{ave}
Ammonia	673	0.238	0.217	0.255	0.236	0.504	0.514	0.505	0.507
Urea	673	0.133	0.125	0.136	0.131	0.280	0.282	0.275	0.279
Ammonium chloride	673	0.059	0.063	0.064	0.062	0.126	0.120	0.137	0.128
Hydrazine hydrate	673	3.316	3.324	3.307	3.315	7.696	7.682	7.568	7.648

2. Photocatalytic activity

2.1 Photodegradation of phenanthrene

2.1.1 Effect of titania precursors

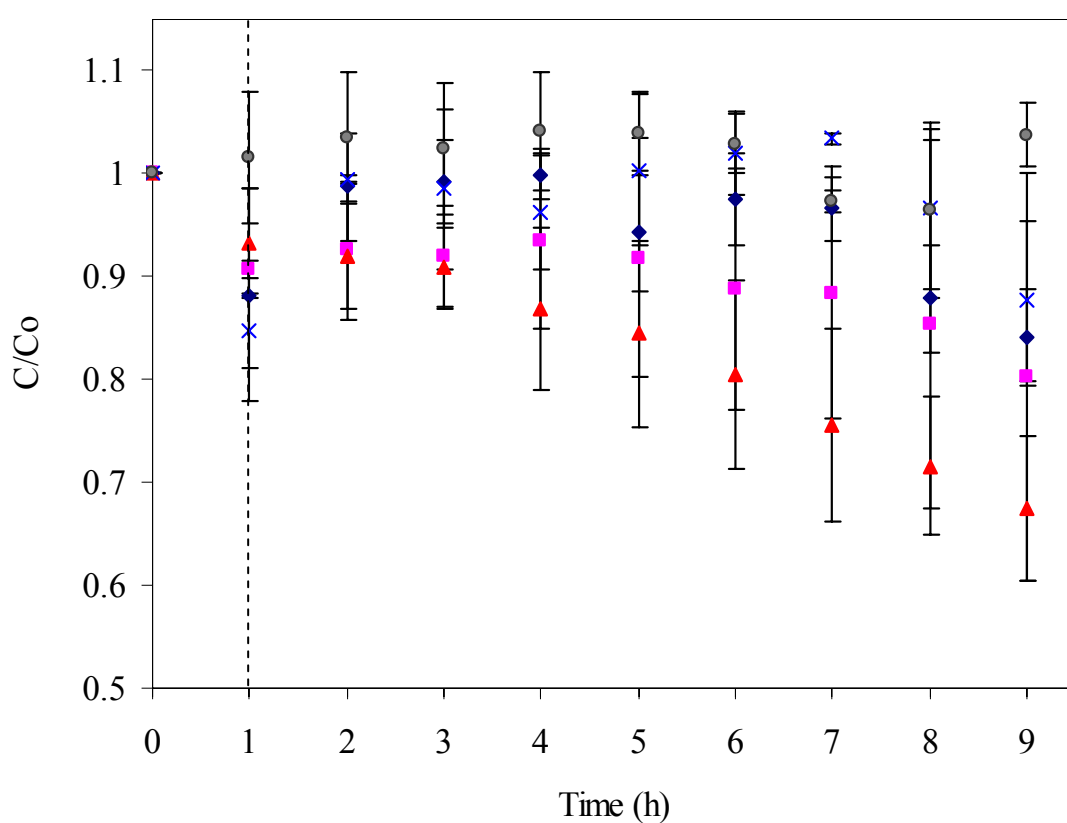


Figure 47 Photodegradation of phenanthrene by N-doped TiO_2 using NH_3 and various types of titania precursors; (a) titanium(IV) tetraisopropoxide (\blacktriangle), (b) titanium(IV) tetra-n-butoxide (\blacksquare) and (c) titanium(IV) bis(ethyl acetoacetato)diisopropoxide (\blacklozenge), and calcined at 673 K, compared to (d) P25 TiO_2 (\times) and without catalysts (\bullet).

(Note: raw data are shown in Appendix D.)

The results of photocatalytic activities (Figure 47) and rate constants (Table 11) of each type of N-doped TiO₂ calcined at 673 K, including P25 TiO₂ indicates that N-doped TiO₂ using titanium(IV) tetraisopropoxide provided the best catalytic efficiency. It was able to degrade phenanthrene with the highest conversion of 33% and rate constant of 0.058 h⁻¹ because of its crystallinity, morphology and the amount of doped nitrogen as Ti-N. Meanwhile, N-doped TiO₂ using titanium(IV) tetra-n-butoxide gave 19% conversion of phenanthrene with the rate constant of 0.034 h⁻¹. This suggests that although it has smaller crystallite size (9.41 nm), its catalytic activity under visible light is not high proportionally because there has been a small amount of strongly-bonded nitrogen in its structure. In other words, the 16% conversion and 0.054 h⁻¹ rate constant belongs to N-doped TiO₂ using titanium(IV) bis(ethyl acetoacetato)diisopropoxide, indicating that even though this N-doped TiO₂ photocatalyst has the high amount of nitrogen, its catalytic activity is not enhanced. This can be assumed that, firstly, some nitrogen species entrapped in TiO₂ are inactive species to photocatalytic degradation such as weakly-adsorbed nitrogen species on the surface of TiO₂. Secondly, some parts of the N-doped TiO₂ are still amorphous because the XRD peak at 2θ of 25.4° is so broad. Thirdly, the surface morphology has the mixture between fluffy grains and semisolid mass. The later morphology normally provided the bigger size, which reduced the specific surface area. Hence, the photocatalytic efficiency is the lowest. Moreover, P25 TiO₂ was also capable of degrading phenanthrene at the 12% conversion of phenanthrene with the rate constant of 0.052 h⁻¹. This phenomenon can be explained by the synergistic interaction between anatase and rutile phases. As previous study (Smirniotis *et al.*, 2003), when anatase attached to rutile, it would cause band bending which reduced the possibility of electron-hole recombination. This might enhance the photocatalytic activity of P25 TiO₂. In case of without catalysts, there is no change in the relative concentration of phenanthrene. This result can be implied that all of degraded phenanthrene originated from the photocatalytic reaction rather than the thermal decomposition reaction.

Besides, under dark reaction in the first one hour, it is evident that the relative concentration of phenanthrene was decreased, suggesting that

phenanthrene was physically adsorbed on the surface of N-doped TiO₂. After switching the light on, the relative concentration of phenanthrene gradually decreased in case of N-doped TiO₂ using titanium(IV) tetraisopropoxide. On the contrary, the other photocatalysts show the increase of the relative concentration of phenanthrene again. This can be implied that N-doped TiO₂ using titanium(IV) tetraisopropoxide was able to degrade phenanthrene immediately that the light was turned on. However, N-doped TiO₂ using titanium(IV) tetra-n-butoxide, N-doped TiO₂ using titanium(IV) bis(ethyl acetoacetato)diisopropoxide and P25 TiO₂ led to the desorption of phenanthrene from their surface rather than sudden degradation of phenanthrene after turning the light on. It is inferred that rate of phenanthrene desorption was higher than that of phenanthrene degradation on their surface. After that, they had just abilities to gradually degraded phenanthrene, especially on the last period of degrading time.

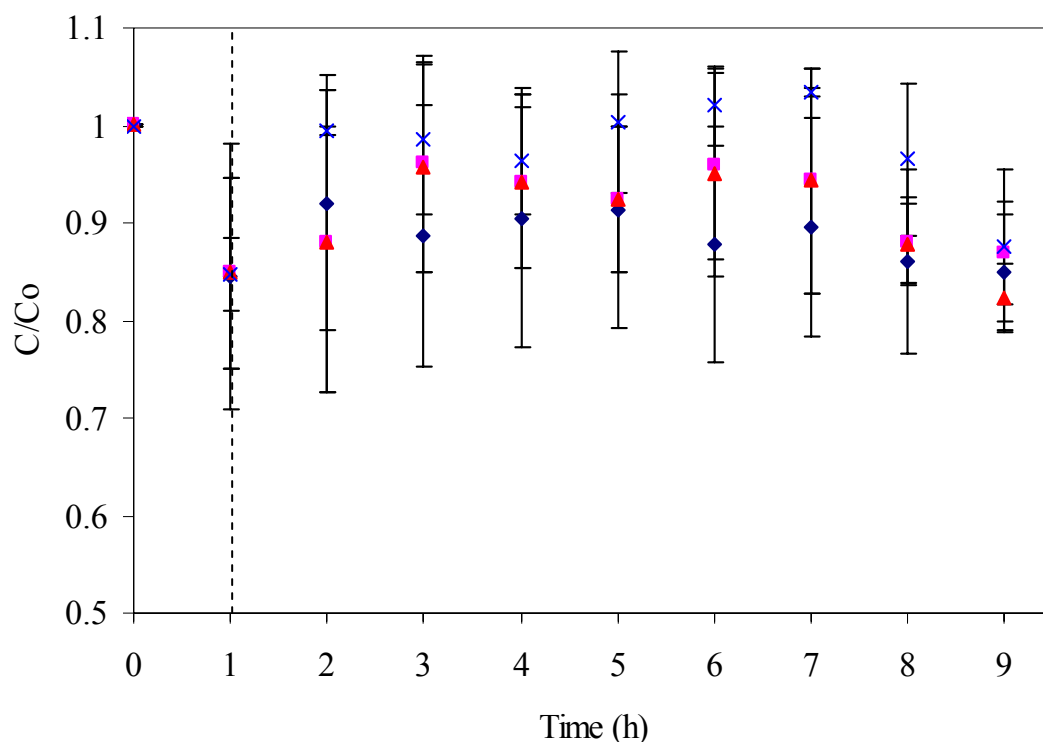


Figure 48 Photodegradation of phenanthrene by N-doped TiO_2 using NH_3 and various types of titania precursors; (a) titanium(IV) tetraisopropoxide (\blacktriangle), (b) titanium(IV) tetra-n-butoxide (\blacksquare) and (c) titanium(IV) bis(ethyl acetoacetato)diisopropoxide (\blacklozenge), and calcined at 773 K, compared to (d) P25 TiO_2 (\times).

(Note: raw data are shown in Appendix D.)

The photocatalytic activities (Figure 48) and rate constants (Table 11) of each N-doped TiO_2 calcined at 773 K demonstrate that it has lower abilities in degrading phenanthrene compared to N-doped TiO_2 calcined at 673 K. Its catalytic efficiency determined by the conversion of phenanthrene is 18% for N-doped TiO_2 using titanium(IV) tetraisopropoxide, 13% for N-doped TiO_2 using titanium(IV) tetra-n-butoxide and 15% for N-doped TiO_2 using titanium(IV) bis(ethyl acetoacetato)diisopropoxide. In particular, N-doped TiO_2 using titanium(IV) tetraisopropoxide abruptly changes in its efficiency though the amount of nitrogen still remains at the high extent because of its larger crystallite size with increasing

temperature. Generally speaking, the bigger size causes the decrease of active surface area so the catalytic efficiency is reduced. Furthermore, the degrading pattern of N-doped TiO₂ using titanium(IV) tetraisopropoxide calcined at 773 K quite differs from the other one that was calcined at 673 K. This points out that rate of desorption was higher than that of degradation in the first few hours. The catalytic efficiency of N-doped TiO₂ using titanium(IV) tetra-n-butoxide has a change also because of its larger crystallite size and the lower amount of nitrogen. N-doped TiO₂ using titanium(IV) bis(ethyl acetoacetato)diisopropoxide has a little bit change in catalytic efficiency since its crystallite size was not much increased. Additionally, it also showed a small fraction of rutile which brought about synergistic effect between anatase and rutile, like P25 TiO₂.

From all of these results, it can be concluded that N-doped TiO₂ using titanium(IV) tetraisopropoxide with NH₃ and calcined at 673 K gave rise to the highest photocatalytic activity of phenanthrene degradation. Additionally, the higher calcination temperature has an adverse impact on the catalytic efficiency of N-doped TiO₂.

Table 11 %Conversion and rate constants of photodegradation reactions of phenanthrene by N-doped TiO₂ using NH₃ and various types of titania precursors at two different temperatures and by P25 TiO₂.

Photocatalyst	Titania precursor	Calcination temperature (K)	Phenanthrene		
			%Conversion ^a	R ²	Rate constant ^b (h ⁻¹)
N-doped TiO ₂	Titanium(IV) bis(ethyl acetoacetato)diisopropoxide	673	16	0.9207	0.054
		773	15	0.6045	0.014
	Titanium(IV) tetra-n-butoxide	673	19	0.8680	0.034
		773	13	0.9227	0.036
	Titanium(IV) tetraisopropoxide	673	33	0.9991	0.058
		773	18	0.9264	0.050
P25 TiO ₂	-	-	12	0.8093	0.052

^a%Conversion was calculated from $(C_{\text{initial}} - C_{\text{final}} / C_{\text{initial}}) \times 100\%$.

^bThe procedure to calculate rate constants are also shown in Appendix E.

2.1.2 Effect of nitrogen sources

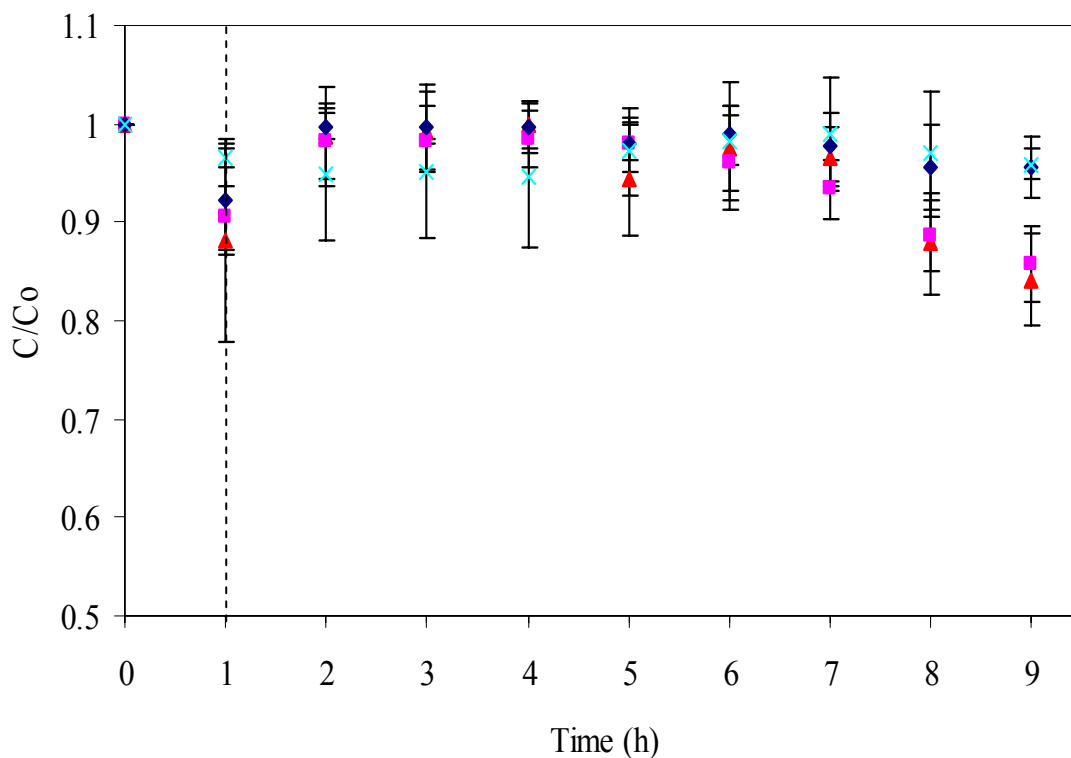


Figure 49 Photodegradation of phenanthrene by N-doped TiO_2 using titanium(IV) bis(ethyl acetoacetato)diisopropoxide and various types of nitrogen sources; (a) NH_3 (▲), (b) $(\text{NH}_2)_2\text{CO}$ (■), (c) NH_4Cl (◆) and (d) $\text{N}_2\text{H}_4\cdot\text{H}_2\text{O}$ (×), calcined at 673 K.

(Note: raw data are shown in Appendix D.)

Although titanium(IV) bis(ethyl acetoacetato)diisopropoxide was not quite appropriate as a titania precursor for preparing N-doped TiO_2 , it gave something different in the variation of nitrogen sources as shown in photocatalytic activity (Figure 49) and rate constants (Table 12). The result can be implied that NH_3 is the best nitrogen source because N-doped TiO_2 using NH_3 had 16% conversion of phenanthrene with the 0.054 h^{-1} rate constant, both of which are the highest values compared to N-doped TiO_2 using other nitrogen sources. The sensible reason used to substantiate this idea is to its small crystallite size. Moreover, N-doped TiO_2 using

$(\text{NH}_2)_2\text{CO}$ was able to catalyze the photodegradation of phenanthrene with 14 % conversion and the rate constant of 0.040 h^{-1} . Although it has close properties, like N-doped TiO_2 using NH_3 , its crystallite size is a bit bigger than that of N-doped TiO_2 using NH_3 . As for N-doped TiO_2 using NH_4Cl , it provided only 4% conversion of phenanthrene and very slow rate (0.012 h^{-1}). This assumes that Cl^- could act as electron donors or hole scavengers which transferred electrons into holes of N-doped TiO_2 after illumination. Thus, the photodegradation of phenanthrene was hampered by the presence of Cl^- . With regard to $\text{N}_2\text{H}_4\cdot\text{H}_2\text{O}$, N-doped TiO_2 using this nitrogen source seems to be inactive to degradation of phenanthrene because it is amorphous and its morphology looks like big semisolid mass. However, it shows a very little change of the relative concentration of phenanthrene (3% conversion) within nine hours owing to its adsorption ability.

Table 12 %Conversion and rate constants of photodegradation reactions of phenanthrene by N-doped TiO₂ using titanium(IV) tetraisopropoxide and various types of nitrogen sources at 673 K.

Photocatalyst	Nitrogen sources	Calcination temperature (K)	Phenanthrene		
			%Conversion ^a	R ²	Rate constant ^b (h ⁻¹)
N-doped TiO ₂	NH ₃	673	16	0.9207	0.054
	(NH ₂) ₂ CO	673	14	0.9871	0.040
	NH ₄ Cl	673	4	0.9001	0.012
	N ₂ H ₄ .H ₂ O	673	3	0.7371	0.0093

^a%Conversion was calculated from $(C_{\text{initial}} - C_{\text{final}} / C_{\text{initial}}) \times 100\%$.

^bThe procedure to calculate rate constants are also shown in Appendix E.

2.1.3 Intermediate products from photodegradation of phenanthrene

Figure 50 shows the structures of two main intermediate products, bis(2-ethylhexyl)benzene-1,2-dicarboxylate ($m/z = 390$) and dimethyl-4-methyl-1,2-benzene dicarboxylate ($m/z = 208$), obtained from the photodegradation of phenanthrene detected by GC/MS and the gas chromatogram is shown in Appendix F. This suggests that the degradation mechanism of phenanthrene involves oxidation reaction by OH radicals, followed by ring opening of phenanthrene in accordance with the previous study by Wen *et al.* (2002). Based on two detectable intermediates, the possible mechanism was also proposed as shown in Figure 51.

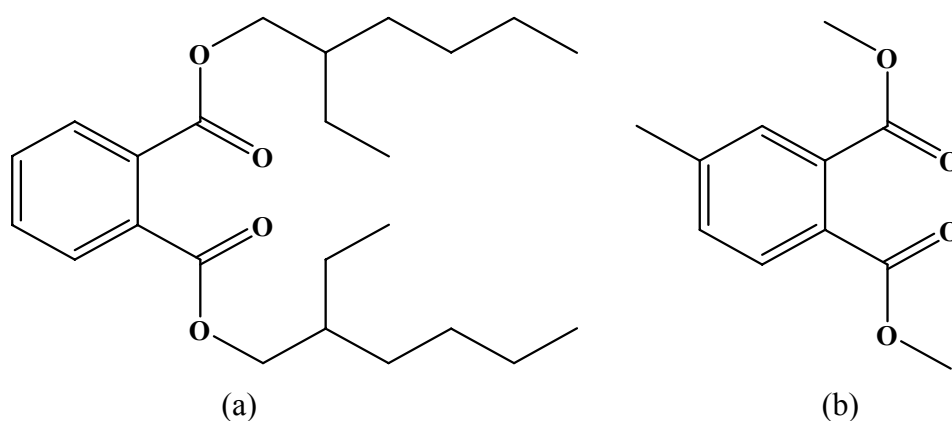


Figure 50 The chemical structures of two detected intermediate products;
(a) bis(2-ethylhexyl)benzene-1,2-dicarboxylate and
(b) dimethyl-4-methyl-1,2-benzene dicarboxylate.

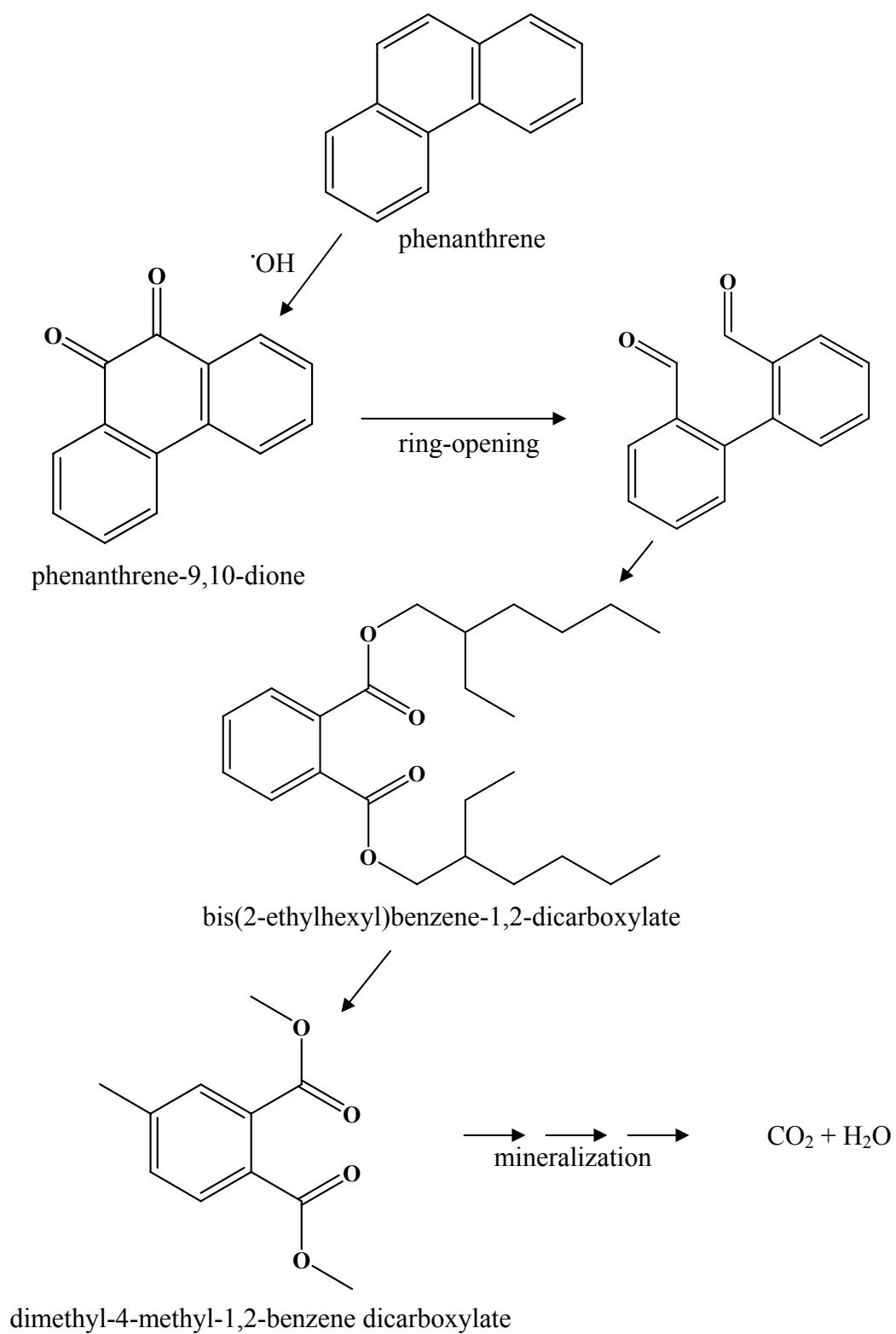


Figure 51 Possibly proposed mechanism of photodegradation of phenanthrene by using N-doped TiO_2 calcined at 673 K.

2.2 Photodegradation of benz[a]anthracene

This section made only use of N-doped TiO₂ using titanium(IV) tetraisopropoxide mixed with NH₃ and calcined at 673 K as a photocatalyst due to its most appropriate photocatalytic properties such as crystallinity, phase composition, surface morphology as well as nitrogen quantity.

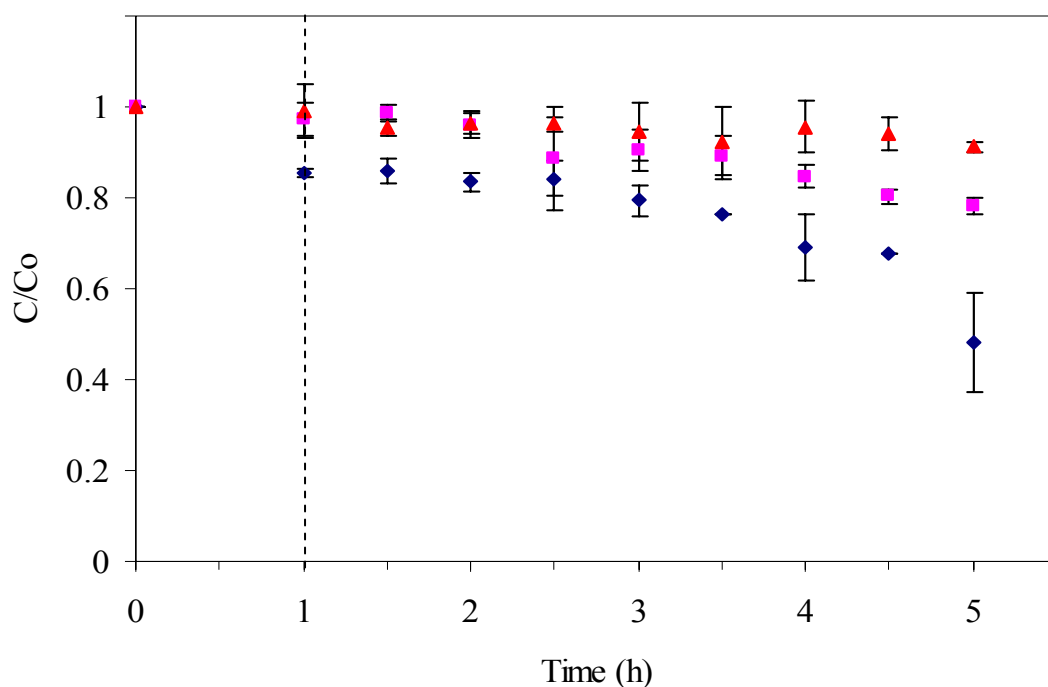


Figure 52 Photodegradation of benz[a]anthracene by using; (a) N-doped TiO₂ calcined at 673 K (♦), (b) P25 TiO₂ (■) and (c) without catalysts (▲).

(Note: raw data are shown in Appendix D.)

The result as shown in Figure 52 suggests that N-doped TiO₂ could catalyze the photodegradation reaction of benz[a]anthracene with 52% conversion. It degraded with the rate constant of 0.074 h⁻¹ as shown in Table 13. In spite of no results about detected intermediate products, it is assured that the reduction of relative concentration of benz[a]anthracene originated from the N-doped TiO₂ effect. Because, in case of no catalyst, there was simply 8% conversion of benz[a]anthracene

which resulted from thermal decomposition. Meanwhile, P25 TiO₂ has a good ability to degrade benz[a]anthracene up to 22% conversion with the rate constant of 0.058 h⁻¹ because of synergistic effect between anatase and rutile, like photodegradation of phenanthrene.

2.3 Photodegradation of phenol

This part also employed N-doped TiO₂ which was prepared by titanium(IV) tetraisopropoxide mixed with NH₃ and calcined at 673 K as a photocatalyst.

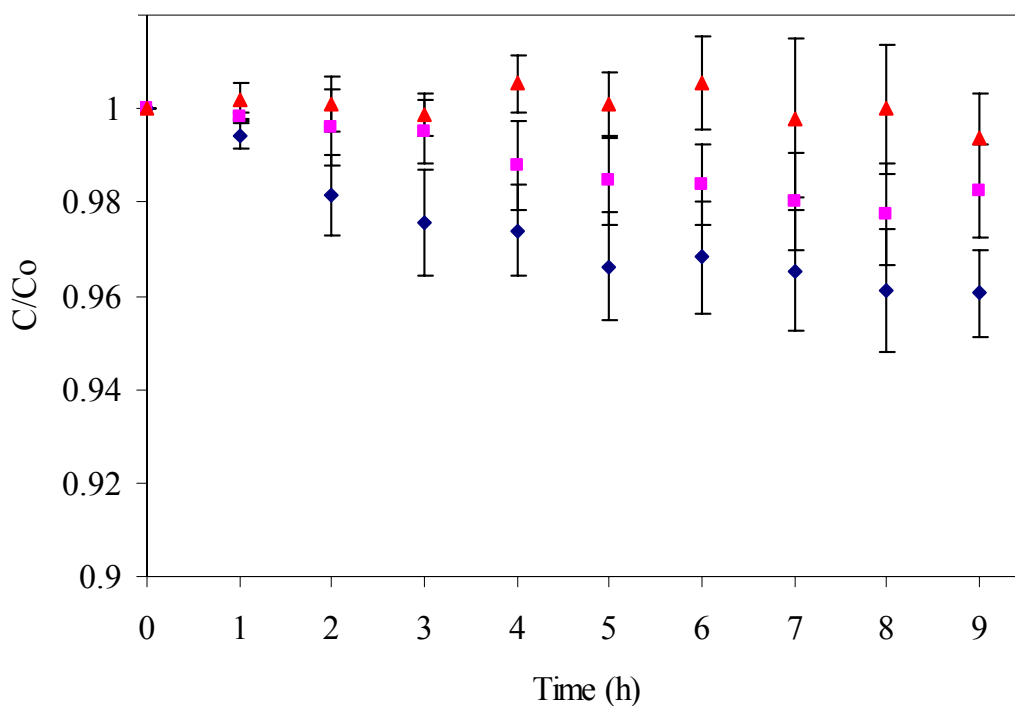


Figure 53 Photodegradation of phenol by using; (a) N-doped TiO₂ calcined at 673 K (♦), (b) P25 TiO₂ (■) and (c) without catalysts (▲).

(Note: raw data are shown in Appendix D.)

As shown in Figure 53, the result shows that only 4% conversion of phenol could be detected from the photodegradation by N-doped TiO₂ whilst P25

TiO₂ provided 2% conversion. Both of two photocatalysts had very slow degradation rate which can be seen from their rate constants as shown in Table 13. These results indicate that phenol was too difficult to be mineralized by this photocatalyst.

Regarding the thermal effect, there was only 0.6% conversion of phenol in case of no catalyst. That's why the effect from the thermal decomposition can be ignored.

Table 13 %Conversion and rate constants of photodegradation reactions of three substrates by N-doped TiO₂ using titanium(IV) tetraisopropoxide mixed with NH₃ and calcined at 673 K.

Photocatalyst	Phenanthrene			Benz[a]anthracene			Phenol		
	%Conversion ^a	R ²	Rate constant ^b (h ⁻¹)	%Conversion	R ²	Rate constant (h ⁻¹)	%Conversion	R ²	Rate constant (h ⁻¹)
N-doped TiO ₂	33	0.9991	0.058	52	0.9215	0.074	4	0.9185	0.0036
P25 TiO ₂	12	0.8093	0.052	22	0.9227	0.058	2	0.8737	0.0026

^a%Conversion was calculated from $(C_{\text{initial}} - C_{\text{final}} / C_{\text{initial}}) \times 100\%$.

^bThe procedure to calculate rate constants are also shown in Appendix E.

CONCLUSION AND RECOMMENDATIONS

Conclusion

N-doped TiO₂ prepared with the variation of titania precursors and nitrogen sources was able to be synthesized by the sol-gel method. From all characterization techniques, it can be implied that the calcination temperature had a significant impact on the crystal structure of N-doped TiO₂. With the increasing temperature, N-doped TiO₂ got the larger crystallite size, the higher crystallinity and anatase-to-rutile phase transformation. The smallest crystallite size, the highest anatase crystallinity and the large amount of strongly-bonded nitrogen are the ideal properties of N-doped TiO₂ for the maximum photocatalytic activity under visible light. Compared to all N-doped TiO₂, N-doped TiO₂ using titanium(IV) tetraisopropoxide as a titania precursor mixed with NH₃ as a nitrogen source and calcined at 673 K seemed to be closely within the scope of the ideal photocatalyst. It provided high crystallinity and spherical surface morphology although its crystallite size is 16 nm. Its phase transformation was retarded by the effect of the strongly-bonded nitrogen in TiO₂ lattice. Moreover, the structural determination did also support that the structure of titanium(IV) tetraisopropoxide was easy to be hydrolyzed by ammonia or water molecules.

With regard to photocatalytic activity, N-doped TiO₂ using titanium(IV) tetraisopropoxide mixed with NH₃ and calcined at 673 K provided the highest %conversion among three substrates; 33% of 20 ppm phenanthrene, 52% of 20 ppm benz[a]anthracene and 4% of 20 ppm phenol. It also rendered the fastest rate of reactions, which was able to be observed from the rate constants; 0.058 h⁻¹ for phenanthrene, 0.074 h⁻¹ for benz[a]anthracene and 0.036 h⁻¹ for phenol. Interestingly, the elevating temperature had an adverse repercussion on the photocatalytic activity. In addition, the probable mechanism of photodegradation reaction of phenanthrene was proposed based on the two detectable intermediates.

Recommendations

1. In case of using titanium(IV) tetrachloride as a titania precursor, it should be handled under nitrogen or inert atmosphere. You must be aware of your glass sets in that they have to be dried before use because this titania precursor is very sensitive to moisture.

2. Regarding the effect of nitrogen sources, titanium(IV) bis(ethyl acetoacetato)diisopropoxide was the most inapplicable titania precursor to synthesize N-doped TiO₂. Therefore, I recommend you using titanium(IV) tetraisopropoxide instead of other titania precursors which are easy to be hydrolyzed in order to obtain more obvious results.

3. Concerning the kinetic aspect, in fact, the photodegradation by using TiO₂ or modified TiO₂ usually has the pseudo-first order kinetic based on the Langmuir-Hinshelwood law (LH). Hence, you should vary the substrate concentrations and calculate the rate values in each concentration by plotting between 1/r and 1/c. Then, you will obtain both the rate constant (k) and the adsorption equilibrium constant (K_{ad}). All of these can be seen in the case study of Sano *et al.* (2008).

4. If your facilities are available, I suggest to you that GC/MS be very suitable for not only detecting intermediates but also measuring the substrate concentration in each time concomitantly.

LITERATURE CITED

- Asahi, R., T. Morikawa, T. Ohwaki, K. Aoki and Y. Taga. 2001. Visible-light photocatalysts in nitrogen-doped titanium oxides. **Science**. 293:269-271.
- Cai, W., Z. Wang, X. Hong, X. Zhao, F. Xu and C. Cai. 2005. Photocatalytic degradation of phenol in aqueous nitrogen-doped TiO₂ suspensions with light sources. **Appl. Catal. B: Environ.** 57: 223-231.
- Callahan, M.A., M.W. Slimak, N.W. Gabelc, I.P. May, C.F. Fowler, J.R. Freed, P. Jennings, R.L. Durfee, F.C. Whitmore, B. Maestri, W.R. Mabey, B.R. Holt, and C.Gould. 1979. **Water-Related Environmental Fate of 129 Priority Pollutants**. US Environmental Protection Agency, Washington, DC. EPA-440/4-79-029.
- Cao, L., Z. Gao, S.L. Suib, T.N. Obee, S.O. Hay, and J.D. Freihaut. 2000. Photocatalytic oxidation of toluene on nanoscale TiO₂ catalyst: studies of deactivation and regeneration. **J. Catal.** 196: 253-261.
- Carp, O., C.L. Huisman and A. Reller. 2004. Photoinduced reactivity of titanium dioxide. **Prog. Solid State Chem.** 32: 33-177.
- Chambers, S.A., S.H. Cheung, P. Nachimuthu, A.G. Joly and M.H. Bowman. 2007. N incorporation and electronic structure in N-doped TiO₂ (110) rutile. **Surf. Sci.** 601:1754-1762.
- Chen, J., J. Shen, S. Zhang, J. Lian and L. Kong. 2007. Benz[a]anthracene heterogeneous photochemical reaction on the surface of TiO₂ particles. **Acta Phys. -Chim. Sin.** 23: 1531-1536.

- Cheng, H.M., G. Liu, F. Li, Z. Chen and G.Q. Lu. 2006. The role of NH_3 atmosphere in preparing nitrogen-doped TiO_2 by mechanochemical reaction. **J. Solid State Chem.** 179: 331-335.
- Datye, A.K., G. Riegel, J.R. Bolton, M. Huang and M.R. Prairie. 1995. Microstructure characterization of a fumed titanium dioxide photocatalyst. **J. Solid State Chem.** 115: 236-239.
- Fang, X., Z. Zhang, Q. Chen., H. Ji and X. Gao. 2007. Dependence of nitrogen doping TiO_2 precursor annealed under NH_3 flow. **J. Solid State Chem.** 180: 1325-1332.
- Feng, J.Y., L. Wan, J.F. Li, W. Sun and Z.Q. Mao. 2007. Improved optical response and photocatalysis for N-doped titanium oxide (TiO_2) films prepared by oxidation of TiN. **Appl. Surf. Sci.** 253: 4764-4767.
- Fernandes, J.B. and A.R. Gandhe. 2005. A simple method to synthesize N-doped rutile titania with enhanced photocatalytic activity in sunlight. **J. Solid State Chem.** 178: 2953-2937.
- _____, S.P. Naik and A.R. Ganghe. 2005. Selective synthesis of N-doped mesoporous TiO_2 phase having enhanced photocatalytic activity. **Micropor. Mesopor. Mater.** 87: 103-109.
- Fornasiero, P., V. Gombac, L. De Rogatis, A. Gasparotto, G. Vicario, T. Montini, D. Barreca, G. Balducci, E. Tondello and M. Graziani. 2007. TiO_2 nanopowders doped with boron and nitrogen for photocatalytic applications. **Chem. Phys.** 339: 111-123.

- Gnaser, H., A. Orendorz, A. Brodyanski, J. Losch, L.H. Bai, Z.H. Chen, Y.K. Le and C. Ziegler. 2007. Phase transformation and particle growth in nanocrystalline anatase TiO₂ films analyzed by X-ray diffraction and Raman spectroscopy. **Surf. Sci.** 601: 4390-4394.
- Hoffmann, M.R., S.T. Martin, W. Choi, and D.W. Bahnemann. 1995. Environmental applications of semiconductor photocatalysis. **Chem. Rev.** 95: 69-96.
- Huang, D., S. Liao, S. Quan, L. Liu, Z. He, J. Wan and W. Zhou. 2008. Synthesis and characterization of visible light responsive N-TiO₂ mixed crystal by a modified hydrothermal process. **J. Non-Crystal. Solids.** 354: 3965-3972.
- Ihara, T., M. Miyoshi, Y. Iriyama, O. Matsumoto and S. Sugihara. 2003. Visible-light-active titanium oxide photocatalyst realized by an oxygen-deficient structure and by nitrogen doping. **Appl. Catal. B: Environ.** 42: 403-409.
- Ireland, J.C., B. Davila, H. Moreno, S.K. Fink and S. Tassos. 1995. Heterogeneous photocatalytic decomposition of polyaromatic hydrocarbons over titanium dioxide. **Chemosphere.** 30: 965-984.
- Khan, S., C. Xu, R. Killmeyer and M.L. Gray. 2006. Photocatalytic effect of carbon-modified *n*-TiO₂ nanoparticles under visible light illumination. **Appl. Catal. B: Environ.** 64: 312-317.
- Ksibi, M., S. Rossignol, J.M. Tatibouet and C. Trapalis. 2008. Synthesis and solid characterization of nitrogen and sulfur-doped TiO₂ photocatalysts active under near visible light. **Mater. Lett.** 62: 4204-4206.
- Kumar, K-N. P. 1995. Growth of rutile crystallites during the initial stage of anatase-to-rutile transformation in pure titania and titania-alumina nanocomposites. **Scr. Metall. Mater.** 32(6): 873-877.

- Lange, N.A. 1956. **Handbook of Chemistry**. 9th ed. Handbook Publisher, Ohio.
- Lee, J.S., J.S. Jang, H.G. Kim, S.M. Ji, S.W. Bae, J.H. Jung and B.H. Shon. 2006. Formation of crystalline $\text{TiO}_{2-x}\text{N}_x$ and its photocatalytic activity. **J. Solid State Chem.** 179: 1067-1075.
- Li, D., X. Fu, H. Huang, X. Chen, Z. Chen, W. Li and D. Ye. 2007. New synthesis of excellent visible-light $\text{TiO}_{2-x}\text{N}_x$ photocatalyst using a very simple method. **J. Solid State Chem.** 180: 2630-2634.
- Lide, D.R. 1995. **Handbook of Chemistry and Physics**. 76th ed. CRC Press, New York.
- Matsumura, M., T. Ohno, K. Sarukawa and K. Tokieda. 2001. Morphology of a TiO_2 photocatalyst (Degussa, P-25) consisting of anatase and rutile crystalline phases. **J. Catal.** 203: 82-86.
- Mills, A. and S.L. Hunte. 1997. An overview of semiconductor photocatalysis. **J. Photochem. Photobiol. A: Chem.** 108: 1-35.
- Morawski, A.W., B. Kosowska, S. Mozia, B. Grzmil, M. Janus and K. Kalucki. 2005. The preparation of TiO_2 -nitrogen doped by calcination of $\text{TiO}_2 \cdot x\text{H}_2\text{O}$ under ammonia atmosphere for visible light photocatalysis. **Sol. Energy Mater. Sol. Cell.** 88: 269-280.
- Muggli, D.S. and L. Ding. 2001. Photocatalytic performance of sulfated TiO_2 and Degussa P-25 TiO_2 during oxidation of organics. **Appl. Catal. B: Environ.** 32: 181-194.
- Nakato, Y., R. Nakamura and T. Tanaka. 2004. Mechanism for visible light responses in anodic photocurrents at N-Doped TiO_2 film electrodes. **J. Phys. Chem. B.** 108: 10617-10620.

- Namura, K. 2002. **Minerals**. Crystal structure gallery. Available Source: <http://staff.aist.go.jp/nomura-k/english/itscgallery-e.htm>, February 17, 2009.
- Nasoka, Y., M. Matsushita, J. Nishino and A.Y. Nosaka. Nitrogen-doped titanium dioxide photocatalysts for visible response prepared by using organic compounds. **Sci. Technol. Adv. Mater.** 6: 143-148.
- Palgrave, R.G., I. Takahashi, D.J. Payne and R.G. Egdell. 2008. High resolution X-ray photoemission study of nitrogen doped TiO₂ rutile single crystal. **Chem. Phys. Lett.** 454: 314-417.
- Patterson, A.L. 1939. The Scherrer formula for X-Ray particle size determination. **Phys. Rev.** 56: 978 – 982.
- Ravindra, K., R. Sokhi and R.V. Grieken. 2008. Atmospheric polycyclic aromatic hydrocarbons: Source attribution, emission factors and regulation. **Atmos. Environ.** 42: 2895-2921.
- Sano, T., N. Negishi, K. Koike, K. Takeuchi and S. Matsuzawa. 2004. Preparation of a visible light-responsive photocatalyst from a complex Ti⁴⁺ with a nitrogen-containing ligand. **J. Mater. Chem.** 14: 380-384.
- _____, E. Puzenat, C. Guillard, C. Geantet and S. Matsuzawa. 2008. Degradation of C₂H₂ with modified TiO₂ photocatalysts under visible light irradiation. **J. Mol. Catal. A: Chem.** 284: 127-133.
- Sato, S., R. Nakamura and S. Abe. 2005. Visible-light sensitization of TiO₂ photocatalysts by wet-method N doping. **Appl. Catal. A: Gen.** 284: 131-137.
- Shifu, C., C. Lei, G. Shen and C. Gengyu. 2005. The preparation of nitrogen-doped photocatalyst TiO_{2-x}N_x by ball milling. **Chem. Phys. Lett.** 413: 404-409.

- Shouxin, L., C. Xiaoyun and C. Xi. 2006. Preparation of N-doped visible-light response nanosize TiO_2 photocatalyst using the acid-catalyzed hydrolysis method. **Chin. J. Catal.** 27: 697-702.
- Smirniotis, P.G. and B. Sun. 2003. Interaction of anatase and rutile TiO_2 particles in aqueous photooxidation. **Catal. Today.** 88: 49-59.
- Spurr, R.A. and H. Myers. 1957. Quantitative analysis of anatase-rutile mixtures with an X-Ray diffractometer. **Anal. Chem.** 29(5): 760-762.
- Su, C., B.Y. Hong and C.M. Tseng. 2004. Sol-gel preparation and photocatalysis of titanium dioxide. **Catal. Today.** 96: 119-126.
- Valentin, C.D., E. Finazzi, G. Pacchioni, A. Selloni, S. Livraghi, M.C. Paganini and E. Giamello. 2007. N-doped TiO_2 : Theory and experiment. **Chem. Phys.** 339: 44-56.
- Viswanath, R.P., M. Sathish and B. Viswanathan. 2007. Characterization and photocatalytic activity of N-doped TiO_2 prepared by thermal decomposition of Ti-melamine complex. **Appl. Catal. B: Environ.** 74: 307-312.
- Wang, W. and J.P. Lewis. 2006. Second-generation photocatalytic materials: anion-doped TiO_2 . **J. Phys.: Condens. Matter.** 18: 421-434.
- Wen, S., J. Zhao, G. Sheng, J. Fu, P. Peng. 2002. Photocatalytic reactions of phenanthrene at TiO_2 /water interfaces. **Chemosphere.** 46 (6): 871-877.
- Yamashita, H., M. Harada, J. Misaka, M. Takeuchi, B. Neppolian and M. Anpo. 2003. Photocatalytic degradation of organic compounds diluted in water using visible light-responsive metal ion-implanted TiO_2 catalysts: Fe ion-implanted TiO_2 . **Catal. Today.** 84: 191-196.

- Yates, J.T., A.L. Linsebigler and G. Lu. 1995. Photocatalysis on TiO₂ Surfaces: Principles, Mechanisms, and Selected Results. **Chem. Rev.** 95: 735-758.
- Yaun, Z.Y., G.S. Shao and X.J. Zhang. 2008. Preparation and photocatalytic activity of hierarchically mesoporous-macroporous TiO_{2-x}N_x. **Appl. Catal. B: Environ.** 82: 208-218.
- Yin, S., Y. Aita, M. Komatsu and T. Sato. 2004. Phase-compositional control and visible light photocatalytic activity of nitrogen-doped titania via solvothermal process. **J. Solid State Chem.** 177: 3235-3238.
- Yu, J., H. Yu, B. Cheng, M. Zhou and X. Zhao. 2006. Enhanced photocatalytic activity of TiO₂ powder (P25) by hydrothermal treatment. **J. Mol. Catal. A: Chem.** 253: 112-118.
- Zhang, J., D.R. Park, K. Ikeue, H. Yamashita and M. Anpo. 1999. Photocatalytic oxidation of ethyl to CO₂ and H₂O on ultrafine powdered TiO₂ photocatalysts in the presence of O₂ and H₂O. **J. Catal.** 185: 114-119.
- Zhao, J., S. Wen, G. Sheng, J. Fu and P. Peng. 2002. Photocatalytic reaction of phenanthrene at TiO₂/water interfaces. **Chemosphere.** 46: 871-877.

APPENDICES

APPENDIX A

Calculation of crystallite sizes, phase composition and unit cell volume

Note: All labelled numbers were average values from the XRD raw data; not be estimated by naked eyes.

The content of anatase was also calculated applying Spurr-Myers equation as shown in equation 2.

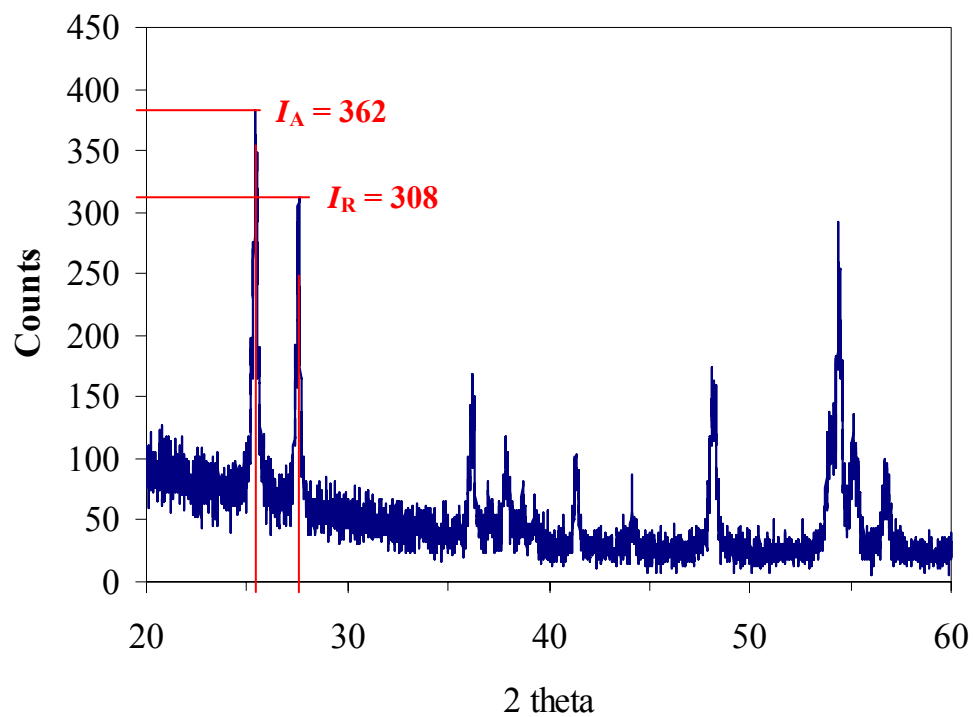
$$w_A = \frac{1}{(1 + 1.26 \frac{I_R}{I_A})} \quad \dots(2)$$

where w_A is the weight fraction of anatase in the mixture

I_R is the intensity of the diffraction peak of rutile

I_A is the intensity of the diffraction peak of anatase

This is an example of finding all constants involved in the Spurr-Myers equation.



Appendix Figure A2 The XRD pattern of N-doped TiO₂ using titanium(IV) tetra-n-butoxide mixed with NH₃ and calcined at 873 K.

Note: All labelled numbers were average values from the XRD raw data; not be estimated by naked eyes.

The unit cell volume was calculated from the product of three lattice parameters (a, b and c), which can be equated for the tetragonal system ($a \neq b = c$) as follows;

$$\frac{1}{d^2} = \frac{h^2 + k^2}{a^2} + \frac{l^2}{c^2} \quad \text{.....(3)}$$

where d is a lattice spacing between the planes in the atomic lattice

h, k and l are the Miller indices

a, b and c are the lattice parameters

This is an example of finding all constants involved in the equation 3. Firstly, a d -spacing value was calculated from Bragg's equation as shown below.

$$2d\sin\theta_B = n\lambda \quad \text{.....(4)}$$

where θ_B is a Bragg's angle

n is an integer determined by the order given ($n = 1$)

λ is the wavelength of x-rays ($\lambda_{\text{Cu K}\alpha} = 0.154 \text{ nm}$)

From the XRD pattern as depicted in Appendix Figure A3, at $2\theta_B$ of 25.355° and 38.875° the d -spacing values were 0.3509 and 0.2373 nm, respectively. Secondly, the d -spacing values and the Miller indices were replaced into the equation 3.

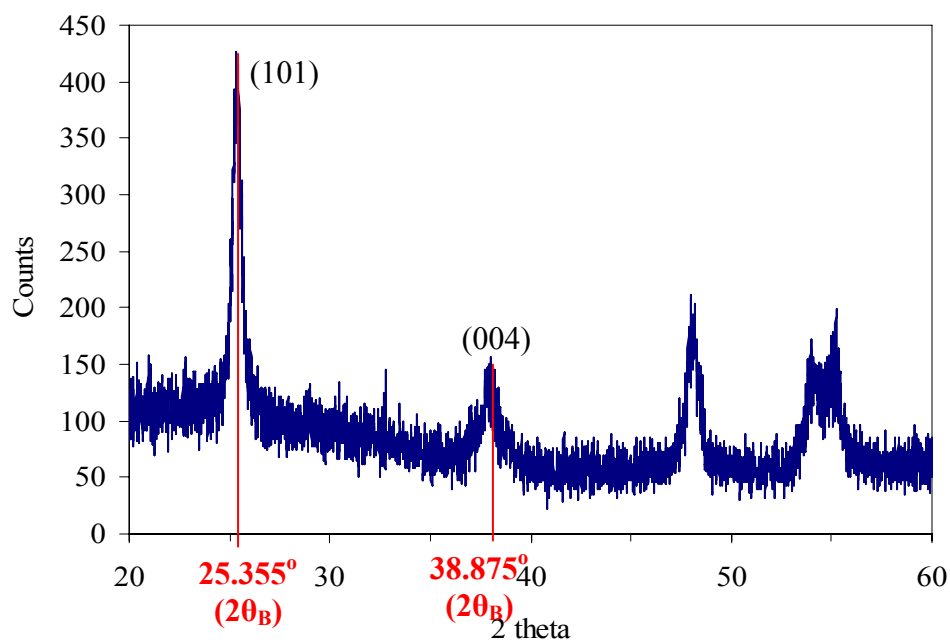
For the (101) plane;

$$\frac{1}{0.3509^2} = \frac{1^2 + 0^2}{a^2} + \frac{1^2}{c^2} \quad \text{.....(5)}$$

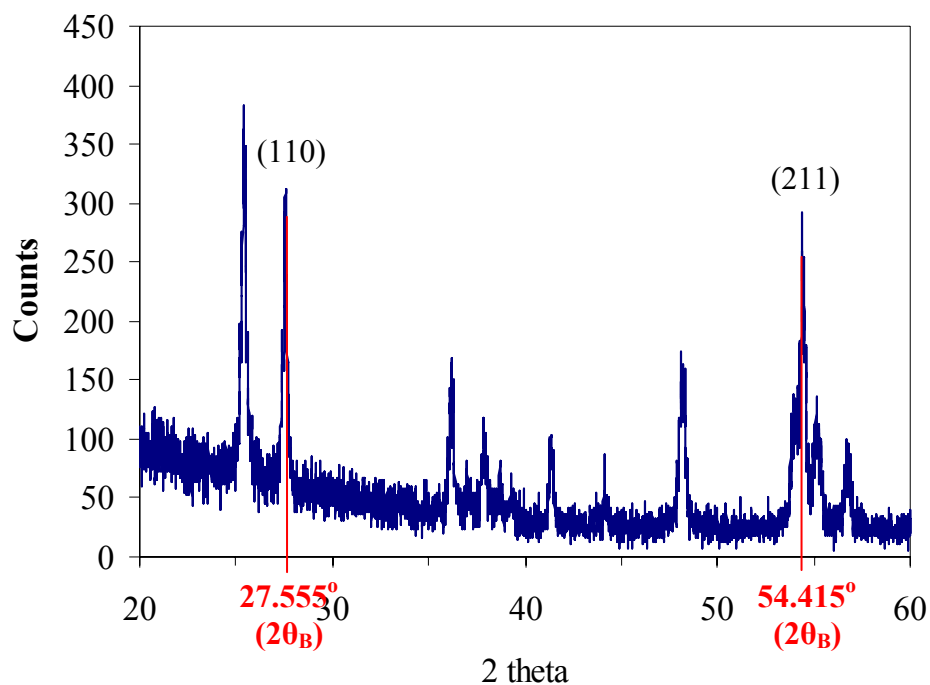
For the (004) plane;

$$\frac{1}{0.2373^2} = \frac{0^2 + 0^2}{a^2} + \frac{4^2}{c^2} \quad \text{.....(6)}$$

Last, from the equations 5 and 6, a and c lattice constants will be obtained; $a = 0.3777 \text{ nm}$ and $c = 0.9492 \text{ nm}$. Hence, the unit cell volume is finally equal to 0.1354 nm^3 . Regarding the rutile case, the specified $2\theta_B$ positions were shown in Appendix Figure A4.



Appendix Figure A3 The XRD pattern of N-doped TiO₂ using titanium(IV) tetraisopropoxide mixed with NH₃ and calcined at 673 K.

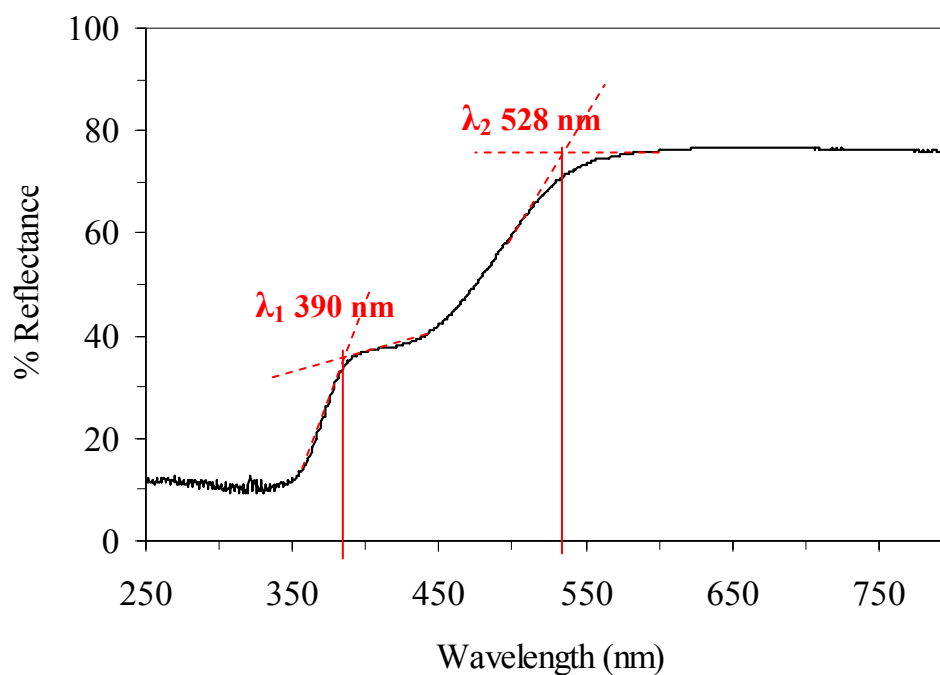


Appendix Figure A4 The XRD pattern of N-doped TiO₂ using titanium(IV) tetra-n-butoxide mixed with NH₃ and calcined at 873 K.

APPENDIX B

The procedure for the determination of the absorption edge of UV-Vis/DR results

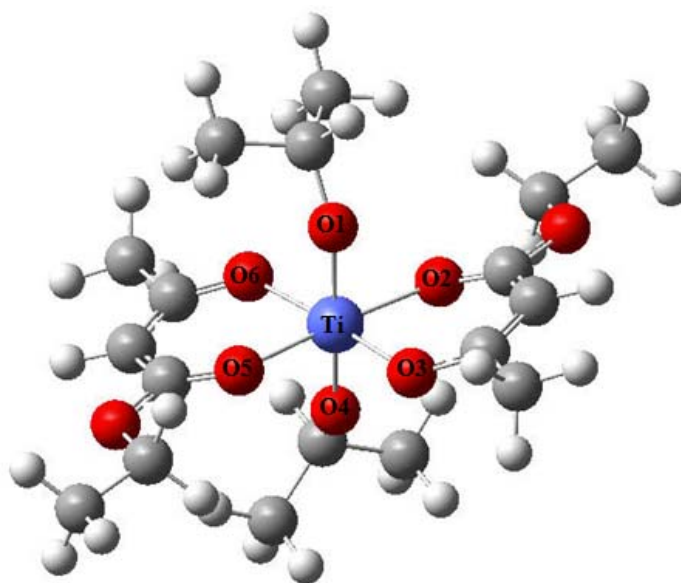
The procedure that was used to find the absorption edge of each UV-Vis /DR spectrum conformed to previous research by Feng *et al.* (2007) as follows;



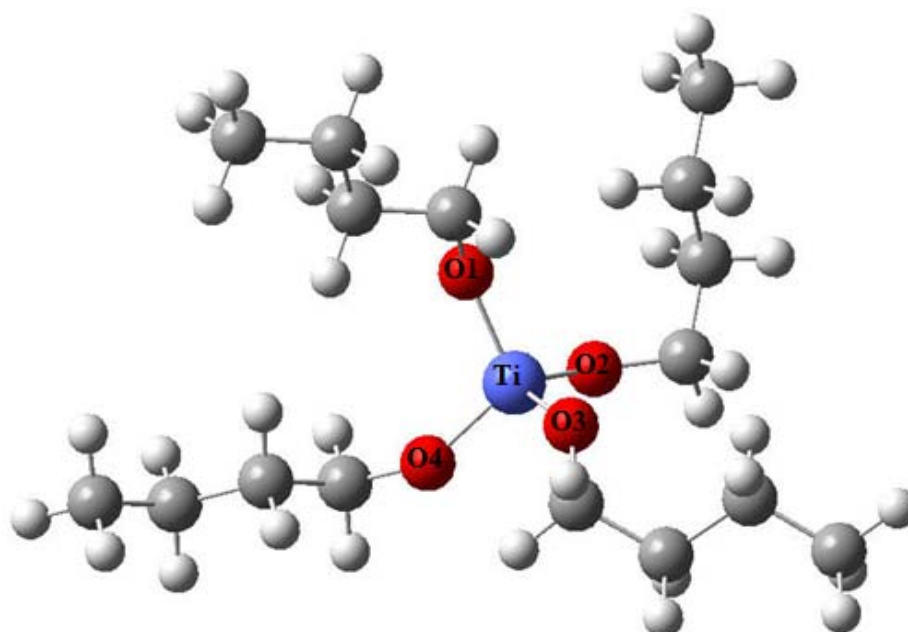
Appendix Figure B1 The UV-Vis/DR spectrum of N-doped TiO₂ using titanium(IV) tetraisopropoxide mixed with NH₃ and calcined at 773 K.

APPENDIX C

The supplementary data on the structural determination by using
quantum chemical calculation



Appendix Figure C1 The optimized structure of titanium(IV) bis(ethyl acetoacetato) diisopropoxide.



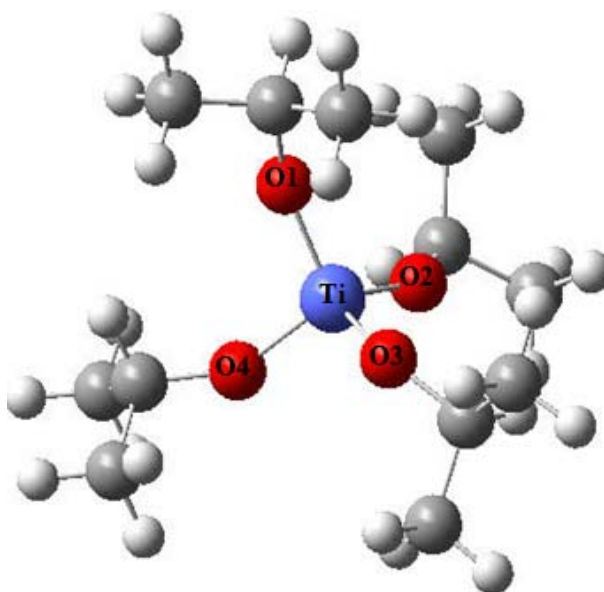
Appendix Figure C2 The optimized structure of titanium(IV) tetra-n-butoxide.

Appendix Table C1 The total energy, optimized bond lengths and bond angles of titanium(IV) bis(ethyl acetoacetato)diisopropoxide.

Titanium alkoxide precursor	Total energy (kcal/mol)	Bond	Distant (Å)	Angle	Degree
Titanium(IV) bis(ethyl acetoacetato) diisopropoxide	-2156.68	O1-Ti	1.81	O1-Ti-O2	87.05
		O2-Ti	2.08	O1-Ti-O3	93.16
		O3-Ti	1.97	O1-Ti-O4	169.53
		O4-Ti	1.81	O1-Ti-O5	93.62
		O5-Ti	2.04	O1-Ti-O6	86.74
		O6-Ti	2.05	O2-Ti-O3	85.42
				O2-Ti-O4	88.07
				O2-Ti-O5	175.62
				O2-Ti-O6	98.98
				O3-Ti-O4	95.68
				O3-Ti-O5	90.22
				O3-Ti-O6	175.58
				O4-Ti-O5	91.96
				O4-Ti-O6	84.89
				O5-Ti-O6	85.31

Appendix Table C2 The total energy, optimized bond lengths and bond angles of titanium(IV) tetra-n-butoxide.

Titanium alkoxide precursor	Total energy (kcal/mol)	Bond	Distant (Å)	Angle	Degree
Titanium(IV) tetra-n-butoxide	-1781.94	O1-Ti	1.80	O1-Ti-O2	109.02
		O2-Ti	1.80	O1-Ti-O3	107.88
		O3-Ti	1.79	O1-Ti-O4	111.11
		O4-Ti	1.79	O2-Ti-O3	110.02
				O2-Ti-O4	110.10
				O3-Ti-O4	108.66



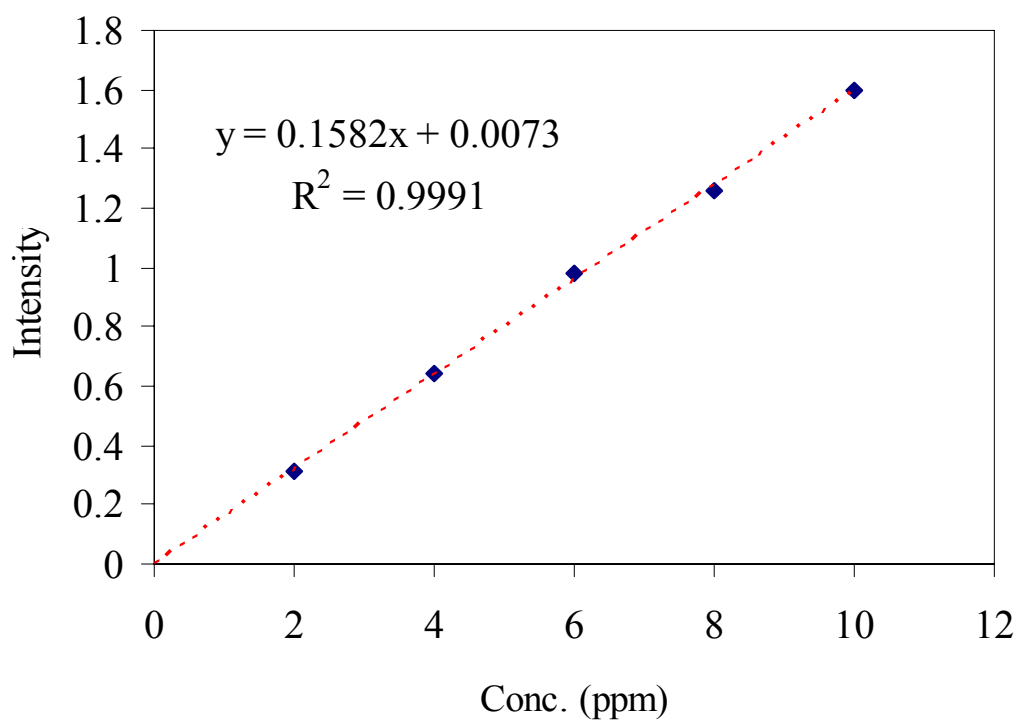
Appendix Figure C3 The optimized structure of titanium(IV) tetraisopropoxide.

Appendix Table C3 The total energy, optimized bond lengths and bond angles of titanium(IV) tetraisopropoxide.

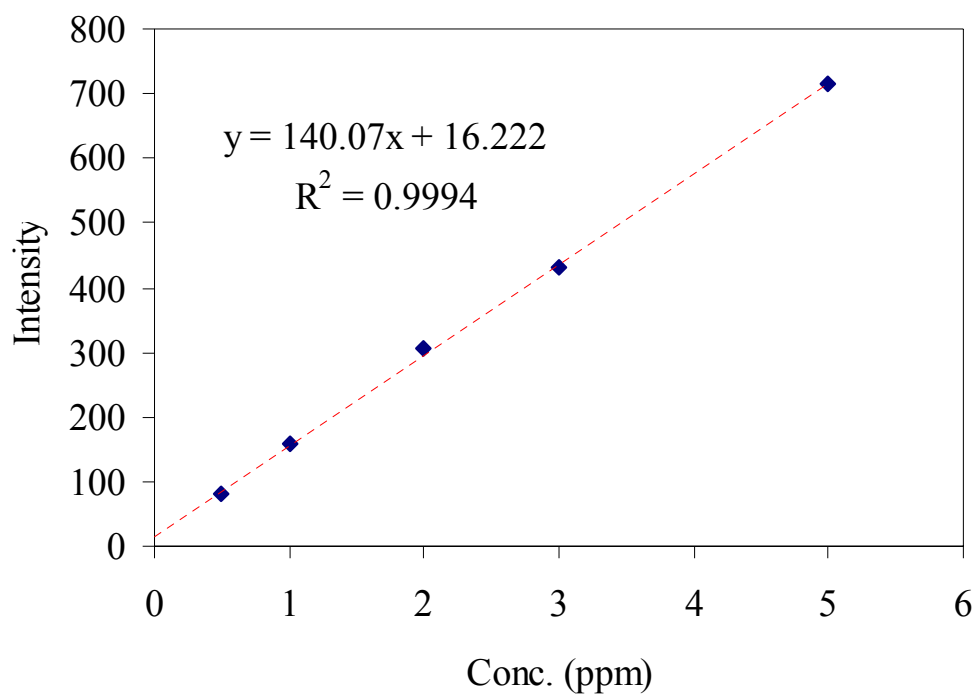
Titanium alkoxide precursor	Total energy (kcal/mol)	Bond	Distant (Å)	Angle	Degree
Titanium(IV) tetraisopropoxide	-1642.71	O1-Ti	1.78	O1-Ti-O2	111.43
		O2-Ti	1.79	O1-Ti-O3	110.42
		O3-Ti	1.80	O1-Ti-O4	107.75
		O4-Ti	1.80	O2-Ti-O3	107.87
				O2-Ti-O4	108.49
				O3-Ti-O4	110.88

APPENDIX D

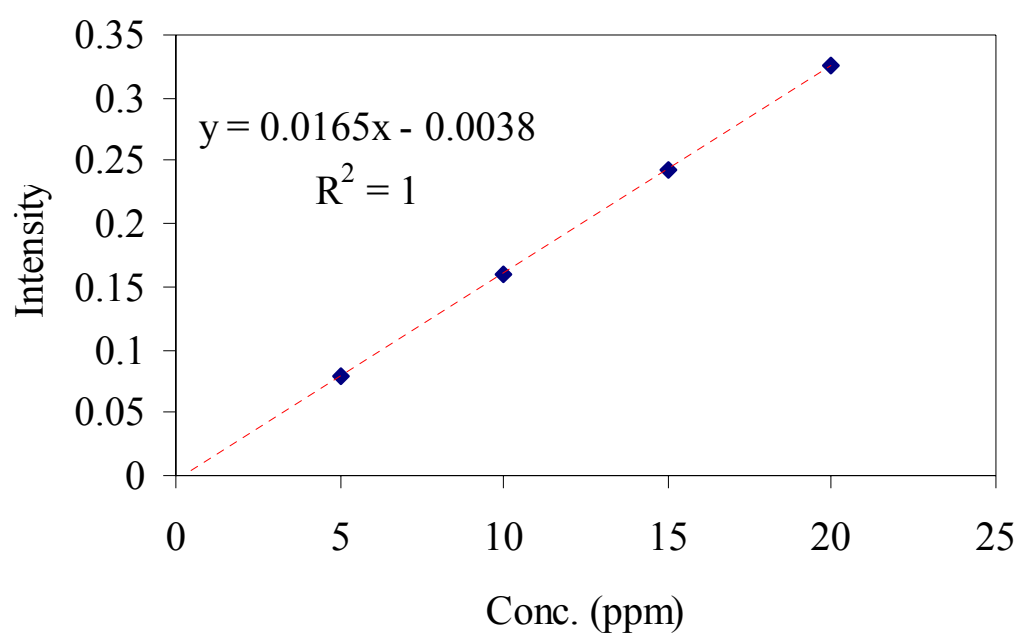
Linear calibration curves of three substrates and raw data of all
photodegradation reactions



Appendix Figure D1 The linear calibration curve of phenanthrene.



Appendix Figure D2 The linear calibration curve of benz[a]anthracene.



Appendix Figure D3 The linear calibration curve of phenol.

Appendix Table D1 Raw data of the photodegradation reaction of phenanthrene by N-doped TiO₂ using titanium(IV) bis(ethyl acetoacetato)diisopropoxide mixed with NH₃ and calcined at 673 K.

Degrading time (h)	Absorbance at λ_{max} 251 nm			Concentration ^a (ppm)			Relative concentration (C/C ₀)				
	Abs ₁	Abs ₂	Abs ₃	C ₁	C ₂	C ₃	C ₁ /C ₀	C ₂ /C ₀	C ₃ /C ₀	(C/C ₀) _{ave}	Std (C/C ₀)
before lamp on	1.527	1.2185	1.286	9.6062	7.6561	8.0828	1	1	1	1	6E-08
0	1.169	1.1223	1.2353	7.3432	7.048	7.7623	0.7644	0.9206	0.9604	0.8818	0.1036
1	1.4202	1.2538	1.2892	8.9311	7.8793	8.103	0.9297	1.0291	1.0025	0.9871	0.0515
2	1.471	1.2651	1.2519	9.2522	7.9507	7.8673	0.9632	1.0385	0.9733	0.9917	0.0409
3	1.4865	1.245	1.291	9.3502	7.8236	8.1144	0.9733	1.0219	1.0039	0.9997	0.0245
4	1.3839	1.232	1.178	8.7016	7.7415	7.4001	0.9058	1.0111	0.9155	0.9442	0.0582
5	1.4147	1.2064	1.299	8.8963	7.5796	8.165	0.9261	0.99	1.0102	0.9754	0.0439
6	1.4249	1.21	1.2523	8.9608	7.6024	7.8698	0.9328	0.993	0.9736	0.9665	0.0307
7	1.3458	1.0068	1.1953	8.4608	6.318	7.5095	0.8808	0.8252	0.9291	0.8783	0.052
8	1.2963	1.078	1.02	8.1479	6.768	6.4014	0.8482	0.884	0.792	0.8414	0.0464

^aconcentrations were converted from absorbance by using linear calibration of phenanthrene as shown above.

Appendix Table D2 Raw data of the photodegradation reaction of phenanthrene by N-doped TiO₂ using titanium(IV) bis(ethyl acetoacetato)diisopropoxide mixed with NH₃ and calcined at 773 K.

Degrading time (h)	Absorbance at λ_{max} 251 nm			Concentration ^a (ppm)			Relative concentration (C/Co)				
	Abs ₁	Abs ₂	Abs ₃	C ₁	C ₂	C ₃	C ₁ /C ₀	C ₂ /C ₀	C ₃ /C ₀	(C/C ₀) _{ave}	Std _(C/C₀)
before lamp on	1.1372	1.3594	1.0121	7.1422	8.5468	6.3515	1	1	1	1	2E-08
0	1.0245	1.2867	0.701	6.4298	8.0872	4.385	0.9003	0.9462	0.6904	0.8456	0.1364
1	1.1754	1.2929	0.7885	7.3837	8.1264	4.9377	1.0338	0.9508	0.7774	0.9207	0.1308
2	1.1737	1.1695	0.7781	7.3729	7.3464	4.8723	1.0323	0.8596	0.7671	0.8863	0.1346
3	1.1891	1.208	0.7919	7.4703	7.5898	4.9595	1.0459	0.888	0.7809	0.9049	0.1333
4	1.1522	1.2832	0.7907	7.237	8.0651	4.9522	1.0133	0.9436	0.7797	0.9122	0.1199
5	1.1353	1.1943	0.7691	7.1302	7.5033	4.8154	0.9983	0.8779	0.7582	0.8781	0.1201
6	1.1497	1.2075	0.7987	7.2212	7.5865	5.0025	1.0111	0.8876	0.7876	0.8954	0.1119
7	1.0973	1.0654	0.8463	6.89	6.6884	5.3034	0.9647	0.7826	0.835	0.8607	0.0938
8	1.0416	1.0868	0.846	6.5379	6.8236	5.3017	0.9154	0.7984	0.8347	0.8495	0.0599

^aconcentrations were converted from absorbance by using linear calibration of phenanthrene as shown above.

Appendix Table D3 Raw data of the photodegradation reaction of phenanthrene by N-doped TiO₂ using titanium(IV) tetra-n-butoxide mixed with NH₃ and calcined at 673 K.

Degrading time (h)	Absorbance at λ_{max} 251 nm			Concentration ^a (ppm)			Relative concentration (C/C ₀)				
	Abs ₁	Abs ₂	Abs ₃	C ₁	C ₂	C ₃	C ₁ /C ₀	C ₂ /C ₀	C ₃ /C ₀	(C/C ₀) _{ave}	Std _(C/C₀)
before lamp on	1.4474	1.5463	1.4863	9.10303	9.72819	9.34893	1	1	1	1	1.6E-08
0	1.3161	1.4151	1.3338	8.27307	8.89886	8.38496	0.90883	0.91475	0.89689	0.90682	0.0091
1	1.3302	1.5387	1.282	8.3622	9.68015	8.05752	0.91862	0.99506	0.86187	0.92518	0.06684
2	1.2495	1.474	1.4036	7.85209	9.27118	8.82617	0.86258	0.95302	0.94408	0.91989	0.04984
3	1.2122	1.5127	1.4706	7.61631	9.5158	9.24968	0.83668	0.97817	0.98938	0.93474	0.08511
4	1.1396	1.5003	1.4852	7.1574	9.43742	9.34197	0.78626	0.97011	0.99926	0.91854	0.11548
5	1.0908	1.4666	1.4314	6.84893	9.2244	9.0019	0.75238	0.94821	0.96288	0.88782	0.11753
6	1.0823	1.5174	1.3759	6.7952	9.54551	8.65107	0.74648	0.98122	0.92536	0.88435	0.12263
7	0.9424	1.518	1.3862	5.91087	9.5493	8.71618	0.64933	0.98161	0.93232	0.85442	0.17932
8	0.83366	1.4491	1.333	5.22351	9.11378	8.3799	0.57382	0.93684	0.89635	0.80234	0.19893

^aconcentrations were converted from absorbance by using linear calibration of phenanthrene as shown above.

Appendix Table D4 Raw data of the photodegradation reaction of phenanthrene by N-doped TiO₂ using titanium(IV) tetra-n-butoxide mixed with NH₃ and calcined at 773 K.

Degrading time (h)	Absorbance at λ_{\max} 251 nm			Concentration ^a (ppm)			Relative concentration (C/C ₀)				
	Abs ₁	Abs ₂	Abs ₃	C ₁	C ₂	C ₃	C ₁ /C ₀	C ₂ /C ₀	C ₃ /C ₀	(C/C ₀) _{ave}	Std _(C/C₀)
before lamp on	1.5537	1.508	1.229	9.77497	9.48609	7.7225	1	1	1	1	4.6E-08
0	1.1819	1.2582	1.1712	7.42478	7.90708	7.35714	0.75957	0.83354	0.95269	0.8486	0.09744
1	1.2352	1.1916	1.3028	7.76169	7.48609	8.189	0.79404	0.78917	1.06041	0.8812	0.15521
2	1.5076	1.2752	1.31	9.48357	8.01454	8.23451	0.97019	0.84487	1.0663	0.96045	0.11103
3	1.453	1.2962	1.2714	9.13843	8.14728	7.99052	0.93488	0.85887	1.03471	0.94282	0.08819
4	1.484	1.2647	1.2029	9.33439	7.94817	7.55752	0.95493	0.83788	0.97864	0.92381	0.07536
5	1.501	1.2966	1.2903	9.44185	8.14981	8.10999	0.96592	0.85913	1.05018	0.95841	0.09574
6	1.4203	1.2745	1.3157	8.93173	8.01011	8.27054	0.91374	0.84441	1.07097	0.94304	0.11609
7	1.4398	1.2654	1.0815	9.05499	7.95259	6.79014	0.92635	0.83834	0.87927	0.88132	0.04404
8	1.4387	1.2383	1.0583	9.04804	7.78129	6.64349	0.92563	0.82028	0.86028	0.86873	0.05318

^aconcentrations were converted from absorbance by using linear calibration of phenanthrene as shown above.

Appendix Table D5 Raw data of the photodegradation reaction of phenanthrene by N-doped TiO₂ using titanium(IV) tetraisopropoxide mixed with NH₃ and calcined at 673 K.

Degrading time (h)	Absorbance at λ_{\max} 251 nm			Concentration ^a (ppm)			Relative concentration (C/C ₀)				
	Abs ₁	Abs ₂	Abs ₃	C ₁	C ₂	C ₃	C ₁ /C ₀	C ₂ /C ₀	C ₃ /C ₀	(C/C ₀) _{ave}	Std _(C/C₀)
before lamp on	0.58306	1.2662	1.3275	3.63944	7.95765	8.34513	1	1	1	1	2E-08
0	0.56882	1.1055	1.2633	3.54943	6.94185	7.93932	0.97527	0.87235	0.95137	0.933	0.05386
1	0.56918	1.1083	1.2084	3.55171	6.95954	7.59229	0.97589	0.87457	0.90979	0.92008	0.05144
2	0.5526	1.1018	1.2076	3.4469	6.91846	7.58723	0.9471	0.86941	0.90918	0.90856	0.03885
3	0.55293	1.1008	1.0516	3.44899	6.91214	6.60114	0.94767	0.86862	0.79102	0.8691	0.07833
4	0.54398	1.0754	1.001	3.39241	6.75158	6.28129	0.93212	0.84844	0.75269	0.84442	0.08979
5	0.49928	1.0898	0.93015	3.10986	6.8426	5.83344	0.85449	0.85988	0.69902	0.80446	0.09135
6	0.47556	1.0212	0.86173	2.95992	6.40898	5.40095	0.81329	0.80539	0.6472	0.75529	0.0937
7	0.44353	0.95432	0.8494	2.75746	5.98622	5.32301	0.75766	0.75226	0.63786	0.71593	0.06766
8	0.41456	0.91712	0.792	2.57434	5.75107	4.96018	0.70734	0.72271	0.59438	0.67481	0.07008

^aconcentrations were converted from absorbance by using linear calibration of phenanthrene as shown above.

Appendix Table D6 Raw data of the photodegradation reaction of phenanthrene by N-doped TiO₂ using titanium(IV) tetraisopropoxide mixed with NH₃ and calcined at 773 K.

Degrading time (h)	Absorbance at λ_{max} 251 nm			Concentration ^a (ppm)			Relative concentration (C/C ₀)				
	Abs ₁	Abs ₂	Abs ₃	C ₁	C ₂	C ₃	C ₁ /C ₀	C ₂ /C ₀	C ₃ /C ₀	(C/C ₀) _{ave}	Std _(C/C₀)
before lamp on	1.5537	1.508	1.229	9.77497	9.48609	7.7225	1	1	1	1	4.6E-08
0	1.1819	1.2582	1.1721	7.42478	7.90708	7.36283	0.75957	0.83354	0.95343	0.84885	0.09783
1	1.2352	1.1916	1.3028	7.76169	7.48609	8.189	0.79404	0.78917	1.06041	0.8812	0.15521
2	1.5076	1.2752	1.301	9.48357	8.01454	8.17762	0.97019	0.84487	1.05893	0.958	0.10755
3	1.453	1.2962	1.2714	9.13843	8.14728	7.99052	0.93488	0.85887	1.03471	0.94282	0.08819
4	1.484	1.2647	1.2029	9.33439	7.94817	7.55752	0.95493	0.83788	0.97864	0.92381	0.07536
5	1.501	1.2661	1.2901	9.44185	7.95702	8.10872	0.96592	0.83881	1.05001	0.95158	0.10633
6	1.4203	1.2745	1.3157	8.93173	8.01011	8.27054	0.91374	0.84441	1.07097	0.94304	0.11609
7	1.4298	1.265	1.0815	8.99178	7.95006	6.79014	0.91988	0.83808	0.87927	0.87907	0.0409
8	1.2297	1.2383	1.0583	7.72693	7.78129	6.64349	0.79048	0.82028	0.86028	0.82368	0.03502

^aconcentrations were converted from absorbance by using linear calibration of phenanthrene as shown above.

Appendix Table D7 Raw data of the photodegradation reaction of phenanthrene by P25 TiO₂.

Degrading time (h)	Absorbance at λ_{max} 251 nm			Concentration ^a (ppm)			Relative concentration (C/C ₀)				
	Abs ₁	Abs ₂	Abs ₃	C ₁	C ₂	C ₃	C ₁ /C ₀	C ₂ /C ₀	C ₃ /C ₀	(C/C ₀) _{ave}	Std (C/C ₀)
before lamp on	1.22	0.86222	1.3541	7.66561	5.40405	8.51327	1	1	1	1	7E-08
0	1.059	0.6954	1.178	6.64791	4.34956	7.40013	0.86724	0.80487	0.86925	0.84712	0.0366
1	1.2191	0.85509	1.3436	7.65992	5.35898	8.4469	0.99926	0.99166	0.9922	0.99437	0.00424
2	1.2992	0.78668	1.3245	8.16625	4.92655	8.32617	1.06531	0.91164	0.97802	0.98499	0.07707
3	1.1673	0.7863	1.3822	7.33249	4.92415	8.6909	0.95654	0.9112	1.02086	0.96287	0.05511
4	1.301	0.7972	1.3813	8.17762	4.99305	8.68521	1.06679	0.92395	1.0202	1.00365	0.07285
5	1.3014	0.86188	1.3447	8.18015	5.4019	8.45386	1.06712	0.9996	0.99302	1.01992	0.04102
6	1.2676	0.88721	1.4	7.9665	5.56201	8.80341	1.03925	1.02923	1.03408	1.03419	0.00501
7	1.089	0.90273	1.2974	6.83755	5.66011	8.15487	0.89198	1.04738	0.9579	0.96575	0.078
8	0.9895	0.82966	1.1611	6.2086	5.19823	7.2933	0.80993	0.96191	0.8567	0.87618	0.07784

^aconcentrations were converted from absorbance by using linear calibration of phenanthrene as shown above.

Appendix Table D8 Raw data of the photodegradation reaction of phenanthrene without catalysts.

Degrading time (h)	Absorbance at λ_{\max} 251 nm			Concentration ^a (ppm)			Relative concentration (C/C ₀)				
	Abs ₁	Abs ₂	Abs ₃	C ₁	C ₂	C ₃	C ₁ /C ₀	C ₂ /C ₀	C ₃ /C ₀	(C/C ₀) _{ave}	Std (C/C ₀)
before lamp on	1.2216	1.4397	1.4665	7.67573	9.05436	9.22377	1	1	1	1	4.5E-08
0	1.3312	1.4086	1.4375	8.36852	8.85777	9.04046	1.09026	0.97829	0.98013	1.01622	0.06412
1	1.3492	1.4136	1.495	8.4823	8.88938	9.40392	1.10508	0.98178	1.01953	1.03546	0.06318
2	1.329	1.3855	1.4998	8.35461	8.71176	9.43426	1.08845	0.96216	1.02282	1.02448	0.06316
3	1.3523	1.439	1.491	8.5019	9.04994	9.37863	1.10763	0.99951	1.01679	1.04131	0.05808
4	1.3054	1.5206	1.4553	8.20544	9.56574	9.15297	1.06901	1.05648	0.99232	1.03927	0.04114
5	1.2701	1.515	1.4608	7.9823	9.53034	9.18774	1.03994	1.05257	0.99609	1.02953	0.02964
6	1.204	1.38969	1.4247	7.56448	8.73824	8.95954	0.98551	0.96509	0.97135	0.97398	0.01046
7	1.0914	1.5247	1.3837	6.85272	9.59166	8.70038	0.89278	1.05934	0.94326	0.96513	0.08541
8	1.225	1.5078	1.3705	7.69722	9.48483	8.61694	1.0028	1.04754	1.06226	1.03753	0.03097

^aconcentrations were converted from absorbance by using linear calibration of phenanthrene as shown above.

Appendix Table D9 Raw data of the photodegradation reaction of phenanthrene by N-doped TiO₂ using titanium(IV) bis(ethyl acetoacetato)diisopropoxide mixed with (NH₂)₂CO and calcined at 673 K.

Degrading time (h)	Absorbance at λ_{max} 251 nm			Concentration ^a (ppm)			Relative concentration (C/C ₀)				
	Abs ₁	Abs ₂	Abs ₃	C ₁	C ₂	C ₃	C ₁ /C ₀	C ₂ /C ₀	C ₃ /C ₀	(C/C ₀) _{ave}	Std _(C/C₀)
before lamp on	0.1659	1.2309	1.4638	1.00253	7.73451	9.2067	1	1	1	1	2.4E-07
0	0.15677	1.0866	1.3066	0.94482	6.82238	8.21302	0.94243	0.88207	0.89207	0.90552	0.03235
1	0.16925	1.1633	1.4407	1.0237	7.30721	9.06068	1.02112	0.94475	0.98414	0.98334	0.03819
2	0.16272	1.213	1.4366	0.98243	7.62137	9.03477	0.97995	0.98537	0.98133	0.98222	0.00282
3	0.1598	1.2033	1.4866	0.96397	7.56005	9.35082	0.96154	0.97744	1.01565	0.98488	0.02781
4	0.15958	1.2199	1.451	0.96258	7.66498	9.12579	0.96015	0.99101	0.99121	0.98079	0.01787
5	0.15089	1.2207	1.4438	0.90765	7.67004	9.08028	0.90536	0.99166	0.98627	0.9611	0.04835
6	0.1508	1.1473	1.412	0.90708	7.20607	8.87927	0.90479	0.93168	0.96444	0.93363	0.02987
7	0.14703	1.0496	1.3522	0.88325	6.5885	8.50126	0.88102	0.85183	0.92338	0.88541	0.03597
8	0.14691	1.001	1.2876	0.88249	6.28129	8.09292	0.88027	0.81211	0.87903	0.85713	0.039

^aconcentrations were converted from absorbance by using linear calibration of phenanthrene as shown above.

Appendix Table D10 Raw data of the photodegradation reaction of phenanthrene by N-doped TiO₂ using titanium(IV) bis(ethyl acetoacetato)diisopropoxide mixed with NH₄Cl and calcined at 673 K.

Degrading time (h)	Absorbance at λ_{\max} 251 nm			Concentration ^a (ppm)			Relative concentration (C/C ₀)				
	Abs ₁	Abs ₂	Abs ₃	C ₁	C ₂	C ₃	C ₁ /C ₀	C ₂ /C ₀	C ₃ /C ₀	(C/C ₀) _{ave}	Std _(C/C₀)
before lamp on	0.59062	1.3213	1.264	3.68723	8.30594	7.94374	1	1	1	1	5.9E-08
0	0.57221	1.1362	1.192	3.57086	7.1359	7.48862	0.96844	0.85913	0.94271	0.92343	0.05715
1	0.5978	1.3147	1.247	3.73262	8.26422	7.83628	1.01231	0.99498	0.98647	0.99792	0.01317
2	0.5818	1.3814	1.2145	3.63148	8.68584	7.63085	0.98488	1.04574	0.96061	0.99708	0.04385
3	0.58129	1.3573	1.2374	3.62826	8.5335	7.7756	0.98401	1.0274	0.97883	0.99675	0.02667
4	0.57217	1.3357	1.2126	3.57061	8.39697	7.61884	0.96837	1.01096	0.9591	0.97948	0.02766
5	0.5651	1.3442	1.254	3.52592	8.4507	7.88053	0.95625	1.01743	0.99204	0.98857	0.03074
6	0.56186	1.34259	1.2189	3.50544	8.44052	7.65866	0.9507	1.0162	0.96411	0.977	0.0346
7	0.55124	1.3293	1.1772	3.43831	8.35651	7.39507	0.93249	1.00609	0.93093	0.9565	0.04295
8	0.56985	1.2997	1.165	3.55594	8.16941	7.31795	0.96439	0.98356	0.92122	0.95639	0.03193

^aconcentrations were converted from absorbance by using linear calibration of phenanthrene as shown above.

Appendix Table D11 Raw data of the photodegradation reaction of phenanthrene by N-doped TiO₂ using titanium(IV) bis(ethyl acetoacetato)diisopropoxide mixed with N₂H₄.H₂O and calcined at 673 K.

Degrading time (h)	Absorbance at λ_{max} 251 nm			Concentration ^a (ppm)			Relative concentration (C/C ₀)				
	Abs ₁	Abs ₂	Abs ₃	C ₁	C ₂	C ₃	C ₁ /C ₀	C ₂ /C ₀	C ₃ /C ₀	(C/C ₀) _{ave}	Std (C/C ₀)
before lamp on	0.17836	1.3743	1.3696	1.08129	8.64096	8.61125	1	1	1	1	2.4E-07
0	0.1727	1.3137	1.333	1.04551	8.2579	8.3799	0.96691	0.95567	0.97313	0.96524	0.00885
1	0.1727	1.3819	1.1983	1.04551	8.689	7.52845	0.96691	1.00556	0.87426	0.94891	0.06748
2	0.1694	1.4024	1.2156	1.02465	8.81858	7.6378	0.94762	1.02056	0.88696	0.95171	0.06689
3	0.16872	1.4038	1.2022	1.02035	8.82743	7.5531	0.94365	1.02158	0.87712	0.94745	0.07231
4	0.16864	1.4057	1.3012	1.01985	8.83944	8.17889	0.94318	1.02297	0.94979	0.97198	0.04428
5	0.16352	1.4069	1.384	0.98748	8.84703	8.70228	0.91325	1.02385	1.01057	0.98255	0.06039
6	0.16517	1.4058	1.4016	0.99791	8.84008	8.81353	0.92289	1.02304	1.02349	0.98981	0.05795
7	0.1609	1.4055	1.3528	0.97092	8.83818	8.50506	0.89793	1.02282	0.98767	0.96947	0.0644
8	0.16931	1.3096	1.33931	1.02408	8.23198	8.41979	0.94709	0.95267	0.97777	0.95918	0.01634

^aconcentrations were converted from absorbance by using linear calibration of phenanthrene as shown above.

Appendix Table D12 Raw data of the photodegradation reaction of benz[a]anthracene by N-doped TiO₂ using titanium(IV) tetraisopropoxide mixed with NH₃ and calcined at 673 K.

Degrading time (h)	Absorbance at λ_{\max} 251 nm			Concentration ^a (ppm)			Relative concentration (C/C ₀)				
	Abs ₁	Abs ₂	Abs ₃	C ₁	C ₂	C ₃	C ₁ /C ₀	C ₂ /C ₀	C ₃ /C ₀	(C/C ₀) _{ave}	Std (C/C ₀)
before lamp on	769.41	757.86	657.71	5.37723	5.29477	4.57977	1	1	1	1	5.9472E-08
0	655.24	658.16	582.36	4.56213	4.58298	4.04182	0.84842	0.86557	0.88254	0.86551	0.01706066
30	680.52	657.59	548.74	4.74261	4.57891	3.8018	0.88198	0.8648	0.83013	0.85897	0.02641303
60	649.17	648.74	547.26	4.5188	4.51573	3.79123	0.84036	0.85287	0.82782	0.84035	0.01252199
90	621.94	637.67	542.31	4.32439	4.4367	3.75589	0.80421	0.83794	0.82011	0.82075	0.01687636
120	585.71	614.88	540.33	4.06574	4.27399	3.74176	0.7561	0.80721	0.81702	0.79344	0.03270805
150	-	-	505.07	-	-	3.49003	-	-	0.76205	0.76205	-
180	475.44	539.87	500.24	3.27849	3.73847	3.45554	0.6097	0.70607	0.75452	0.6901	0.07372172
210	-	-	451.63	-	-	3.1085	-	-	0.67875	0.67875	-
240	372.85	298.13	399.67	2.54607	2.01262	2.73755	0.47349	0.38012	0.59775	0.48378	0.10918074

^aconcentrations were converted from absorbance by using linear calibration of benz[a]anthracene as shown above.

Appendix Table D13 Raw data of the photodegradation reaction of benz[a]anthracene by P25 TiO₂.

Degrading time (h)	Absorbance at λ_{max} 251 nm			Concentration ^a (ppm)			Relative concentration (C/C ₀)				
	Abs ₁	Abs ₂	Abs ₃	C ₁	C ₂	C ₃	C ₁ /C ₀	C ₂ /C ₀	C ₃ /C ₀	(C/C ₀) _{ave}	Std (C/C ₀)
before lamp on	567.03	569.08	690	3.93238	3.94701	4.81029	1	1	1	1	6.9022E-08
0	559.78	531.15	688.34	3.88062	3.67622	4.79844	0.98684	0.93139	0.99754	0.97192	0.03550469
30	562.1	570.84	666.25	3.89718	3.95958	4.64074	0.99105	1.00318	0.96475	0.98633	0.01964648
60	555.42	553.79	641.21	3.84949	3.83785	4.46197	0.97892	0.97234	0.92759	0.95962	0.02793332
90	538.16	546.24	525.93	3.72627	3.78395	3.63895	0.94759	0.95869	0.75649	0.88759	0.11366823
120	536.05	523.46	593.2	3.7112	3.62132	4.11921	0.94376	0.91748	0.85633	0.90586	0.04485605
150	530.76	510.94	588.2	3.67343	3.53193	4.08352	0.93415	0.89484	0.84891	0.89263	0.04266251
180	484.77	497.09	568.73	3.3451	3.43305	3.94451	0.85066	0.86979	0.82001	0.84682	0.02510632
210	453.21	471.2	549.65	3.11978	3.24822	3.8083	0.79336	0.82296	0.7917	0.80267	0.01758775
240	451.91	453.39	529.05	3.1105	3.12107	3.66123	0.791	0.79074	0.76112	0.78095	0.01717483

^aconcentrations were converted from absorbance by using linear calibration of benz[a]anthracene as shown above.

Appendix Table D14 Raw data of the photodegradation reaction of benz[a]anthracene without catalysts.

Degrading time (h)	Absorbance at λ_{max} 251 nm			Concentration ^a (ppm)			Relative concentration (C/C ₀)				
	Abs ₁	Abs ₂	Abs ₃	C ₁	C ₂	C ₃	C ₁ /C ₀	C ₂ /C ₀	C ₃ /C ₀	(C/C ₀) _{ave}	Std _(C/C₀)
before lamp on	688.68	592.61	544.24	4.80087	4.115	3.76967	1	1	1	1	8.4057E-08
0	671.49	625.15	512.36	4.67815	4.34731	3.54207	0.97444	1.05645	0.93962	0.99017	0.05998409
30	654.84	558.13	529.85	4.55928	3.86884	3.66694	0.94968	0.94018	0.97275	0.9542	0.01674875
60	683.84	563.95	520.15	4.76632	3.91039	3.59769	0.9928	0.95028	0.95438	0.96582	0.02345857
90	674.07	562.27	524.46	4.69657	3.89839	3.62846	0.97827	0.94736	0.96254	0.96272	0.01545682
120	689.05	521.4	522.33	4.80351	3.60661	3.61325	1.00055	0.87645	0.95851	0.94517	0.06311337
150	690.91	545.64	461.95	4.81679	3.77967	3.18218	1.00332	0.91851	0.84415	0.92199	0.0796387
180	690.91	530.49	528.17	4.81679	3.67151	3.65494	1.00332	0.89223	0.96957	0.95504	0.05695291
210	666.23	535.19	520.84	4.64059	3.70506	3.60261	0.96662	0.90038	0.95568	0.94089	0.03550859
240	630.56	548.74	492.5	4.38594	3.8018	3.40029	0.91357	0.92389	0.90201	0.91316	0.01094438

^aconcentrations were converted from absorbance by using linear calibration of benz[a]anthracene as shown above.

Appendix Table D15 Raw data of the photodegradation reaction of phenol by N-doped TiO₂ using titanium(IV) tetraisopropoxide mixed with NH₃ and calcined at 673 K.

Degrading time (h)	Absorbance at λ_{max} 251 nm			Concentration ^a (ppm)			Relative concentration (C/C ₀)				
	Abs ₁	Abs ₂	Abs ₃	C ₁	C ₂	C ₃	C ₁ /C ₀	C ₂ /C ₀	C ₃ /C ₀	(C/C ₀) _{ave}	Std (C/C ₀)
before lamp on	0.32708	0.33573	0.33695	20.0533	20.5776	20.6515	1	1	1	1	2.2372E-07
0	0.32433	0.33148	0.33594	19.8867	20.32	20.5903	0.99169	0.98748	0.99704	0.99207	0.00478794
1	0.31884	0.33172	0.3295	19.5539	20.3345	20.2	0.9751	0.98819	0.97814	0.98047	0.0068522
2	0.31599	0.331	0.32916	19.3812	20.2909	20.1794	0.96648	0.98607	0.97714	0.97656	0.0098053
3	0.315	0.32979	0.32872	19.3212	20.2176	20.1527	0.96349	0.98251	0.97585	0.97395	0.00964803
4	0.31441	0.3285	0.3249	19.2855	20.1394	19.9212	0.96171	0.97871	0.96464	0.96835	0.00908682
5	0.31197	0.3276	0.32822	19.1376	20.0848	20.1224	0.95433	0.97605	0.97438	0.96826	0.01208605
6	0.3112	0.32822	0.32548	19.0909	20.1224	19.9564	0.95201	0.97788	0.96634	0.96541	0.01296207
7	0.31106	0.3276	0.32181	19.0824	20.0848	19.7339	0.95158	0.97605	0.95557	0.96107	0.01313019
8	0.31077	0.32277	0.32639	19.0648	19.7921	20.0115	0.95071	0.96183	0.96901	0.96052	0.00922146

^aconcentrations were converted from absorbance by using linear calibration of phenol as shown above.

Appendix Table D16 Raw data of the photodegradation reaction of phenol by P25 TiO₂.

Degrading time (h)	Absorbance at λ_{\max} 251 nm			Concentration ^a (ppm)			Relative concentration (C/C ₀)				
	Abs ₁	Abs ₂	Abs ₃	C ₁	C ₂	C ₃	C ₁ /C ₀	C ₂ /C ₀	C ₃ /C ₀	(C/C ₀) _{ave}	Std _(C/C₀)
before lamp on	0.3323	0.33578	0.3182	20.3697	20.5806	19.5152	1	1	1	1	1.4461E-07
0	0.3319	0.33534	0.31729	20.3455	20.5539	19.46	0.99881	0.9987	0.99717	0.99823	0.00091542
1	0.33192	0.3365	0.31395	20.3467	20.6242	19.2576	0.99887	1.00212	0.9868	0.99593	0.00807121
2	0.33124	0.33153	0.3185	20.3055	20.323	19.5333	0.99685	0.98748	1.00093	0.99509	0.00689404
3	0.33196	0.32962	0.31262	20.3491	20.2073	19.177	0.99899	0.98186	0.98267	0.98784	0.0096635
4	0.32534	0.32874	0.31673	19.9479	20.1539	19.4261	0.97929	0.97927	0.99543	0.98466	0.009327
5	0.3266	0.32747	0.31592	20.0242	20.077	19.377	0.98304	0.97553	0.99292	0.98383	0.00872226
6	0.32444	0.3262	0.3156	19.8933	20.000	19.3576	0.97661	0.97179	0.99193	0.98011	0.01051372
7	0.3236	0.32521	0.31484	19.8424	19.94	19.3115	0.97411	0.96887	0.98957	0.97752	0.01075764
8	0.33002	0.3268	0.31179	20.2315	20.0364	19.1267	0.99322	0.97356	0.98009	0.98229	0.0100125

^aconcentrations were converted from absorbance by using linear calibration of phenol as shown above.

Appendix Table D17 Raw data of the photodegradation reaction of phenol without catalysts.

Degrading time (h)	Absorbance at λ_{\max} 251 nm			Concentration ^a (ppm)			Relative concentration (C/C ₀)				
	Abs ₁	Abs ₂	Abs ₃	C ₁	C ₂	C ₃	C ₁ /C ₀	C ₂ /C ₀	C ₃ /C ₀	(C/C ₀) _{ave}	Std _(C/C₀)
before lamp on	0.32356	0.31443	0.31397	19.84	19.2867	19.2588	1	1	1	1	8.7495E-08
0	0.32329	0.31432	0.31594	19.8236	19.28	19.3782	0.99918	0.99965	1.0062	1.00168	0.00392443
1	0.32163	0.31546	0.3156	19.723	19.3491	19.3576	0.9941	1.00324	1.00513	1.00082	0.00589534
2	0.32364	0.31522	0.3119	19.8448	19.3345	19.1333	1.00024	1.00248	0.99349	0.99874	0.00468376
3	0.32346	0.31584	0.31772	19.8339	19.3721	19.4861	0.99969	1.00443	1.0118	1.00531	0.00610075
4	0.32133	0.3152	0.31611	19.7048	19.3333	19.3885	0.99319	1.00242	1.00673	1.00078	0.00692031
5	0.32248	0.31567	0.3191	19.7745	19.3618	19.5697	0.9967	1.0039	1.01614	1.00558	0.00983015
6	0.31671	0.31517	0.31788	19.4248	19.3315	19.4958	0.97908	1.00233	1.0123	0.9979	0.01705064
7	0.31858	0.31522	0.31789	19.5382	19.3345	19.4964	0.98479	1.00248	1.01234	0.99987	0.01395899
8	0.31999	0.31598	0.3101	19.6236	19.3806	19.0242	0.98909	1.00487	0.98782	0.99393	0.00949718

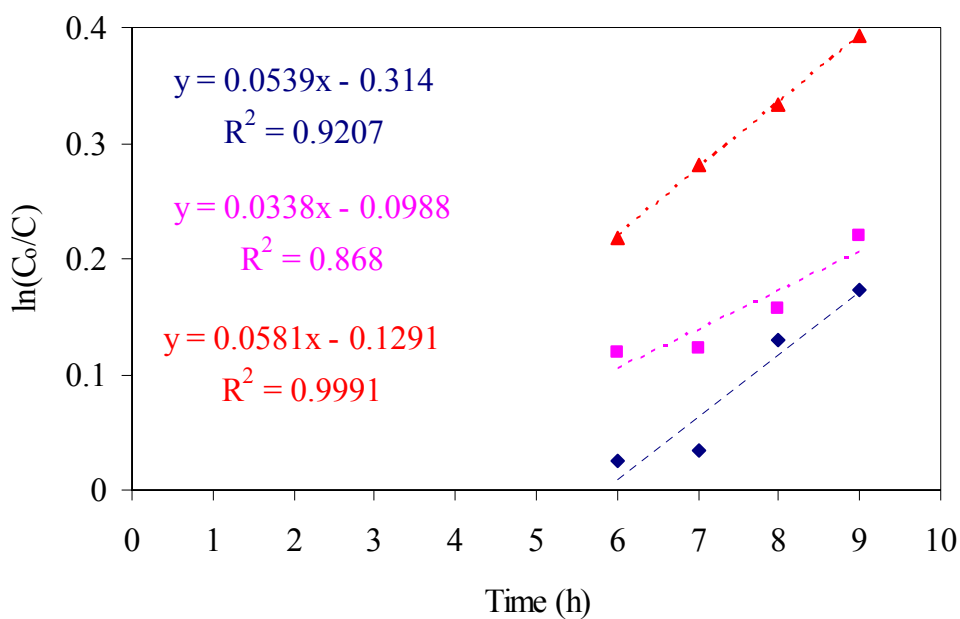
^aconcentrations were converted from absorbance by using linear calibration of phenol as shown above.

APPENDIX E

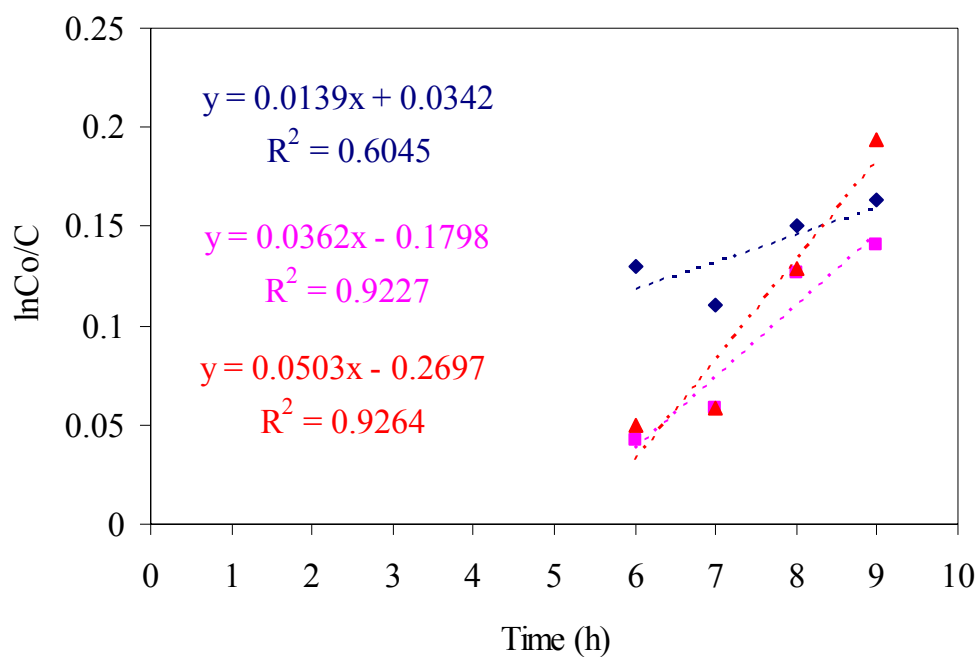
Calculation of rate constants of each photodegradation reactions

The procedure used to find rate constants was adapted from previous research by Fang *et al.* (2007). They assumed that the degradation of methylene blue in the presence of photocatalysts was the first-order kinetic reaction because they plotted a graph between $\ln C_0/C$ and degrading time (h). Then, they obtained the relative coefficient (R^2) was close to 1 and the slope of the graph could be considered as the rate constant of the photodegradation reaction. Therefore, this work properly modified their method to find the rate constants. All raw data are shown in the Appendix D.

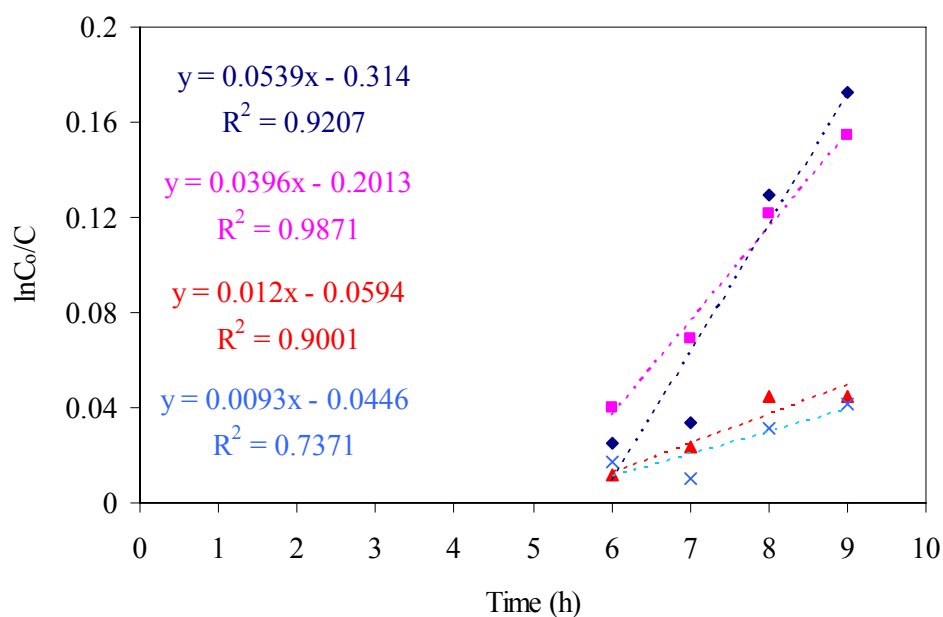
First, all the photodegradation reactions of phenanthrene focused on the three last hours (6-9 h) because most of N-doped TiO_2 could obviously degrade the substrate in this period. Therefore, it is reasonable to find rate constants and compared to one another as shown in Appendix Figure E1-E4.



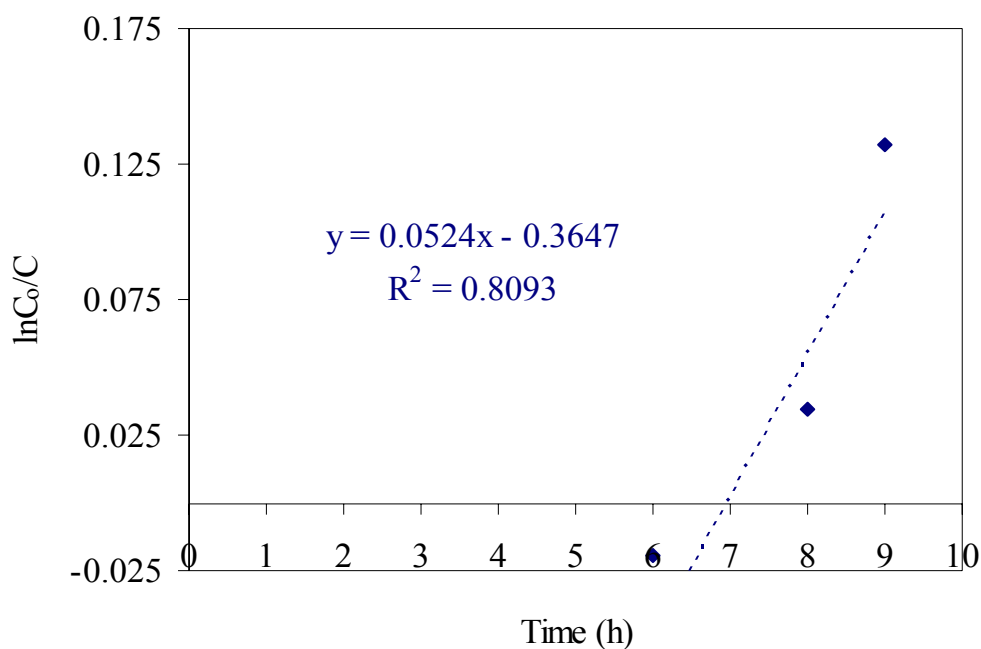
Appendix Figure E1 The relation between $\ln C_0/C$ and time (h) of photodegradation reaction of phenanthrene by N-doped TiO_2 using the variation of titania precursors; (a) titanium(IV) bis(ethyl acetoacetato) diisopropoxide (♦), (b) titanium(IV) tetra-n-butoxide (■) and (c) titanium(IV) tetraisopropoxide (▲), and calcined at 673 K.



Appendix Figure E2 The relation between $\ln C_0/C$ and time (h) of photodegradation reaction of phenanthrene by N-doped TiO_2 using the variation of titania precursors; (a) titanium(IV) bis(ethyl acetoacetato) diisopropoxide (♦), (b) titanium(IV) tetra-n-butoxide (■) and (c) titanium(IV) tetraisopropoxide (▲), and calcined at 773 K.

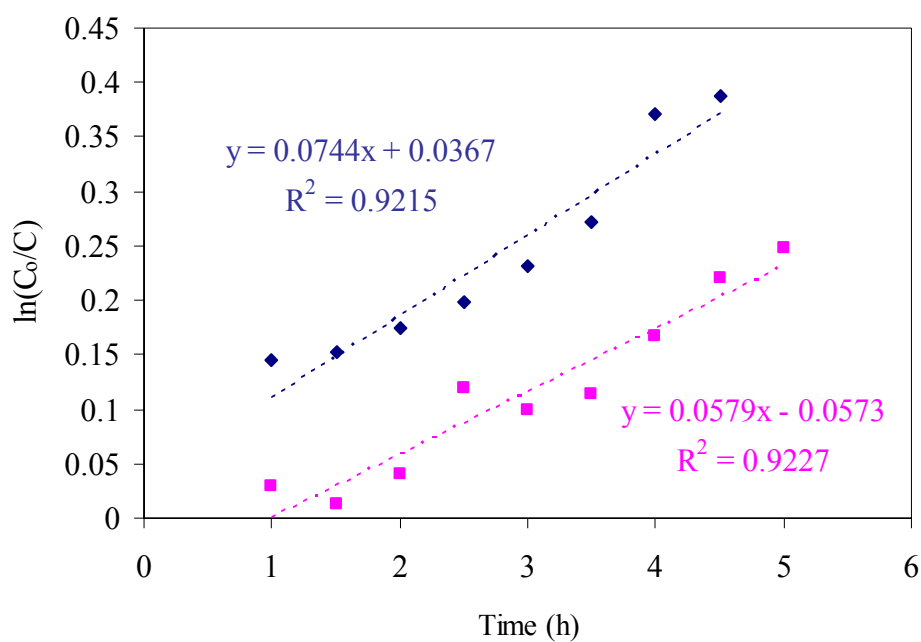


Appendix Figure E3 The relation between $\ln C_0/C$ and time (h) of photodegradation reaction of phenanthrene by N-doped TiO_2 using the variation of nitrogen sources; (a) NH_3 (◆), (b) $(\text{NH}_2)_2\text{CO}$ (■), (c) NH_4Cl (▲) and (d) $\text{N}_2\text{H}_4 \cdot \text{H}_2\text{O}$ (×), and calcined at 673 K.

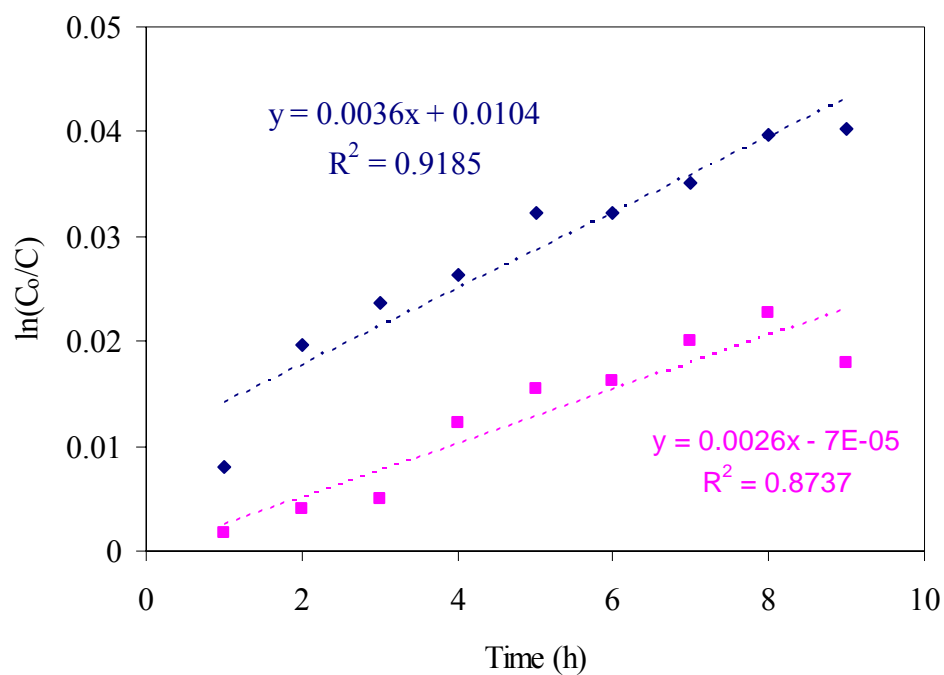


Appendix Figure E4 The relation between $\ln C_0/C$ and time (h) of photodegradation reaction of phenanthrene by P25 TiO_2 .

Regarding the other substrates, benz[a]anthracene and phenol, their photodegradation rate constants were able to be found with the full range of irradiation time: 1-5 h for benz[a]anthracene and 1-9 h for phenol as illustrated in Appendix Figure E5 and E6.



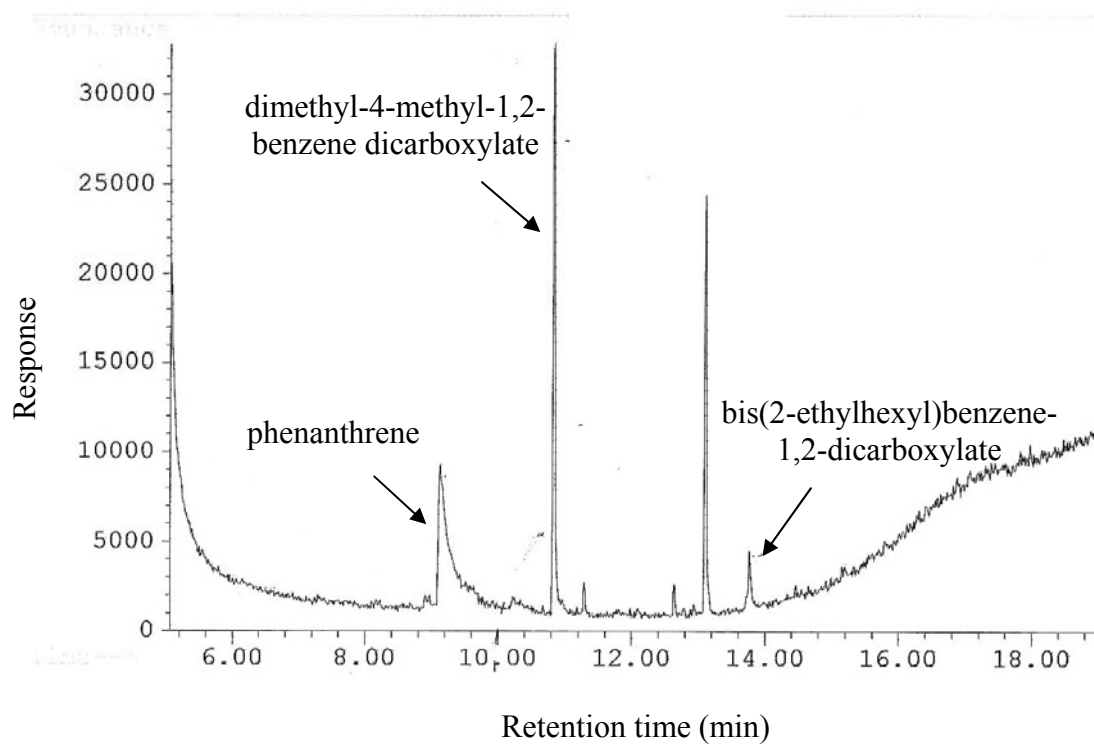
Appendix Figure E5 The relation between $\ln C_0/C$ and time (h) of photodegradation reaction of benz[a]anthracene by (a) N-doped TiO₂ using titanium(IV) tetraisopropoxide mixed with NH₃ and calcined at 673 K (♦) and (b) P25-TiO₂ (■).



Appendix Figure E6 The relation between $\ln C_0/C$ and time (h) of photodegradation reaction of phenol by (a) N-doped TiO₂ using titanium(IV) tetraisopropoxide mixed with NH₃ and calcined at 673 K (♦) and (b) P25-TiO₂ (■).

APPENDIX F

The gas chromatogram of phenanthrene and intermediate products



Appendix Figure F1 The gas chromatogram of phenanthrene and intermediate products.

CIRRICULUM VITAE

NAME : Mr. Weekit Sirisaksoontorn

BIRTH DATE : March 17, 1985

BIRTH PLACE : Pathum Thani, Thailand

EDUCATION	: <u>YEAR</u>	<u>INSTITUTE</u>	<u>DEGREE/DIPLOMA</u>
	2007	Kasetsart Univ.	B.Sc. (Chemistry)

POSITION/TITLE : Postgraduate student

WORKPLACE : Faculty of Science, Kasetsart University

SCHOLARSHIP/AWARDS :

- Development and Promotion of Science and Technology Talents Project (DPST)
- Center for Innovation in Chemistry:
Postgraduate Education and Research Program in Chemistry (PERCH-CIC)
- Outstanding Poster Award at PACCON 2008 (Pure and Applied Chemistry International Conference) 31 Jan – 2 Feb 2008